Novel Electroactive Soft Actuators Based on Ionic Gel/Gold Nanocomposites Produced by Supersonic Cluster Beam Implantation

Yunsong Yan

University of Milan, Milan

Matricola n. R10346

Supervisor: Prof. Paolo Milani

Interdisciplinary Centre for Nanostructured Materials and Interfaces (CIMaINa)

University of Milan, Milan

Anno accademico 2015-2016

1.Table of Contents

2. Figures Index

3. List of abbreviations

1- Butyl-3-methylimidazolium tetrafluoroborate [Bmim] [BF4]

Carbon nanotubes (CNTs)

Carbon-polymer-composites (CPCs)

Electric double-layer capacitors (EDLCs)

Electro-active polymers (EAPs)

Electrochemical impedance spectroscopy (EIS)

Ethylene glycol dimethacrylate (EGDMA)

1-Ethyl-3-methylimidazolium bis(trifluoromethylsulfonyl)imide [Emim][Tf2N]

1- Ethyl-3-methylimidazolium tetrafluoroborate (EMIM.BF4)

Equivalent series resistance (ESR)

Anion exchange membranes (AEM)

Fourier transform infrared spectroscopy (FT-IR)

Graphitic carbon nitride (g-CN)

Halloysite nanoclays (HNC)

Hexagonal-cylindrical (HEX)

Ion exchange capacity (IEC)

Ionic electroactive polymers (IEAPs)

Ionic gel/metal nanocomposite (IGMN)

Ionic gel/metal nanocomposite without TEA+ (tetraethylammonium) (IGMN-WTEA+)

Ionic gel/metal nanocomposite without nanoclays (IGMN-WNC)

Ionic-polymer-metal composites (IPMC)

Multi-wall nanotubes (MWNTs)

Nitrile butadiene rubber (PEO-NBR)

Poly (vinylpyrrolidone) (PVP)

Poly styrene sulfonate (PSS)

Poly(acrylic acid) (PAA)

Poly acrylic acid-co-poly acrylonitrile (PAA-co-PAN)

Polyvinylidene difluoride (PVDF)

Proton exchange membrane (PEM)

Single wall nanotubes (SWNTs)

Supersonic Cluster Beam Implantation (SCBI)

Tetrabuthylammonium (TBA+)

Tetrabutylammonium hydroxide (TBA.OH),

Tetraethyl ammonium (TEA+)

Tetraethylammonium fluoride hydrate (TEAF)

Tetraethylammonium tetrafluoroborate (TEA.BF4)

Tetramethylammonium (TMA+)

Ttetraethylammonium hydroxide (TEA.OH),

X-ray Diffraction (XRD)

X-ray photoelectron spectroscopy (XPS)

4. Abstract

Ionic electro-active polymers (IEAPs) constitute a promising solution for developing self-regulating, flexible and adaptive mechanical actuators in the area of soft robotics, micromanipulation and rehabilitation [1-3]. These smart materials have the ability to undergo large bending deformations as a function of a low applied voltage (1 to 5 V), as a result of the ions migration through their inner structure when the network is liquid filled. Among this broad family of materials, ionic-polymer-metal composites (IPMC) based on DuPont's Nafion® have attracted an increasing interest for the production of light weight controllable soft machines due to their easiness to be metalized (e.g. by mean of electroless plating), fast response and capability of working exposed to air. However, the high cost of the material, its relatively low working density (i.e. the maximum mechanical work output per unit volume of active material that drives the actuation) and weak force output, as well as the considerable fatigue effects endured by the surface electrodes upon cycling, is limiting the performance of these IPMC actuators and hindering their implementation in traditional mechatronic and robotic systems [8]. On the other hand, ionic hydrogels, such as poly(acrylic acid) (PAA) and poly-styrene sulfonate (PSS) based polymers [9-10], exhibit controllable mechanical properties and porosity and have shown to be excellent candidates to be used as electrically triggered artificial muscles and miniaturized robots operating in aqueous environments. Although the relatively low cost of these materials render them appealing for mass production scale up, the applicability of these polymeric actuators is limited to a liquid environment, which is intrinsically facilitating the solvent evaporation when the hydrogels are exposed to air. Furthermore, because of the difficulty encountered in fabricating stable and anchored metal structures on these polymer surfaces, these smart soft systems operate in a non-contact configuration with respect to the pilot electrodes, therefore increasing the actuators response time up to few tenths of seconds. In order to achieve an efficient

electromechanical transduction along with a stable and durable performance for electro-active actuators operating in air, two main interplaying characteristics must be tailored when designing the system. On one hand side, the need of electrodes that are physically interpenetrating with the polymeric basis is of absolute priority, since the intercalation of ions into the electrode layers and the resulting material volumetric change are fundamental for strain generation. On the other hand, the formulation and engineering of new low cost materials able to merge highly elastic properties and efficient ionic transport features is of crucial importance.

The present thesis work deals with the formulation, synthesis and manufacturing of a novel ionic gel/metal nanocomposite (IGMN) that was designed and developed to merge the advantageous properties of both IPMCs and ionic hydrogel actuators and to contextually overcome many of the above mentioned drawbacks characteristic of these two families of polymers. These composites were obtained by mean of Supersonic Cluster Beam Implantation (SCBI)[1]. This technique, developed in-house, relies on the use of supersonically accelerated gas-phase metal cluster beams directed onto a polymeric substrate in order to generate thin conductive layers (few tenths to few hundreds of nanometers thick) anchored to the polymer. This scalable approach already proved to be suitable for the manufacturing of elastomer/metal functional nanocomposites, and, as described in this work, it enabled the production of cluster-assembled gold electrodes (100 nm thick) interpenetrating with an engineered ionic gel matrix[2]. This novel approach led to the fabrication of highly conductive metal nanostructures, large surface area for ions storage and providing minimal interfacial stresses between the metal layer and the polymeric basis upon deformation. The key features of this novel system comprise the control on the polymer elasticity, bending actuation in air from 0.1V to 5V, fast response time (< 300 ms), high displacement (> 5 cm), high work density (>10 J/cm^3), minimal electrodes fatigue upon cycling and low manufacturing costs.

A bottom-up approach was firstly adopted to engineer and produce Uv photo-cross-linked ionic co-polymers (iongel) with tailored mechanical properties and provided with inorganic nano-structures embedded in the macromolecular matrix which show excellent long-term performance. The polymer is based on poly(acrylic acid)-co-poly(acrylonitrile) (PAA-co-PAN) co-polymers, which are chemically cross-linked in a hydrogel-like fashion and swollen with suitable imidazolium-based ionic liquid. The materials are produced as 100 μm freestanding layers using a one-pot synthesis and a simple molding process. Due to the incommensurably low vapor pressure of the ionic liquid, issues concerning the shrinkage of traditional water swollen gels operating exposed to air could be avoided. An organic cation (tetraethyl ammonium, TEA+) is stably coordinated to the carboxyl groups of the PAA and free to move in the polymer sieve-like structure when a small voltage is applied at the electrodes. PAN was introduced to enhance the elastic properties of whole polymer. In the bulk polymer, halloysite nanoclays (HNC) are physically embedded into the gel in order to both improve the toughness of the gel and to improve the ionic conductivity of the system. In fact, the nanostructures interacts with the imidazolium cation of the ionic liquid through an oxygen reduction reaction, and therefore the latter is able to contribute to the charge transport phenomena induced by the electric field due to the solvent partial dissociation. Furthermore, the porosity of the polymer, tailored by the cross-linker, creates physical channels to favor the mobility of positive ions when an electric field is applied. The contribution of both the positive charged species (TEA+ and cations of ionic liquid) that accumulates at the nanostructured electrode in a double layer capacitance regime generates a differential swelling at the opposite sides of the actuator, which bends towards the anode.

A schematic of the composite is reported in Figure 1, while a simplified representation of the actuation mechanism is reported in Figure 2.

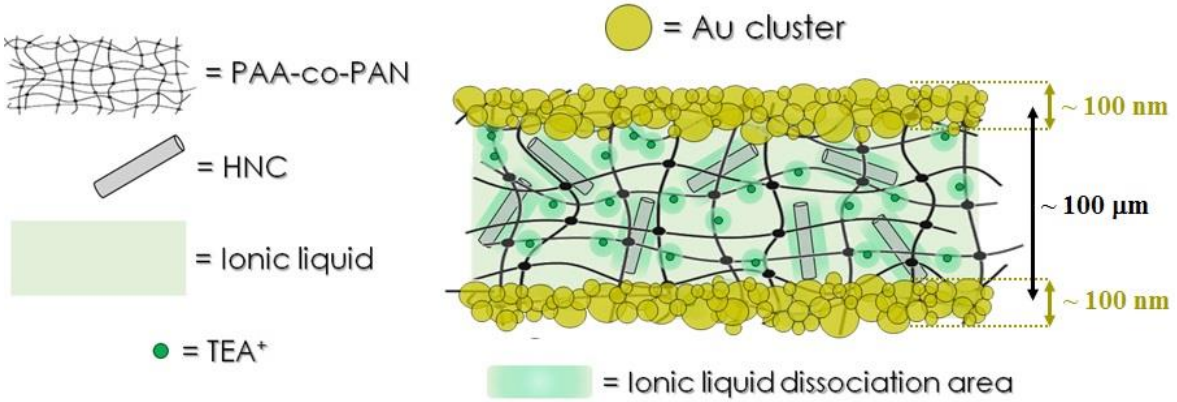

Figure 1. Schematic of IGMN actuator.

As it will be shown in the next sections, the actuation mechanism of the IGMN could be modeled according to both the material structure and design, as well as to the experimental data on its electrochemical and electro-mechanical properties.

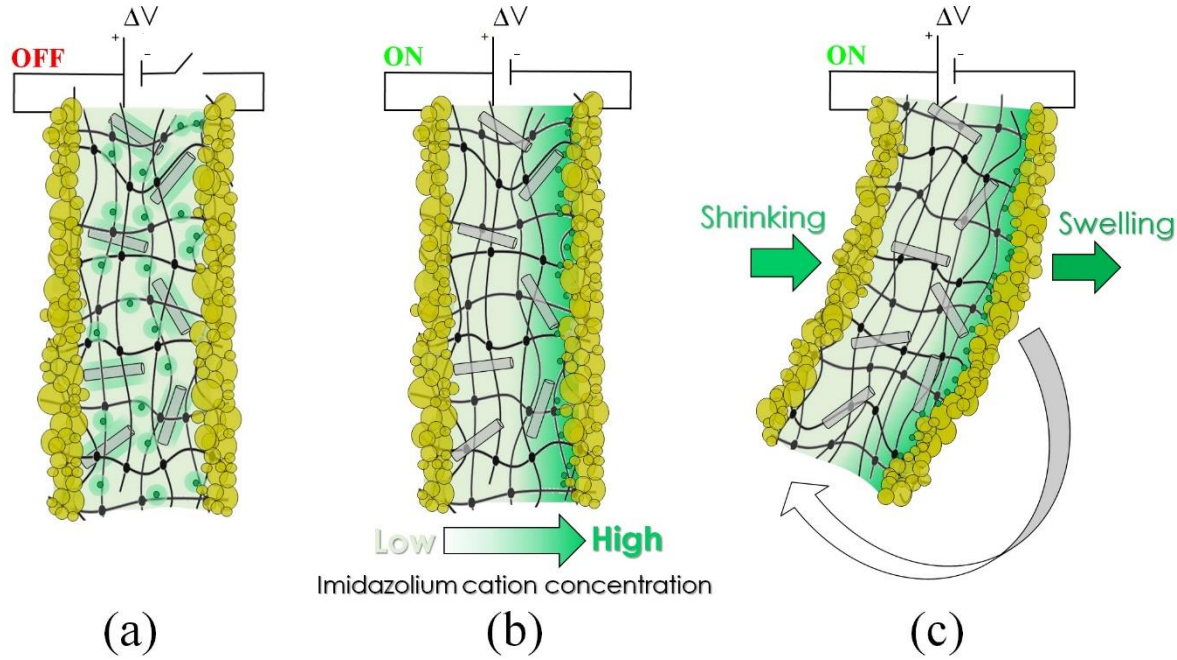

Figure 2. Actuation mechanism of the IGMN. a) IGMN-based actuator. b) When the electrical stimulus is applied, both the TEA+ and Emim (1- Ethyl-3-methylimidazolium) cations migrate towards the cathode. c) The differential swelling at the anodic and cathodic side of the IGMN induces the bending of the actuator towards the anode.

Comparing with traditional soft polymers incompatibility with current metallization processes, like

electroless plating or surface silver laminated electrodes fabrication, which are not suitable to guarantee long-term actuation of the components, SCBI demonstrated to be a suitable technique for the production of next generation electro-active soft actuators. The IGMN-based actuators showed superior performance, such as large bending displacement, fast response time, long durability in a low voltage regime during the actuation process. The combination of the SCBI fabrication technology with the ionic gel synthesis and fabrication renders the manufacturing of these systems time-saving and costs-effective, and the unique properties of these actuators render them good candidates for potential scale up and for applications in micro-electromechanical systems, microfluidics, soft robotics, and rehabilitation.

5. Introduction

5.1 The brief of different ionic electroactive polymer actuators

The rapidly advancing field of materials science has introduced many ‘smart’ materials with novel sensing and actuation capabilities. The ability of electroactive polymer (EAP) to change their shape or size under electrical excitation is offering appealing alternatives to conventional sensors and actuators[3]. Two functionally similar classes of such materials are IPMCs and carbon-polymer-composites (CPCs). Both are IEAPs consisting of a polymeric membrane provided with surface metal electrodes, that change their curvature under electrical stimulus and, conversely, they generate an electrical signal when they are bent. Since their first introduction over two decades ago [4], their properties have been greatly improved, e.g., both the power consumption and surface resistance have been significantly reduced. In this sense, IEAP have been proposed as materials for various applications in the field of robotics, due to their technological potential and advantages over conventional actuators, including easy scalability, light weight, and low actuation voltage. To make a deep understanding of such materials behavior and characteristics, IPMCs and CPCs will be discussed in the next sections.

5.1.1 Ionic polymer metal composites (IPMCs)

A typical IPMC consists of a polyelectrolyte membrane (usually Nafion® or Flemion®) plated on both faces by a noble metal, and neutralized with certain counter ions that balance the electrical charge of the anions covalently fixed to the back-bone membrane. The transport of hydrated cations within an IPMC beam under the applied voltage and the associated electrostatic interactions leads to the bending of an IPMC beam. In 1992, the electro-active characteristics and the electromechanical

coupling mechanism of IPMCs were discovered by three groups of researchers in Japan and in the United States[4].

The principle of such ion-exchange polymer-metal composites (IPMC) has been modeled and ionic polymeric actuators/sensors were studied in term of their ion-exchange capabilities. An ionic polymer is a polyelectrolyte that contains ionic groups such as sulfuric or carboxylic acid attached to the backbone of a polymer chain (with electrically neutral repeating units). The composition forms highly ionic clusters that facilitate selectively the transport of the mobile ions (either cations or anions) across the backbone. The mobile ions inside the polymer can be transported and accumulated at one side of the polymer by applying a small electrical field, which results in the physical bending of the system, as shown in Figure 3.

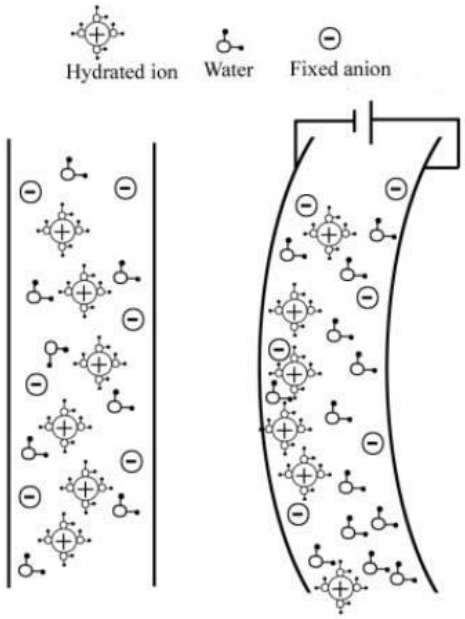

Figure 3. Schematic illustration of the IPMC actuation mechanism[4].

For example, IPMCs were fabricated and tested by Oguro's group in 1992. They found that the bending displacement was dependent on the applied voltage for the cantilevered IPMC and that the magnitude of the output electrical signal was in turn related to the magnitude and direction of the applied deformation as shown in Figure 4 [5].

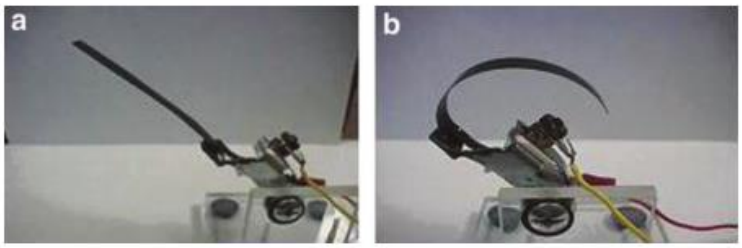

Figure 4. Successive photographs of an IPMC strip before actuation (a) and after actuation (b). IPMC, ionic polymer–metal composite[6].

Also, they proved that IPMCs were active actuators that showed large deformation in the presence of a low applied voltage and exhibited to low impedance. Activated by this idea, many improvements have been developed by different research groups. Due to the major role of ions transport and storing ability of the polymers in determining the actuation performance, their properties of maintaining the required mobility for counterions across the membrane by forming hydrophilic clusters or channels providing a certain degree of porosity for charge transport when swollen in the presence of suitable diluent were engineered. It was revealed that the proton exchange membrane (PEM) and anion exchange membranes (AEM) are two broad categories of ionic polymers that facilitate the transport of the cations and anions, respectively. In this case, acidity or the ion exchange capacity (IEC) of the ionic polymer becomes an indication of its capacity to store the counterions at the ionic sites, and the ion conductivity of the ionic polymer becomes an indication of the ions mobility across the membrane. IEC, highly depends on the structure of the membrane, while the ion conductivity depends on the size and charge of the counterions as well as on the electrolyte type, diluents uptake and conductivity. Among the most reported PEMs, the proton conductivity is strongly related to the amount of ionic groups (sulfonic or carboxylic acid groups), and membranes with more acid groups typically have higher proton conductivity [7]. However, the tensile modulus of the polymer typically scales inversely with the ionic conductivity and with higher diluent uptake. Based on such properties, the main effort in this

research area is to synthesize ionic polymers with high ionic conductivity in hydrated conditions, improved chemical and thermal stability, and improved mechanical properties. A considerable number of potential polymer backbone and side-chain combinations have been synthesized to meet these requirements. DuPont's Nafion continues to hold a place of prominence in the field because of its high proton conductivity and good mechanical properties, and thus it provides a useful standard for comparison with other perfluorinated sulfonic acid (PFSA) candidate membranes. The reason why the structure of the DuPont's Nafion (shown in Figure 5) became a good candidate is that it consists of perfluorinated alkenes with short side chains terminated by ionic groups (typically sulfonate group) for cation exchange or ammonium cations for anion exchange. The large polymer backbones determine their mechanical strength. Short side chains provide ionic groups that interact with water or other diluents and favor the passage of appropriate ions[8].

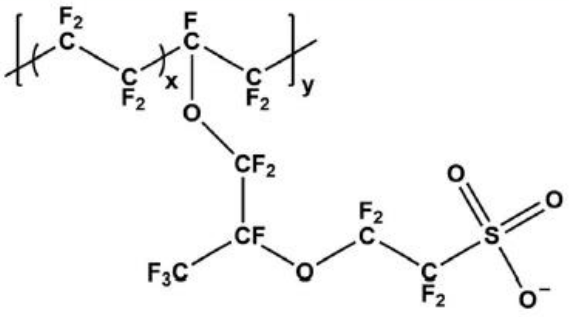

Figure 5. The chemical structure of Nafion[9].

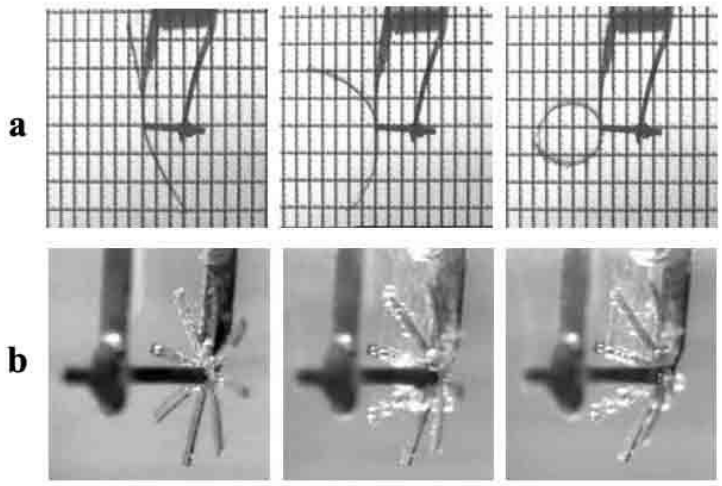

Figure 6. The actaution of biomimic underwater robot a) 2-legs IPMCs actuator which can be controlled to undergo a grasping motion under 4.5V in water. b) Time-sequence images of micro underwater Nafion actuators. The actuator shown has the dimensions of w=500mm, l=4000mm, t=200mm for each leg. The actuator was actuated with 15V input voltage with 50mA current to a tip deflection of ~1mm[8].

Kwok's group prepare 0.18 um thick ionic conducting polymer films based on Dupont Co. (Nafion SE-5012) and fabricated micro-cantilever structures composed of Au/Nafion/Au film layers. By using this film, the displacement test was successfully carried out, and for a 24mm long IPMC actuator strip, the maximum deflecting angle could even attain about 155° (corresponding to a displacement of 48mm). Based on this discover, Grippers with multi-fingers configurations were successfully developed; the grippers could be actuated in water at ~5V DC voltages (shown in Figure 6).

Also, to improve the displacement of the IPMC actuator, salts are considered to influence the actuator performance. A hydrated ion is usually referred to a tightly held sheath of water molecules, bound to the ionic specie even under an applied electric field. Following a chemical reduction process, the mobile cation in the membrane can be exchanged with any suitable ion by immersing the membrane in a salt solution of that ion. Alkali metal ions (Li+, Na+, K+, Rb+ , and Cs+) may be exchanged by soaking them in an appropriate salt solution such as chloride salts (LiCl, NaCl, and KCl) at

moderate temperatures (30℃) for 1–3 days. Alkyl ammonium ions TBA+ (tetrabuthylammonium) and TMA+ (tetramethylammonium) may be exchanged using TBA+ and TMA+. In table 1 the advantages and disadvantages of different alkali metals in the IPMCs are reported. Comparing with other salts, the IPMC with Li + ions shows the fastest and largest displacements[10].

Cation Form	**Advantages**	**Disadvantages**
Li+, Na+, K+, Rb+, Cs+,.	**1. Fast response** **2. Large amplitude under high-frequency alternate current (AC)**	**1. Nation-based IPMCs do not hold strain under DC** **2. Small overall displacement** **3. Low voltage limit due to water electrolysis(<1.5 V)**
TBA+	**1. Do not relax so fast under DC** **2. Large overall displacement** **3. Can suppress water electrolysis at higher voltage (up to 3V)**	**1. Slow response** **2. Small amplitude under high-frequency AC**

Table 1. Advantages and disadvantages of various cation forms in the actuation of ionic polymer–metal composites.

However, many effects have been attributed to the performance of IPMC actuators; the conventional water-based IPMCs significantly loosen their solvent content when operated at voltages larger than 1.23 Volts in air (at which electrolysis of water starts). To overcome such problem, ionic liquids which are room-temperature molten salts, and are considered as sealants due to their very low vapor pressure, have been introduced, while IPMCs can be made as self-contained encapsulated actuators to operate in dry environments as well. IPMCs could be regarded as the one of the most promising smart materials because of their light weight and since they can produce large bending deformation under low driving voltages. Furthermore, they operate both in a humid or liquid environment and in dry environments and can be modeled as both capacitive and resistive elements.

The actuators behave similarly to biological muscle and this provides an attractive mean of actuation for biomechanics and biomimetic applications.

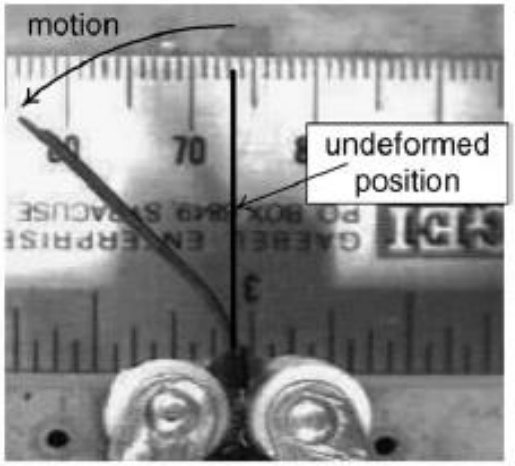

Figure 7. the deflection of IPMC actuators solved with ionic liquid[11].

Bennett's group was the first to fabricate one IPMC actuator which uses highly stable ionic liquids 1-ethyl-3-methylimidazolium bromide to replace water as the solvent[12], due to their advantages, like higher electrochemical stability than water which could offer the possibility of higher actuation voltages (4.1V) and non-volatile properties. 1-ethyl-3-methylimidazolium trifluoromethanesulfonate ionic liquid has been successfully tested as a viable solvent for Nafion based IPMC actuators, which made it a promising candidate to replace water in ionic polymer actuators. What is more, experimental results indicated that Nafion based actuators solvated with this ionic liquid have improved stability when operated in air as compared to the same materials solvated with water, although the magnitude of the response is decreased as compared to the water samples at high frequencies. The main drawback associated with the use of ionic liquids is a reduction in the speed of the response as compared to water, although the initial results were promising and demonstrated the potential for this approach(shown in Figure 7)[11].

To generate a large bending angle and better performance of the IPMCs actuators, the use of thick metal layers interpenetrating with the polymer is necessary. Shahinpoor's group fabricated one IPMCs based artificial muscles which is composed of a perfluorinated ion-exchange membrane, composited with platinum by using a chemical processing technique that employs a platinum salt and appropriate reducing agents. In this case, they used silver as a bright-metal surface electrode layer with a typical thickness of approximately 1–2 um so that the surface resistance is significantly reduced to approximately 1 ohm/cm^2. It was shown that IPMC artificial muscles with silver (or copper) deposited as surface electrodes showed significantly improved actuation performance (roughly 10–20% higher force relative to that without silver layers). It is important to observe that the platinum particulate layer is buried a few microns deep (typically, 5– 10 um) within the IPMC surface and is highly dispersed (As shown in Figure 8)

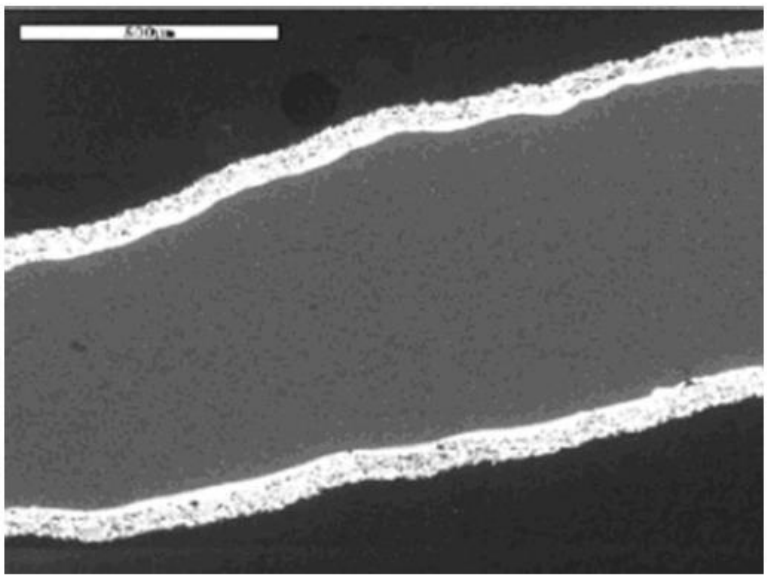

Figure 8. A cross section of an IPMC showing two electrodes (top and bottom) with porous expanded graphite and dense platinum[11].

Oguro's research proves that the platinum electrodes penetrating into the polymer resulted in a very large interfacial area between the polymer and the metal, which led to large capacitance of these

devices (1–5mF/cm^2) [11]. The more the number of electrode layers, the higher strain can be achieved. This experimental result was verified by physics-based modeling efforts that highlighted the role played by the double layer capacitance that forms at the interface of the electrode and the polymer [12].

After that more and more IPMCs actuators which are suitable for working in dry conditions have been developed; however, the high cost of the materials, their relatively low working density, as well as the considerable fatigue effects endured by the electrodes upon cycling, is limiting the performance of IPMCs-based actuators and hindering their implementation in mechatronic and robotic systems.

The most widely used electrode plating method for creating a stable bond between metal and ionic polymer is a chemical reduction process, in which the nanoparticles of a noble metal such as platinum are chemically reduced from its salt, and from a large interface at deposited up to the macromolecular network near the boundary of the polymer. Upon reduction of the salt solution by a reducing agent, nanoparticles are released within the macromolecular matrix of the membrane to form a metallic layer. The most common procedure for metal plating can be summarized as follows [4]: based on the water uptake properties of the ionic polymer, the surface of the polymer is roughened and then immersed in a platinum salt solution such as $Pt(NH_3)_4HCl$ for 24 h. The membrane is then rinsed in distilled water, hydrogen peroxide, and sulfuric acid to remove organic impurities. Next, the membrane is soaked in a proper reducing agent such as $NaBH_4$ to release the platinum nanoparticles. The reduced nanoparticles are trapped in the porous network of the polymer and form a conductive metallic layer up to the surface of the ionic polymer.

It could be concluded that the impregnation–reduction procedure may be repeated 3–5 times to allow the platinum nanoparticles to penetrate up to an optimum depth (10–30 μm) and form a porous cluster structure. The repetition of the procedure directly increases the density of the electrode layer and volume and improves the composite materials surface conductivity. A sheet resistance of 5–

20ohm/sq can be achieved using this method depending on the thickness of the platinum layer. Roughening of the ionic polymer surface by sand blasting has shown to facilitate the formation of fractal-like electrode structure inside the polymer membrane, enabling the formation of a larger surface area and larger capacitance in the electrode layer.

As described above, the key point to fabricate IPMC actuators is to make an interpenetrating metal layer inside of the actuator and highly elastically electrode on the surface; however, the manufacture process is time-consuming and complex and the electrode on the surface is relatively fragile to offer durability for actuating. Furthermore, high costs and complexiity of the manufacture process still constitutes the drawbacks in the design and the industrial production.

Physical metal loading has been proposed to hasten the actuators manufacture, at 1/10th of conventional method. The method consists of a direct physical loading of a conductive primary powder into the ionic polymer, forming a dispersed particulate layer[13]. However, this still requires the generation of a second layer of smaller secondary particles via chemical plating, similarly to the conventional methods.

Another improvement was the casting method, which is to mix the metal particles and the polymer in its liquid state with a solvent and then after stirring, sonication and a thermal treatment, to cast a polymer film, boiled in a hydrogen peroxide solution at a temperature between 75°C -100°C for 1 hour and then boiled in the distilled water for 1 hour, onto a substrate. The thermal treatment increases the mechanical stiffness of the cast Nafion® film by increasing the strength of the molecules' bonding structure. However, this method requires the delicate tuning of process variables such as temperature and concentration of a specific solvent, and demonstrated reproducibility problems[14].

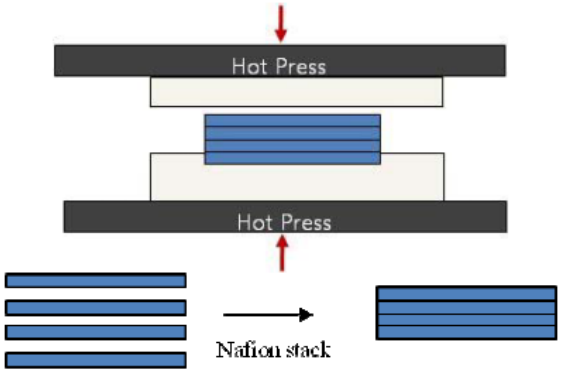

Figure 9. Fabrication of actuator by stacking and hot press[4].

Hot-pressing and electroless plating methods were also applied for fabricating the complete electrode of IPMC actuators. The hot-pressing method consists of using a hot-pressing system to make several thin Nafion® films adhere together, which enhances the bending stiffness, the force performance and the reproducibility (shown in Figure 9). However, the surface roughness of the produced electrode is not regular after hot-pressing. Although other techniques like hot-embossing and polymer coating were also used to increase the adhesion between the layers, the problem of high cost and complex procedures in manufacturing are still remaining[4].

Besides the adhesion problems between the polymer and the electrode during the IPMC fabrication, and the problems deriving from having a thick polymer/metal composite region, patterning electrodes with controlled geometry is extremely challenging. The possibility of patterning metal structure in the composites could enable the local drivability of the deformation, resulting in more complex and sophisticated actuating pathway [15].

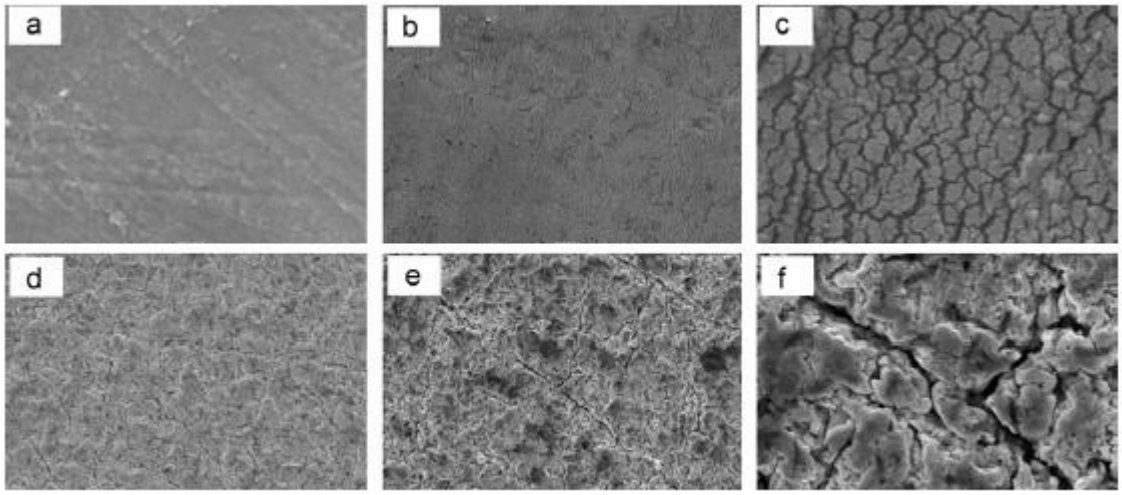

Figure 10. Surface SEM micrographs of IPMCs before and after actuation(100 cycles under 3 V, 0.1 Hz): (a) the C12 actuator before actuation, (b) the C12 actuator after actuation,(c) the magnified image of (b), (d) a conventional IPMC before actuation, (e) a conventional IPMC after actuation, and (f) the magnified image of (e)[16].

To overcome this problem, many methods used for improving the adhesive ability of electrodes are also applied for fabricating the electrodes on the surface. Among them, sputtering became a promising method for electrodes long term operation. For example, Pandita's group proves that by using the gold sputtering method, the electrodes could experience a long term performance without significant fatigue, which proves a promising method of fabrication(Figure 10)[16].

As described by Pandita's group, the gold sputtering Nafion-IPMCs actuator showed different loss of electrical conductivity with respect to the conventional Nafion–IPMC fabricated via electroless plating of Pt in view of the failure of metal electrode after actuation. Figure.10 shows the surface SEM morphologies of their respective electrodes before and after actuation (100 cycles under 3 V, 0.1 Hz). In both cases of the gold sputtering and conventional IPMC, fractured electrode surfaces were observed after the severe oscillational actuation. However, there was a large difference in morphology. The outermost Au layer on the Nafion-IPMC was comminuted fractured in the submicron scale, while the fracture of the Pt surface on the conventional IPMCs developed roughly with a wavelength of ca.

10 μm. This is mainly attributed to different deposition processes for fabricating the IPMCs actuators. With the difference in morphology of the electrode failure, the deviation of surface resistances before and after actuation was much lower for the gold sputtered IPMCs actuator than for the conventional IPMCs actuator, i.e. 81% and 168% for the gold sputtered IPMC and conventional IPMCs, respectively. This result also suggested that the Au layer is helpful to maintain the electrode performance.

Although the feature of smooth electrode surface from gold sputtering led to improved durability of the electrode, as compared to a conventional Nafion–IPMC with noble metal electrodes, and that the fabrication method of the electrode enabled IPMC actuators to be fabricated in large scales with batch-to-batch reproducibility, the method still could neither offer large surface area for ions storage, nor a durable performance for a long term application of the actuators (only hundred actuation cycles). So, similarly to other electrodes fabrication methods, the sputtering improved the adhesive ability between the polymer and the electrodes, but did not provide an actual interpenetrating composite region as in the classic electroplating framework.

5.1.2 Carbon-polymer-Composites (CPCs)

Carbonaceous materials, like functionalized carbon nanotubes and doped graphene, were introduced as an alternative to noble metals for the production of chemically modified porous electrodes with higher flexibility. In this framework, layer-by-layer fabrication techniques were used for the manufacturing of a new class of composites based on ion-permeable electrolytes, such as polyvinylidene difluoride (PVDF) and PSS, able to generate large strains when electrically stimulated (bucky-gels).

The principle of such design of actuator is based on the discovery of the specific interactions

between CNTs(carbon nanotubes) and the imidazolium ions of the ionic liquid enabling to the forming of bucky gel, which firstly proved the fabrication of dye-sensitized solar cells by using [Emim] [Tf2N] (1-ethyl-3-methylimidazolium bis(trifluoromethylsulfonyl)imide) gels as electrolytes containing MWNTs (Multi-wall nanotubes) and SWNTs (Single wall nanotubes). They showed two main electrochemical properties: a) higher double layer capacitance and a smaller internal electrode resistance, b) higher energy conversion efficiencies. Watanabe's group found out that bucky gels could be used as a component for electric double-layer capacitors (EDLCs)[17]. In that experiment, bucky gel based EDLCs were highly performing energy storage devices and they could accumulate electric charges at the interface between a polarizable electrode and suitable electrolyte. In a constant current mode, an [Emim] [Tf2N]/SWNTs gel, sandwiched by metal electrodes with a separator, showed charging and discharging properties in response to an applied voltage. The capacitance (Ca) of such capacitors could attain around (7 mF/cm^2), which is greater than that fabricated with activated carbon and the same ionic liquid (5.5 mF/cm^2). In the meantime, the gravimetric capacitance (Cw) of the former is lower than that of the latter. Furthermore, as the key step of preparing a bucky gel, the ground process is fundamental; comparing with an unground mixture of SWNTs and [Emim][Tf2N], the capacitance of the resultant EDLC is lower by approximately 30% than that with the corresponding bucky gel containing grounded SWNTs. Moreover, the bucky-gel-based EDLC also displays a smaller internal electrode resistance than others, proving the material important role in offering high capacitance.

Bucky gel based electrolyte has other significantly improved the energy conversion efficiency, comparing with the electrolyte using a bare ionic liquid. For example, Usui's group dispersed different nanoparticles, like carbon nanotubes, carbon fibers, carbon nanoparticles and TiO2 nanoparticles, individually into a solar cells' ionic liquid electrolyte (EMIM-TFSI), and observed that viscosity and conductivity of the ionic nanocomposite gel electrolyte increased[18]. The energy conversion efficiency

of solar cells prepared using them improved from 4.21% for the bare ionic electrolytes to 5% at the maximum value for the electrolyte containing well-dispersed carbon nanotubes.

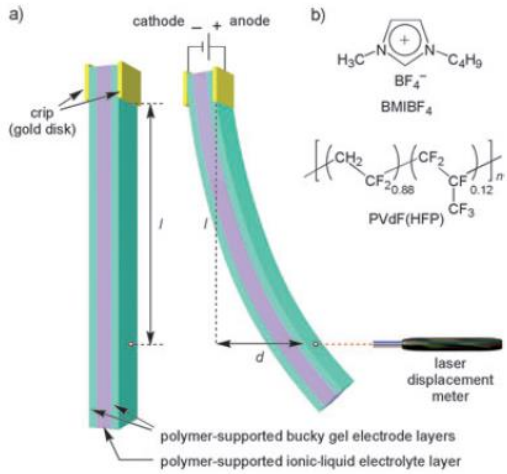

Figure 11. Schematic structure of the actuator strip composed of a polymer-supported ionic-liquid electrolyte layer sandwiched by bucky-gel electrode layers, and experimental setup for cantilever oscillation [19].

Due to this excellent properties of increasing the capacitance of electrolyte and high energy conversion efficiency, the bucky gels were also introduced to produce electro-active actuators. An example of the typical bucky gel based actuator is the one made by Fukushima's group, which operated by the conversion of electrical energy into mechanical energy[19]. Their actuator adopted a bimorph configuration with a polymer-supported internal ionic liquid electrolyte layer sandwiched by bucky-gel electrode layers, which allows quick and long-lived operation in air at low applied voltages (shown in Figure 11).

This bucky gel-based actuator can readily be fabricated through layer-by-layer casting of electrode and electrolyte components in a gelatinous 4-methyl-2-pentanone solution of a vinylidene difluoride-hexafluoropropylene copolymer (PVdF (HFP)). Typically, the electrode layers are composed of SWNTs (13 wt%), [BMIM] [BF4] (1-Butyl-3-methylimidazolium tetrafluoroborate) (54 wt%), and

PVdF- [BMIM] [BF4](33 wt%), while the electrolyte layer includes (67 wt%) and PVdF (HFP) (33 wt%). When an electric potential of 3.5 V is applied with a frequency of 0.01 Hz, the actuator strip undergoes a bending motion toward the anode side with a maximum displacement of 5 mm. The strain and stress, generated in the bucky-gel electrode layer, are 0.9% and 0.1mPa, respectively. The actuation takes place quickly in response to an applied alternating voltage of 3.0 V even at a frequency of 30 Hz. Moreover, the bending motion (2.0 V, 0.1 Hz) can be repeated for at least 8000 cycles in air without a notable decay (20%).

Another typical example was the first bucky gel based paper actuator made by Baughman's group[20]. They fabricated the first carbon nanotube based electromechanical actuator papers that to generate higher stresses than natural muscle (sustainable stress 0.1 MPa, Maximum 0.35MPa) and higher strains than high-modulus ferroelectrics[21]. The bucky-paper-based actuator operates by a dimensional change of SWNTs in the covalently bonded directions, due to quantum chemical and double-layer electrostatic effects caused by a charge injection into SWNTs. It proved that a volume change of the electrode layers, arising from an interlayer ion transport feature, contributes to the bending motion.

Because of its excellent performance and better mechanical properties (flexibility), bucky gel based actuator became promising materials. However, the high cost and potentially complex manufacture process hinders its applicability. Due to the necessity of fabricating the thin layer of bucky gel-based electrode, the hot-pressing and layer by layer fabrication procedures to bind the SWNTs electrode composite layer with intermediate ionic electroactive polymer layer makes the mass production of this system more complicated and difficult, able to increase the cost of fabrication, similarly, to some extent, to the IPMCs formations.

5.2 Other state-of-the-art electro-active actuators

5.2.1 Hierarchical Porous polymers as the actuators

The most important requirement in determining the deformation of ionic polymer based actuators are large displacements in bending motion, fast switching response, low operating voltage, and durable operation in air. Current ionic polymer actuators are yet lacking all of these requirements together, mainly because of the slow actuation response and drastically reduced displacements under low-voltage operation. Many Scientists employed self-assembled block copolymers in actuators and improved electromechanical deformation, compared with that of several conventional polymers lacking active organization for ion transport[22]. However, in particular, there has been no substantial progress in lowering the operation voltage of the actuators. This implied that the nanoscale ionic channels in the polymer layer created by a sacrificial copolymer approach, influences the switching response and the role of self-assembled polymer electrolytes is predominantly necessary to identify a specific bending motion of the actuators.

Kim's group introduced one hierarchical porous polymer to increase the actuator performance (Figure 12). In their study, they introduced a new ionic polymer actuator comprising nanostructured sulphonated block copolymers and ionic liquids with a tailored degree of ionic interaction. This polymer showed architecture of self-assembly hierarchical porous channels at the nanoscale and it exhibited an important actuator performance than the previously reported ionic polymer actuators. These characteristics are intimately related to the fast and organized ion motion along the well-connected ionic channels within the self-assembled polymer layer. The new actuator developed is capable of millimeter-scale displacements in a sub-1-V actuation region, which is a great achievement in the polymer actuators performance.

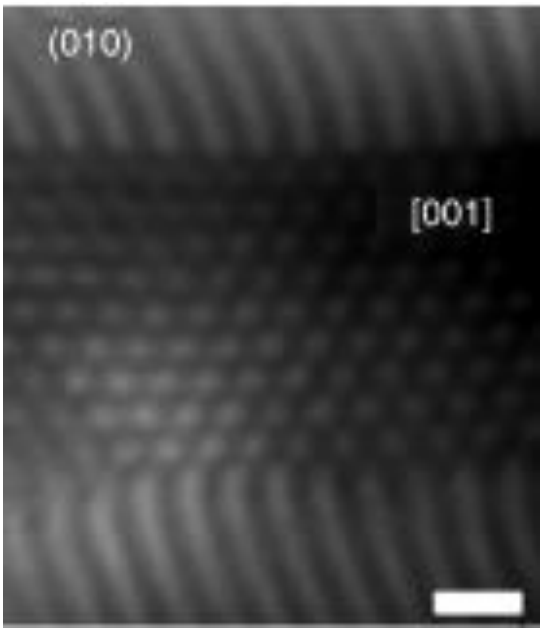

Figure 12. the (010) plane and the [001] view of the HEX (hexagonal-cylindrical) structure. Scale bar, 100 nm; the PSS phases were darkened by RuO_4 staining[23].

The proposed actuation mechanism for this actuators comprising nanostructured block copolymers and an ionic liquid is (illustrated schematically in Figure 13) is described as follows: when a voltage is applied between the two electrodes, the fast electromechanical deformation of the actuator was driven by the rapid creation of dimensional gradients of ionic liquid within the polymer layer, which was responsible for their fast sub-1-V switching response. The bending motion of the actuators was then triggered by the electric charging and discharging at the SWCNTs(single wall carbon nanotubes) electrodes, with non-detectable back relaxation behaviors. The expansion and shrinkage of the electrodes as a result of ion migration are omitted in the drawing for clarity. From the XPS characterization, it was unveiled that the unique internal structure of the polymer layer was found to be unchanged during the actuation. Furthermore, due to the relatively high glass transition temperature (Tg) of the PSS-b- PMB block copolymers containing ionic liquids, ca. 60℃ which slows

down the self-relaxation of ions in the absence of external stimuli, the actuator shows no significantly back-relaxation in the performance. However, the production of such actuator is still requiring the hot pressing method and could not be normalized for mass production.

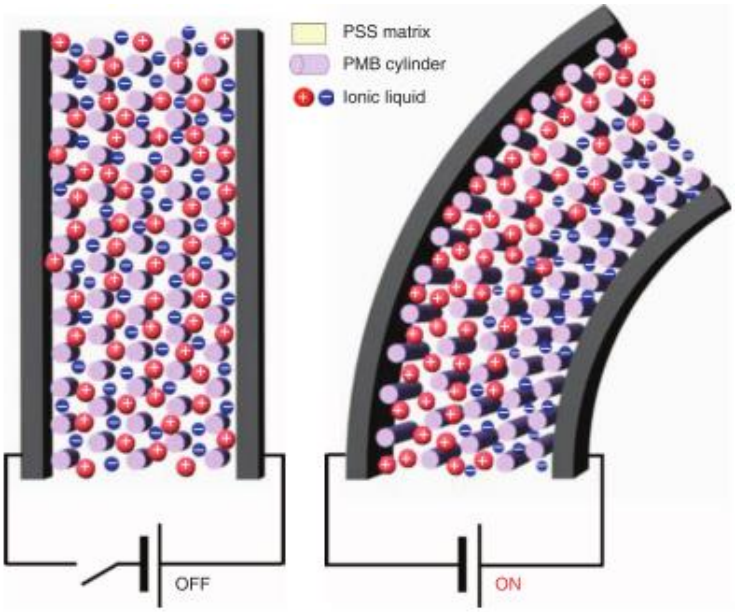

Figure 13. Actuation mechanism in our actuator. Schematic illustration of the internal structure of the actuator as a result of actuation. The creation of dimensional gradients within the polymer layer was responsible for the fast and efficient electromechanical deformation of the actuator[23].

5.2.2 High capacitance polymers as the actuators

Another type of the ionic liquid actuator based on high capacitance electrodes were supercapacitors. Due to the fact that ionic liquid based electrochemical actuators are composed of a layer of polymer electrolyte sandwiched between electrodes, the strain generation depends on their ability to store electrical energy in a double interface and convert it into mechanical output by reversible ion intercalation and deintercalation of electrodes. The electrodes materials, including nature low-dimensional carbon materials with porous networks, large specific surface areas (SSAs) and high electrical conductivity, is of crucial important for high-performance electrochemical–mechanical

behaviors. Wu's group designed a graphitic carbon nitride nanosheet electrode-based ionic actuator that displays high electrochemical activity and electromechanical conversion abilities, including large specific capacitance (259.4 F/g) with ionic liquid as the liquid swollen electrolyte, fast actuation response (0.5±0.03% in 300ms), large electromechanical strain (0.93±0.03%) and high actuation stability (100,000 cycles) under 3V[24].

In their work, based on the physicochemical effects caused by nitrogen doping, an ionic actuator based on a hierarchically porous graphitic carbon nitride (g-CN) nanosheet electrode has been fabricated. To enhance the structural stability of the electrodes, a small portion of CNTs was added to the g-CN network. To provide sufficient ions for rapid migration, an interpenetrating polymer network based on poly(ethylene oxide) and nitrile butadiene rubber (PEO-NBR) was introduced, which has proven to be a promising electrolyte layer with high ion uptake, ionic conductivity and ion transportation(Figure 14). The improvement of the electromechanical motion was attributed to the N-active site, that increases the charge density as well as enhances the binding interaction with cations and the hierarchical porosity structure with dominant size <2 nm, which has a leading effect on the electrode volume expansion.

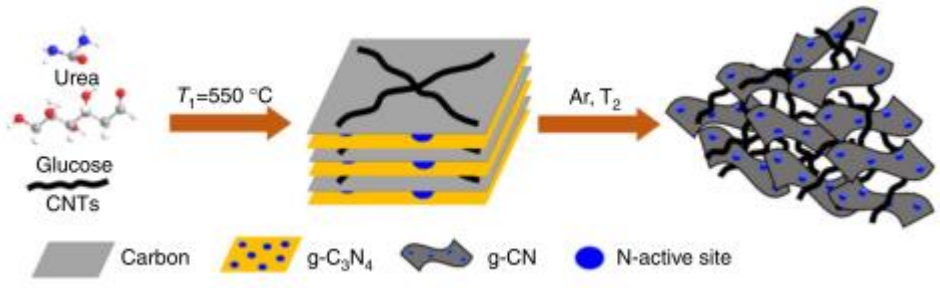

Figure 14. Illustration of the preparation of the g-CN materials[24].

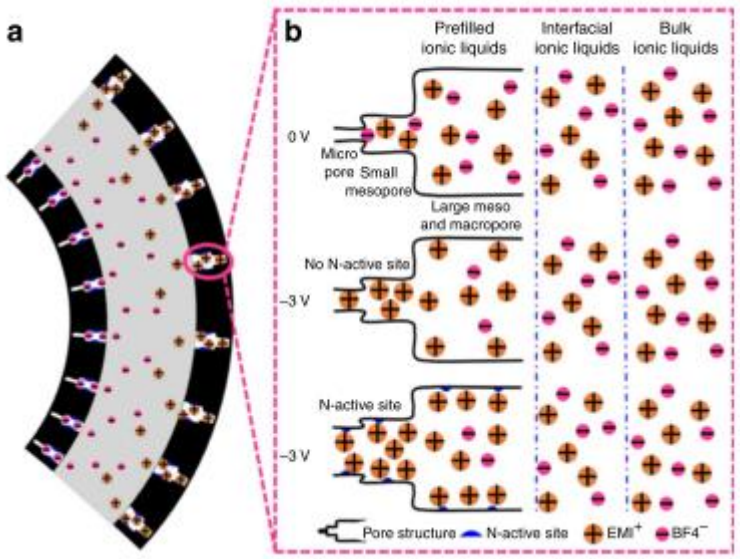

Figure 15. Scheme of bending motion of g-CN actuator (a) Bending motion of the g-CN actuator. (b) Schematic illustration of the pore structure and cation-induced mechanical output of the g-CN actuator[24].

As seen from Figure 15, the actuation mechanism for the g-CN-based actuator on the experiment as follows: For carbon electrode-based actuators, when a voltage was applied between the electrode layers, the ions were intercalated into porous electrodes and the volume of electrodes expanded because of the pressure generated inside them. Because the cations were bigger than the anions, the actuation showed a bending motion resulting from different extent of swelling. A voltage-induced pressure was generated in terms of the balance between the electrostatic and volume exclusion interactions, which were greatly varied along with the pore distribution. When the pore size became smaller, the electrostatic interaction became stronger because the distance between the ion and the electrodes became shorter (several nanometers), whereas the volume exclusion interaction became more significant because the space available for ions became smaller and the number of ions in the pore decreased. The voltage-induced pressure in the pore distribution caused deformation of the carbon electrode-based actuators. For pore sizes larger than 4 nm, the pressure inside of the porous electrode was virtually the same as in the bulk electrolyte. However, with pore widths <4 nm, there

were marked changes of pressure because the effect of the electrostatic interaction was relatively larger than the volume exclusion interaction, indicating that the pores below 4 nm played a fundamental role in the electrode volume change. Therefore, considering the porous structural characteristics of this new materials (see Figure.15b), they utilized the hierarchically porous model (see Figure.15) of a macropore sleeve with meso- and micropores to analyse the mechanism of how the charge storage was converted into mechanical motion. As shown in Figure. 15a, when an electric field was applied on the actuator, the ion was intercalated into the porous structure of the electrode, resulting in a bending motion of the actuator. In this actuators, three types of ionic liquids (ILs), prefilled ILs, interfacial ILs and bulk ILs, played different roles in the contribution of mechanical motion (see Figure.15b). After an electric field was applied to the actuator, the prefilled ion could quickly intercalate into the micro- and small mesopores, and the pore volume expanded, which resulted in a rapidly increasing displacement (300 ms) and diffusion of ions from the electrode–electrolyte interface or PEO-NBR polymer afterwards. When doping nitrogen in carbon materials, the manipulated local electronic structure (N-active site) increased the charge density and enhanced its binding interaction with cations, which accommodated more cations in pores, and the electrode volume expansion was further increased. Furthermore, all pores contribute to capacitance, but only those pores below 4 nm played a role in the electrode volume expansion. g-CN_{800} they produced has considerably more micropores (<2nm), and these pores were closer to the ion sizes, making them more suitable for large volume expansion of the actuator. Therefore, the hierarchically pore structure and N-active site in the actuator displayed a higher actuation performance.

Although this actuator has achieved better performance than normal actuator, the layer by layer manufacture process along with high cost of multi-materials and time-consuming fabrication makes this manufacture approach not easy for a convenient scale-up.

5.3 The new ionic electroactive polymer actuator

Although as described above, the families of IPMCs and bucky-gels consist of highly flexible and light-weight polymeric composite actuators exhibiting good electromechanical performance and they both play an important role in many scientific and technological areas, including microelectromechanical systems, soft robotics and biotechnology, the main drawbacks of both IPMCs and bucky gel based actuators is that their performance is strongly relying on the role of thick layers of the electrode material, interpenetrating with the polymeric basis, which renders the fabrication procedures of such systems time-consuming and rather complex. More specifically, the penetration depth of the metal electrodes into the polymeric substrate and the thickness of the carbon-based electrode layers range from few um up to 30 um, thus covering a significant portion of the overall actuator thickness, which typically ranges from 25 μm to about 100 μm. The presence of such an extended composite region leads to high electrochemical capacitance values (up to hundreds of F/g for bucky-gels), that guarantee an effective ion storage to trigger the bending actuation. However, it also implies a large Young's modulus mismatch between the polymeric basis (from fractions to hundreds of MPa) and the material composing the electrodes (from tenths to hundreds of GPa). The mechanical coupling between layers of different stiffness, but comparable length scales, constitutes the main cause of the electrodes cracking and delamination during actuation, therefore limiting the lifetime of the systems.

In this case, I designed one soft actuator which could perform a long term actuation and be ease for mass production. In the present thesis work the synthesis, fabrication and characterization of a novel family of IGMNs based on ionic conductive PAA-co-PAN network with embedded HNC by mean

of SCBI is presented. The production of cluster-assembled gold thin films (100 nm thick), inter-penetrating with the quasi-solid state electrolyte, enabled the manufacturing of elastic soft actuators provided with flexible electrodes having low surface electric resistance and large surface area for an effective charge storage. The electro-responsive properties of the materials are intermediate between that of IPMCs and bucky-gels. This feature is due to the synergistic effect of the quaternary ammonium TEA^+ counter-ion and HNC on the transport ability and electrochemical characteristics of the functional nanocomposites. Both the organic cation and the inorganic nanostructures confer high ionic conductivity (0.35 mS/cm) and large double layer capacitance (30 uF/cm2) to the composites, by favoring the partial dissociation of the ionic liquid incorporated in the structure (solvent molar uptake is 37%). The materials showed sensitivity to the applied electric field starting at 0.1 V and exhibited high-performance actuation in response to electrical stimuli at low voltages (up to 1.04% net strain at 5 V) and good durability in their frequency response (up to 76000 cycles at 2 V and 1 Hz). The manufacturing process adopted for the actuators fabrication is cost-effective and suitable for mass production production scale up. The novel IGMNs presented here represent a forefront technological solution for the development of smart flexible components suitable for the manufacturing of soft bio-mimetic robots, deformable electronic and haptic systems, and wearable biomedical devices.

6.Materials and Methods

6.1 Ionic gel fabrication and characterization

6.1.1 Materials

The ionic gel samples were manufactured as thin layers of different thickness (100 µm, 150 µm and 350 µm), using a one-pot synthesis, by mean of a free-radical UV photo-cross-linking reaction and a simple molding process. The macromolecular PAA-co-PAN network is cross-linked using EGDMA and has the ability to absorb and retain a high amount of 1-Ethyl-3-methylimidazolium tetrafluoroborate (EmimBF4) ionic liquid, that operate as the transport medium for the migration of the TEA+ cation through the polymer sieve-like structure when an electric field is applied. The solvent uptake of the material i.e. the molar ratio of the ionic liquid with respect to the AA monomer is EmimBF4 : AA = 37% mol/mol, while the TEA+ cation concentration is 0.17 mM. EmimBF4 has been widely used for the production of electroactive ionomeric actuators and quasi-solid-state electrolytes, due to its relatively low viscosity (about 151.7 cp at room temperature) and large electrochemical window (around 4.2 V), while TEA^+ has already been employed as the active charge carrier specie in high-displacement IPMCs membranes. The PAA carboxyl groups, covalently bonded to the main backbone, offers fixed anionic sites for the TEA^+ cations coordination, while PAN was introduced to confer rubbery properties to the polymer matrix. The ratio between AA and AN was set as 8 : 2 (mol/mol). HNC with high ionic exchange capability are embedded in the electrolyte to both increase its ionic conductivity and to operate as a reinforcement for the polymer. The ion capturing ability of the HNC has already been demonstrated and reported in the literature. These tubular nanostructures consist of a rolled up stacking of tetrahedral SiO_4 and octahedral AlO_6 sheets, and present surface siloxanes groups exposed at the outer surface (negatively charged) and aluminum hydroxide pendants in the inner lumen (positively charged).

When dispersed in solution, the zeta potential of both inner and outer surfaces can be tuned by controlling a number of factors, including pH, ionic strength and ionic medium type. Due to their unique surface chemistry features, HNC have been used for the controlled adsorption and intercalation of ionic liquids and various liquid phase electrolytes. HNC were included in the PAA-co-PAN network at a fixed ratio of 5% (w/w) with respect to AA.

All chemicals were purchased from Sigma Aldrich, except the EmimBF4 ionic liquid, which was purchased from Io-li-Tec. The one-pot synthesis was carried out at room temperature, mixing the reagents in a 4 ml glass test tube.

The chemical structure of the compounds for the synthesis of the ionic gel is shown from Figure 16 to Figure 22.

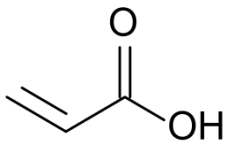

Figure 16. The chemical structure of acrylic acid (AA).

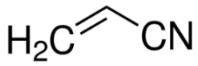

Figure 17. The chemical structure of acrylonitrile (AN).

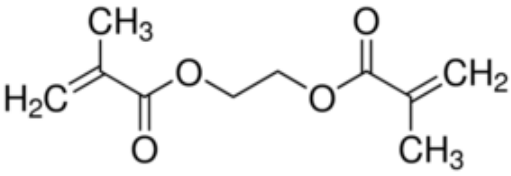

Figure 18. The chemical structure of Ethylene glycol dimethacrylate (EGDMA).

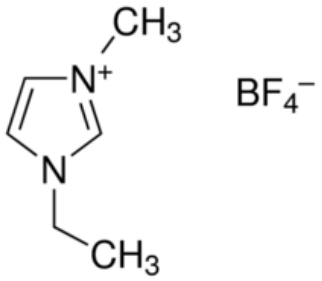

Figure 19. The chemical structure of 1-Ethyl-3-methylimidazolium tetrafluoroborate (EMIM.BF4).

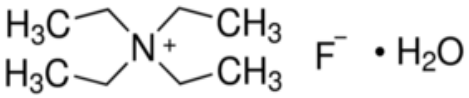

Figure 20. The chemical structure of Tetraethylammonium fluoride hydrate (TEAF).

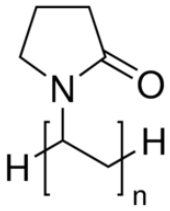

Figure 21. The chemical structure of Poly (vinylpyrrolidone) (PVP).

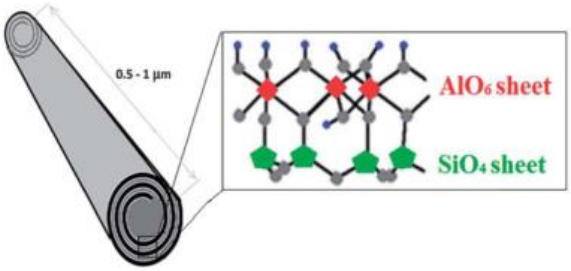

Figure 22. Schematic representation of the halloysite nanoclays (HNC) structure and wall chemistry[25].

6.1.2 Ionic gel synthesis and manufacturing

The synthesis scheme of the ionic gel network is reported in Figure 23.

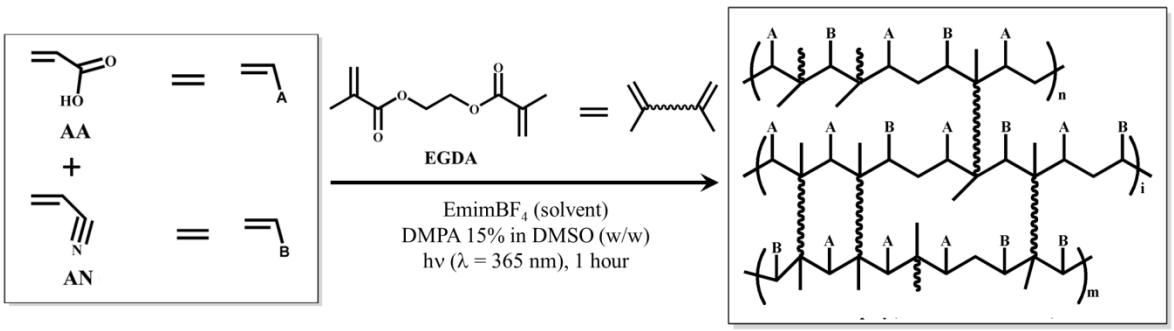

Figure 23. the scheme of synthesis of iongel.

More in details, 547.5 µl of AA were mixed with 130 µl of AN and subsequently added in a 650 µl solution containing EmimBF4 and H2O (EmimBF4 : H2O = 7 : 3 v/v), in which 26 mg of TEAF were previously dissolved under stirring for 3 hours. Then, EGDMA (19 µl) was added in the solution. After manually stirring the tube for 10 minutes, 30 mg of HNC were dispersed in the mixture. Poly (vinyl pyrrolidone) (PVP) was used to facilitate the dispersion of the nanostructures (100 mg). The solution was then stirred overnight at 900 rpm using a magnetic stirrer. The resulting mixture was a viscous opaque liquid with a milky color. After stirring, the initiator was added to the test tube. 30 µl of a dimethyl sulfoxide solution containing 2,2-Dimethoxy-2-phenylacetophenone (0.15 w/w) was added to the test tube. The polymerizing solution was then vigorously stirred and injected in a silicone frame, positioned on a glass slide (2 mm thick). A second glass layer was used as a lid to spread the liquid into the frame and after the molding system was clamped, the apparatus was exposed to UV light for 1 hour. The equipment used to induce the photo-cross-linking was a UVLS-24 EL series (UVP) lamp, endowed with a 4 W light bulb. After polymerization, the formed ionic gel film was peeled off the glass, fixed into a 3D printed poly lactic acid (PLA) frame, and positioned into a dryer overnight to remove water residuals. A schematic of the molding procedure and a picture of a framed ionic gel sample is reported in Figure 24.

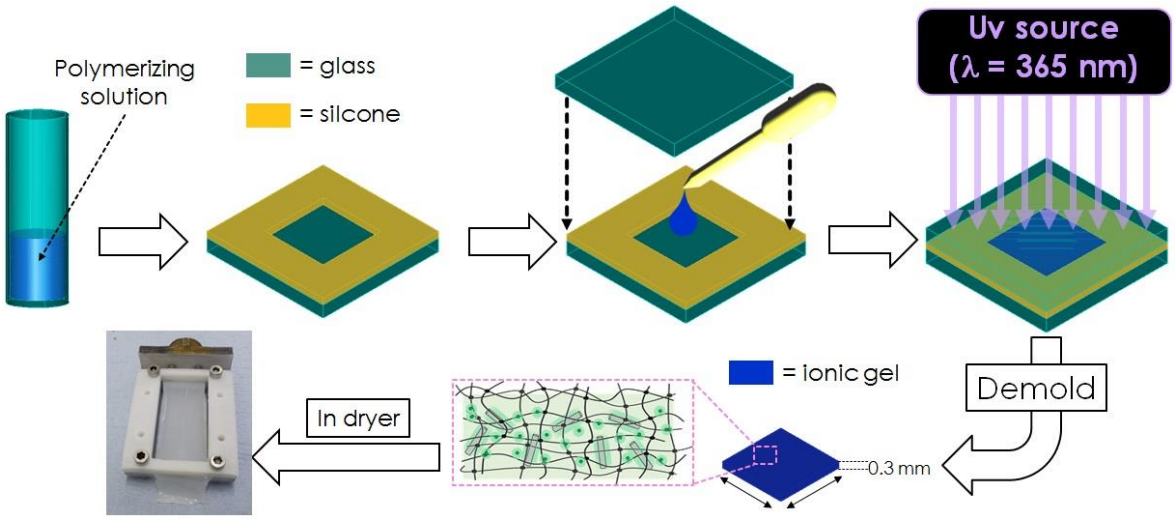

Figure 24. Schematic of the ionic gels manufacturing procedure.

6.1.2 Optical microscopy

To examine the surface morphology of the ionic gel, optical microscopy was carried out on the produced samples and special attention was paid to analyze the heterogeneity of the membrane as well as the smoothness of the surface before the electrode fabrication.

6.1.3 FT-IR

The chemical structure of the ionic gel membranes was characterized by IR attenuated total reflectance spectroscopy (ATR). The equipment used was an Agilent Cary 660 MIR system. For this testing, ionic liquid-swollen films approximately 2 X 5 cm were pressed against a thallium bromoiodide crystal (KRS-5) with 45º beveled ends using a thumbscrew pressure plate assembly. Before testing of the films, a scan of the background emissivity of the ATR system was performed. This standard emissivity was used as a baseline against which the absorbance of each sample was measured. The sample chamber was kept in dry air during the testing in order to reduce the effect of moisture and

CO_2 interference on the results. Then the samples were recorded at room temperature using this FT-IR spectrometer which yielded clean spectra for the ionic liquid-swollen films over a range of wavenumbers from 400 cm^{-1} to 4000 cm^{-1}. The crystal was carefully cleaned by using methyl-ethyl ketone (MEK).

6.1.4 Mechanical testing

To understand the mechanical properties of the iongel membrane, the tensile tests were conducted on ionic gel samples fabricated as dog bones, molded using a procedure similar to the one reported before. The dimensions of the specimens were set according to the standard ISO-527. The equipment used for the Young's modulus determination was a 50 N load cell (Suter, FH 50) fixed in a motorized vertical stand (Sauter, TVN-M). The strain rate was set as 1 mm/s. The applied load was registered as a function of time and subsequently converted into stress according to the samples cross-section. Three samples were measured and the results were then averaged to get the stress-strain curve which was fitted in the linear region (10% strain) in order to obtain the Young's modulus of the material.

6.1.5 XPS

To get insights on the $EmimBF_4$ interaction with the nanostructured silicates, we used XPS on pure HNC powders and on HNC precipitates, recovered after being soaked under stirring overnight in pure $EmimBF_4$ and in a 0.17 mM ionic liquid solution containing the quaternary ammonium cation (HNC are 20% in weight with respect to the ionic liquid).

The samples were characterized in a UHV apparatus (Leybold LHS 10/12) equipped with a

hemispherical electron analyzer and conventional X-ray source (Mg K = 1253.6 eV) operated at 10 kV and 25 mA. The high resolution spectra were acquired in constant pass-energy mode Ep= 30 eV. The overall energy resolution was 0.9 eV. The pressure in the experimental chamber during experiments was below 5 X 10^{-9} mbar. The binding energy scale is calibrated via the Au 4f5/2 core level line (located at 88.5 eV) of a clean polycrystalline Au sample. Charging effects on the samples under investigation were observed during the measurements. The spectra were aligned to adventitious carbon peak placed at 285.0 eV and then accordingly shifted. The line shapes were fitted with mixed singlets of a linear combination of a Gaussian and a Lorentzian profiles sited on a Shirley background. The Si 2p signals were gently smoothed for making the profiles more readable.

6.1.6 XRD

To understand the interaction between the TEA+ slat, ionic liquid and HNC, pure and treated HNC, prepared as described in the previous section, were analyzed using an Oxford X'Calibur X-ray diffractometer. Samples were loaded into 0.5 mm diameter glass capillaries, and diffraction was collected in transmission geometry with a CCD detector. The molybdenum X-ray source provides a wavelength of 0.710 Å.

6.2 IGMN fabrication and characterization

6.2.1 SCBI (Supersonic cluster beam implantation)

As previously demonstrated by the CIMIANA's group, neutral metallic nanoparticles produced in the gas phase and aerodynamically accelerated in a supersonic expansion can be implanted in a

polymeric substrate to form a conductive nanocomposite with superior resilience and outstanding structural and functional properties. More in details, SCBI is based on the use of a highly collimated supersonic beam carrying metallic clusters. Even if the kinetic energy is significantly lower than in ion implantation, neutral clusters are able to penetrate up to tens of nanometers into the polymeric target due to their inertia, therefore forming a conducting nanocomposite and avoiding electrical charging and carbonization. This straightforward approach for metallization (e.g.with Au, Ag, Pt, Pd) of functional soft materials shows huge potential despite conventional techniques, such as ion-gun sputtering or metal vapor deposition (MVD), which promotes a weak surface adhesion of the metallic layers on the polymers, thus favoring a subsequent delamination of the conducting layers even at very low deformations[26].

A schematic of a typical apparatus for the fabrication process is reported in Figure 25.

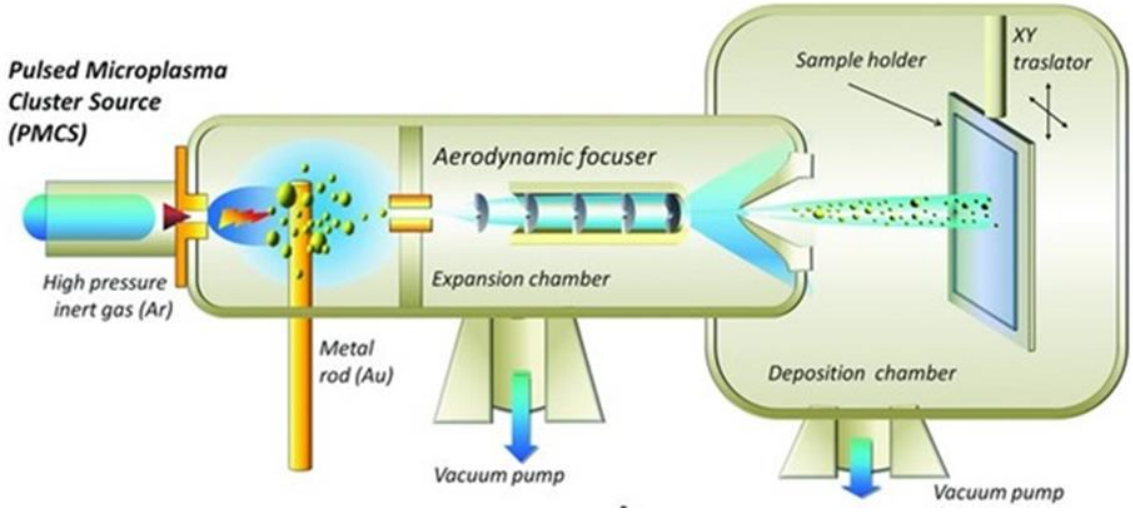

Figure 25. the scheme of a typical apparatus employed for (SCBI).

The cluster source (Pulsed Microplasma Cluster Source, PMCS) consists of a ceramic body with a cavity in which a solid Au target (purity 99.9%) is vaporized by a localized electrical discharge ignited during the injection of a pulse of inert gas (He or Ar) at high pressure (40 bars). The metal atoms, sputtered from the target, aggregate in the source cavity to form metal clusters; the mixture of clusters

and inert gas expands subsequently through a nozzle forming a supersonic beam into an expansion chamber kept at 10^{-6} mbars. Electrically neutral nanoparticles exiting the PMCS are aerodynamically accelerated in a highly collimated beam with divergence lower than 1° and with a kinetic energy typically of 0.5 eV/atom. The central part of the supersonic cluster beam enters, through a skimmer, a second vacuum chamber (implantation chamber) where the beam is intercepted by the polymeric substrate. Ionic gel samples are mounted into the SCBI apparatus sample holder being hold in the PLA frame reported. The custom-made setup for the metallization was as follows. The polymeric substrate is fixed in a motorized frame. During implantation the sample holder is continuously moved in the vertical direction with respect to the cluster beam, in order for the nanoparticles to homogeneously cover the entire surface of the ionic gel and to intercept the sensor of a microbalance, which is used to monitor in real time the amount of gold implanted. Once the target amount is obtained, corresponding to an overall film thickness of approximately 100 nm, the motorized frame undergoes a 180° rotation and the opposite side of the polymer is processed. After the manufacturing, IGMN actuators are cut into strips (30 mm in length and 2.5 mm in width).

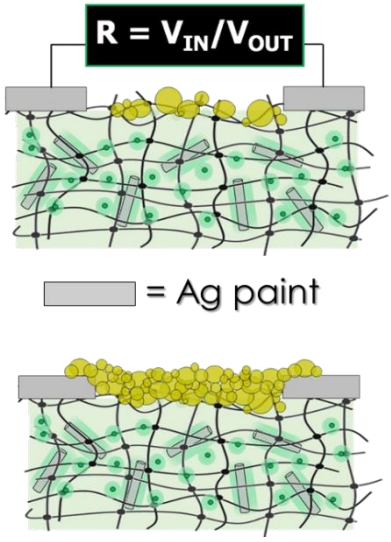

Figure 26. Schematic of the type of sample employed to monitor the electric characteristic of the IGMN as the implantation is carried out.

The electrical properties of the IGMNs were monitored during the SCBI process. An acetate

stencil mask was used to define the geometry of the regions to be implanted into the ionic gel, while Ag electrical contact were previously painted on the polymer using a silicone pencil and a conductive silver paste (SCP, Electrolube). Then, a strip of 2 x 5 mm^2 of gold clusters was implanted between the Ag electrodes, partially covering their surface area. During this process, the resistance between the electrodes is acquired using a multimeter. A scheme of the sample setup for the electrical resistance measurements during SCBI is reported in Figure 26.

6.2.2 Electro-chemical characterization

Electrochemical impedance spectroscopy (EIS) measures the frequency-dependent complex impedance of an electrochemical cell as a function of an applied electrical potential.

One of the aim EIS is to investigate on the boundaries properties of a system of electrodes in contact with an electrolyte. For electro-active actuators, having a chemical inert electrode desirable; in fact, the faradic charge transfer of the active ionic specie at the metal layer (via oxidation and reduction processes) could induce a consumption of the electrodes. Due to their cluster-assembled nature, the electrodes fabricated using SCBI are expected to behave as double layer capacitance with respect to the quasi-solid state electrolyte.

In this work, EIS, has been selected as the method to examine whether the actuators electrodes can be considered as double layer capacitors and to quantitatively measure the electrochemical capacitance and ionic resistance of the system.

In the experiment, all measurements were performed at room temperature, using a Gamry reference 600 potentiostat in a two electrodes configuration. During the experiments, IGMN were positioned in a custom-made aluminum Faraday cage. For the electrochemical impedance

spectroscopy assay, the voltage amplitude was set as (6.4 ± 0.1) mV, while the frequency sweep was from 100 kHz to 0.1 Hz. Cyclic voltammetry was also carried out for the standard ionic gel formulation, using a scan rate of 10 mV/s in a voltage range going from -4 V to +4 V.

6.2.3 Electro-mechanical actuation

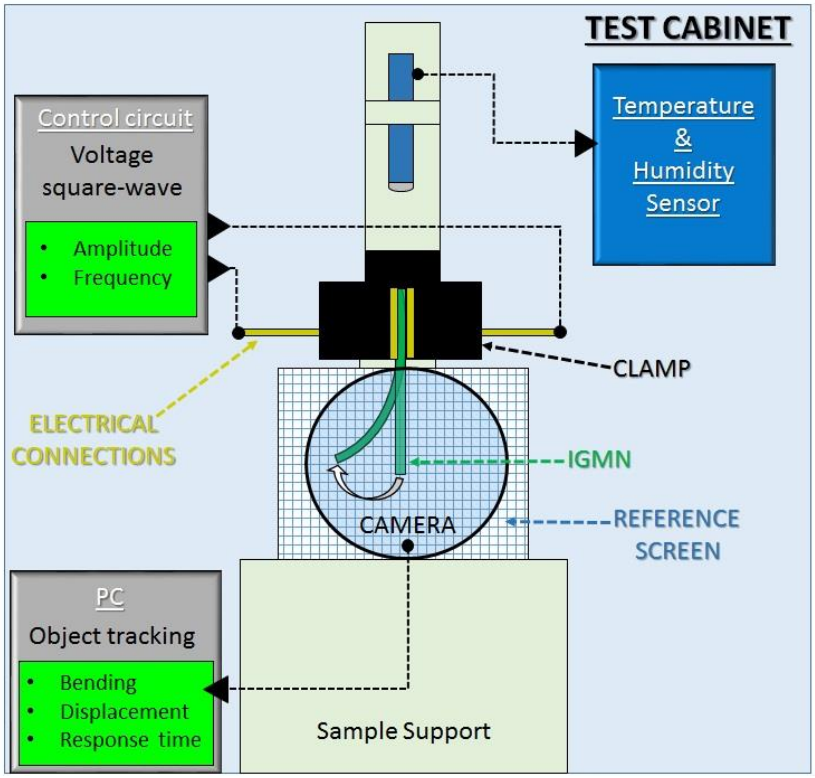

Figure 27. The scheme of electro-mechanical actuation test of IGMN actuator.

The setup employed for the electro-mechanical characterization of the actuators is shown in Figure 27. IGMNs were clamped between two PDMS layers (2 mm thick), having paper sheets metallized with gold glued to one side, in order to operate as the electrical contacts. The Au film (200 nm thick) was fabricated using physical vapor deposition. The equipment used for the metallization was an Edwards Coating System (model E306A). After positioning the cantilever (free length was 25 mm) into a

dedicated support, a custom-made electronic circuit interfacing a power supply (EA-PS 2342-10 B) and a wave function generator (Thandar TG503) was wired to the Au contacts, in order to provide the electrical stimulus to the IGMN. A camera connected to a personal computer was focused on the actuator, while a reference screen was fixed behind it. A temperature and humidity sensor (PCE 313-A) was also fixed to the sample support. All experiments were conducted at a relative humidity of 40% and at 26 °C. The frequency behavior of the IGMNs was observed by applying a 3 V square wave with frequency varying from 0.05 Hz to 5 Hz.

7. Results

7.1 Characterization of iongel

7.1.1 Optical microscopy of iongel

As reported in Figure 28 the surface of the ionic gel after the drying process in the PLA frame resulted uniformly smooth, which characteristic is indeed necessary for the fabrication of electrodes using SCBI. This could be related to the accurate low-temperature molding procedure, as well as to the particular drying method, in which the layers are not constrained along their whole surface area, but only at the lateral borders in contact with the frame, which favors the water release from the polymer avoiding wrinkles or bucklings. A further contribution could also come from the appropriate dispersion of the nanoclays in the mother mixture, which also plays a vital role in synthesizing homogeneous ionic gel-based nanocomposites with respect to other traditional fillers[27].

A low-roughness morphology on the surface is in fact fundamental for the homogeneity of the electrodes themselves and to promote the cluster implantation, which in turn results in a better actuation performance[28].

Figure 28. Optical microscope image of the surface of the produced polymers.

In Figure 29, an image of the cross-section of an ionic gel molded using a 100 μm thick silicone spacer is reported. According to the optical system calibration, the thickness could be measured as 95 μm, which value differs only of the 5% with respect to the nominal thickness of the silicone mold employed. This proves the reliability of the molded procedure, which exhibited similar results for larger silicone spacers thicknesses and good repeatability.

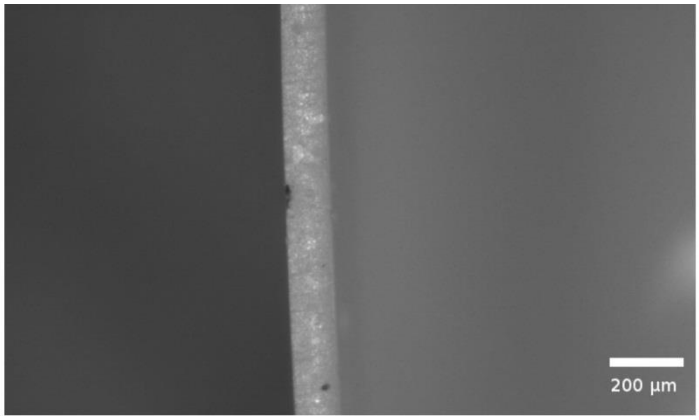

Figure 29. Image of an ionic gel layer cross-section for thickness measurement.

7.1.2 FT-IR

The IR spectrum is reported in Figure 30. The peaks at 3133 cm^{-1} and 3093 cm^{-1} represent the stretching hydrogen bond of the –OH groups, while the peaks at 2852 cm^{-1} and 2909 cm^{-1} is related to the –CH stretching in the main backbone [S1]. The peak at 2206 cm^{-1} is due to the presence of the –OH from the associated carboxylic acid group. Furthermore, the peaks at 1704 cm-1 and 1564 cm-1 prove the C=O stretching and intermolecular hydrogen bonding of the C=O of carboxylic acid group inside the polymer, which demonstrate the presence of PAA in the network [S1]. However, the peak related to acrylonitrile is too weak to be observed, while the peak of EmimBF4 is covered in the range of 500

cm-1. The absence of peaks in the range going from 1620 cm^{-1} to 1680 cm^{-1} proves that the PAA-co-PAN network was successfully synthesized, since all the C=C stretching disappeared [S1]. The peaks related to the nanoclays and TEA are overlapped with the main spectral structure, while the absence of a peak 1617 cm^{-1} can be associated to the PVP incorporation into the polymer.

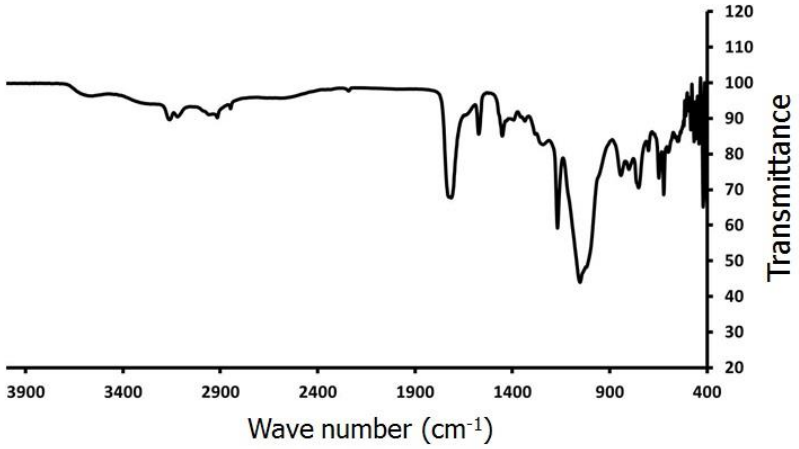

Figure 30. FT-IR spectrum of the ionic gel.

7.1.3 Mechanical testing

The stress-strain curve is reported in Figure 31. The mechanical properties of the materials in the standard formulation were evaluated using uniaxial tensile tests. The Young's modulus of the ionic gel was measured to be 0.347 MPa, while its elongation at break was 255%.

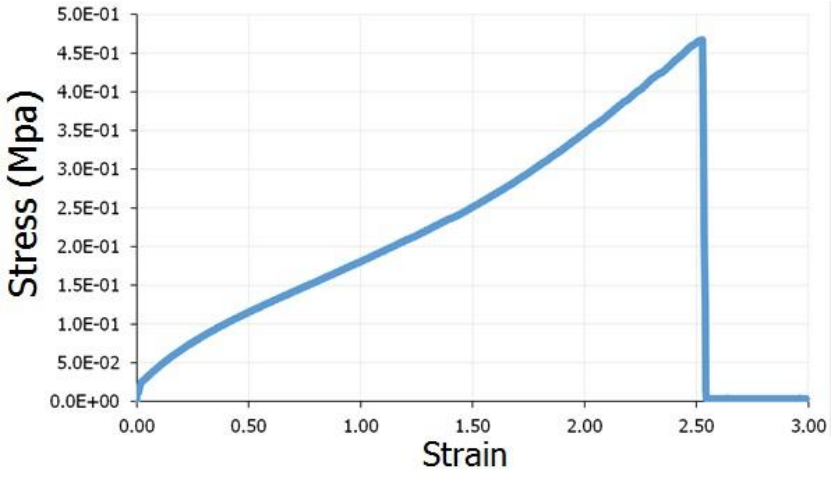

Figure 31. Stress-strain curve for the ionic gel samples.

This value of the Young's modulus is of the order of magnitude of the one reported for silicone elastomers. This suggests the feasibility of the manufacturing approach that will be used for the electrode fabrication, since the metallization of such elastomeric materials for highly deformable stretchable electrodes production on polydimethylsiloxane was already proved using SCBI [2].

7.1.4 XPS

7.1.4.1 XPS of the pure HNC

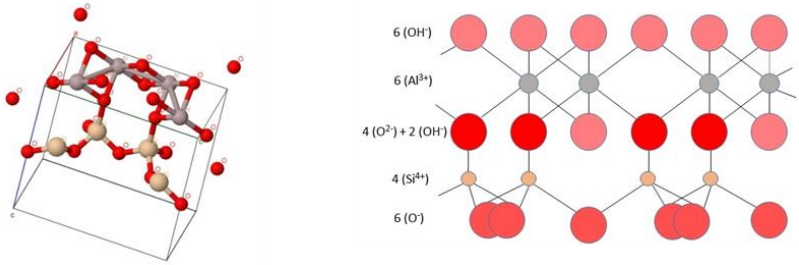

Figure 32. XPS-1 Structure of Halloysite ($Al_2Si_2O_5(OH)_4$) 7A (a= 5.150 Å, b=8.900 Å, c= 7.570 Å, α= 90°, β=100°, γ =90°. Red: oxygen; grey: aluminium and light brown: silicon.

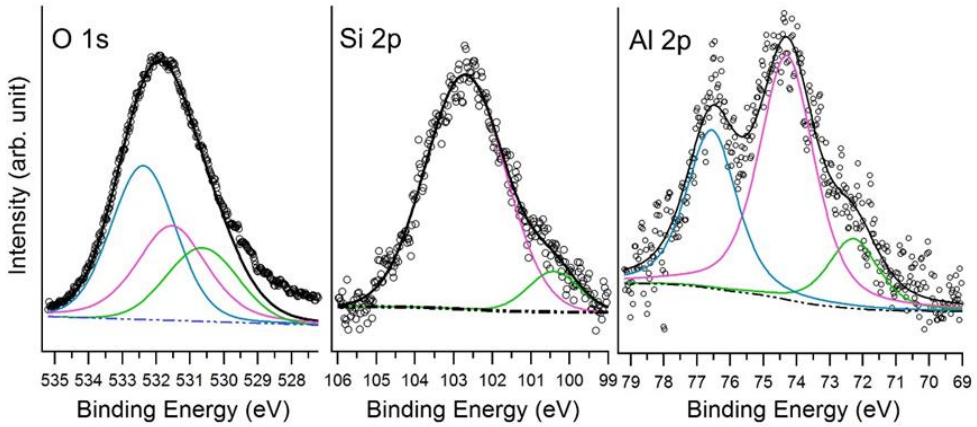

Figure 33. High resolution photoelectron spectra at O1s, Si 2p and Al 2p edges.

To better understand the XPS inside of HNC (Hallosite nanoclays), the single Halloysite stoichiometric unit is shown in Figure 32. It is clear that hydroxyl groups connected with Al+ appear outside and the hydroxyl group connected with Si is shown inside. This structure shows its special function in the whole ionic gel actuator.

Element	Atomic fraction (at.%)		Element ratio	Stoichiometric ratios	
	Expected	Measured		Expected	Measured
O 1s	69.23	68.75	N_O / N_{Al}	4.5	4.16
Al 2p	15.38	16.49	N_O / N_{Si}	4.5	4.65
Si 2p	15.38	14.76	N_{Al} / N_{Si}	1	1.12

Table 2. Atomic fraction and stoichiometric ratios of Aluminium, Oxygen and Silicon in Halloysite calculated from XPS analysis.

Element	Peak assignments	Position (eV)
O 1s	O^{2-}	529.64
	O^{-}	531.18
	OH^{-}	532.30
Al 2p	metallic	72.29
	$Al^{3+}(Al_2Si_2O_5(OH)_4)$	74.31
	AlO_x	76.56
Si 2p	metallic	100.40
	oxide (Si^{4+})	102.71

Table 3. Fitted peak assignments of the high resolution XPS spectra.

The peaks have been fitted by mixed Gaussian-Lorentzian singlets. As shown in Figure 33 the structure of the Halloysite stoichiometric unit involves three different electronic environments for the oxygen electrons: OH- in metal hydroxide (measured 46.0%, expected 44.44%), O-(measured 34.4%, expected 33.33%) in silicon oxide and O2-(measured 19.6%, expected 22.22 %) in aluminium oxide. Thus the larger amount of the oxygen content reported in Table 2. is mainly due to an increment of hydroxyl groups. Moreover a slightly lack of oxygen bounded to metals could be related to oxygen vacancies as assessed by the minor metallic components in aluminum and silicon edges. To distinguish the peak of different elements, the assignments of the deconvolved components are reported in Table 3.

7.1.4.2 Ionic liquid, Halloysite Nanoclays and salt ([Emim][BF4]+HNCs + TEA+)

The obtained value nearly reproduce the stoichiometry of [Emim][BF_4] and no evidence of the quantitative provision of the salt arises. In particular the ratio between C/B is equal, to 6 in both cases as expected for the ionic liquid alone, and the ratio F/B is around 3 in both cases suggesting a loss of

volatile fluorine, perhaps induced by a hydrolysis reaction on the anion BF_4- with the formation of BF_3 /BF_2 containing species.

The peak area of the high resolution photoelectron spectra at O1s, Si2p and Al 2p of halloysite nanotubes (shown in Figure 34) have been used for the quantitative determination of the atomic fraction and the stoichiometric ratios of the elemental constituents (see Table 2). The measured data are in good agreement with the expected values.

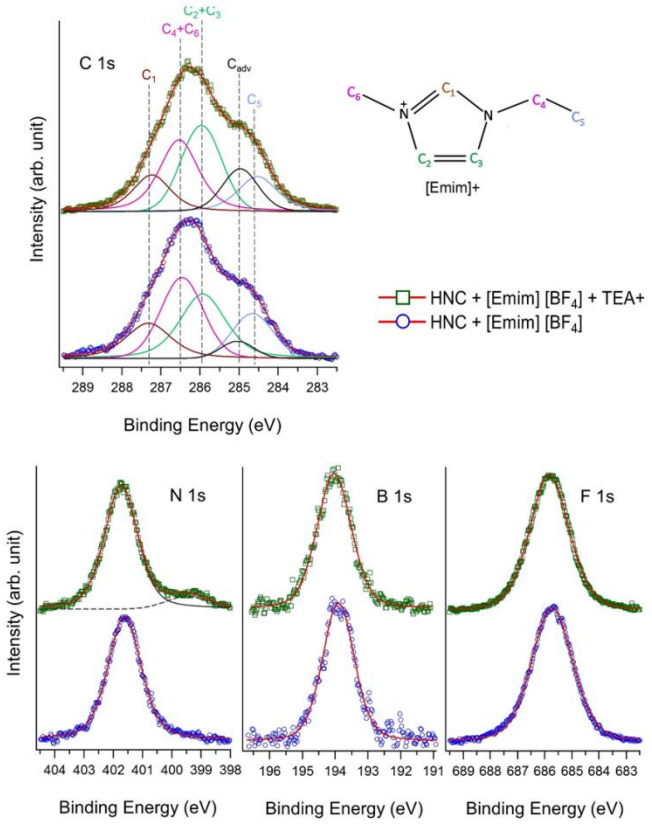

Figure 34. High resolution photoelectron spectra at C 1s, N 1s, B 1s and F 1s edges for [Emim][BF4]+HNCs (blue empty circles) and for [Emim][BF4]+HNCs + TEA+ (green empty squares). The carbon peak has been deconvolved in four components corresponding to the carbon sites in the [Emim]+ cation plus one peak for the adventious carbon. The peak position of the carbon sites are reported in Table 6. The insert shows the molecular structure of [Emim]+.

Element	Atomic fraction (at.%)		
	Expected	Measured	
		[Emim][BF_4]+HNC	[Emim][BF_4]+HNC + TEA^+
C 1s	46.15	51.56	51.62
N 1s	15.38	14.29	15.48
F 1s	30.77	26.05	24.42
B 1s	7.69	8.10	8.47

Table 4. Atomic fraction of the elements contained in [Emim][BF_4] and TEA^+, namely carbon, nitrogen, fluorine and boron without and with the TEA^+ salt.

As shown in Figure 40, the carbon peak has been deconvolved in four components corresponding to the carbon sites in the [Emim]+ cation plus one peak for the adventious carbon. Since the ionic liquid is expected to fully coat the HNCs, the amount of the detectable signal from nanoclays is very low (less than 5%). However the charge polarization effect due to interaction between the [Emim][BF4]+ and HNCs without and with the TEA+ salt has been proved from the oxygen peak, as described in detail in the paper. Thus the atomic fraction (Table 4) has been determined only for the elements present in the ionic liquid and the salt. In the reported data the area of the adventious carbon has been subtracted from the overall carbon peak.

The obtained value nearly reproduce the stoichiometry of [Emim][BF_4] and no evidence of the quantitative provision of the salt arises. In particular the ratio between C/B is equal, to 6 in both cases as expected for the ionic liquid alone, and the ratio F/B is around 3 in both cases suggesting a loss of volatile fluorine, perhaps induced by a hydrolysis reaction on the anion BF_4- with the formation of BF_3 /BF_2 containing species.

In Table 5 the position of the peak maxima are reported. As shown in Figure 34, the F 1s, N 1s and B

1s edges display a narrow peak with a maximum FWHM below 1.7 eV, whereas the C 1s structure is more complicated indicating the expected various chemical environments for the carbon atoms. From the molecular structure of the cation four carbon sites are expected (plus adventious carbon). (see Figure 34).

Element	**Peak position (eV)**	
	[Emim][BF_4]+HNC	[Emim][BF_4]+HNC + TEA+
C 1s	286.28	286.30
N 1s	401.62	401.63
F 1s	685.73	685.83
B 1s	193.90	194.01

Table 5. Peak position of the elements contained in [Emim][BF_4] and TEA^+, namely carbon, nitrogen, fluorine and boron without and with the TEA^+ salt.

Peak	[Emim][BF_4]+HNC		[Emim][BF_4]+HNC + TEA^+	
	Position (eV)	FWHM (eV)	Position (eV)	FWHM (eV)
C_1	286.28	1.37	287.23	1.14
C_2+C_3	285.93	1.38	285.96	1.22

C_4+C_6	286.46	1.28	286.54	1.18
C_5	284.66	1.23	284.53	1.20
C_{adv}	285.00	1.00	285.00	1.09

Table 6. Peak position and FHMW of the deconvolved five components of the carbon peak. The used numbering system is in accordance with the molecular structure given in Figure 34.

The component at lowest BE (C5) has been identified as aliphatic carbon. The features at higher BE correspond to the carbons pairs (C2, C3) of carbon bonded to carbon and nitrogen in the aromatic ring and (C4, C6) of carbon of the alkyl chain directly bonded to the nitrogen of the aromatic ring. Finally the more shifted component (C1) is related to carbon in the aromatic ring between two nitrogen atoms. The fit procedure has been carried out under the following restrictions: the peak FWHM should range between 1.0 – 1.5 eV and the relative peak area ratios should be according to the stoichiometry of equivalent carbon positions. The presence of the adventious carbon (Cadv) has been also taken into account in the procedure fit. All the results are reported in Table 6.

Figure 35 shows the wide spectra of the analyzed samples. As expected, pure HNC shows peaks only of oxygen, silicon and aluminum and an almost negligible contribution of carbon.

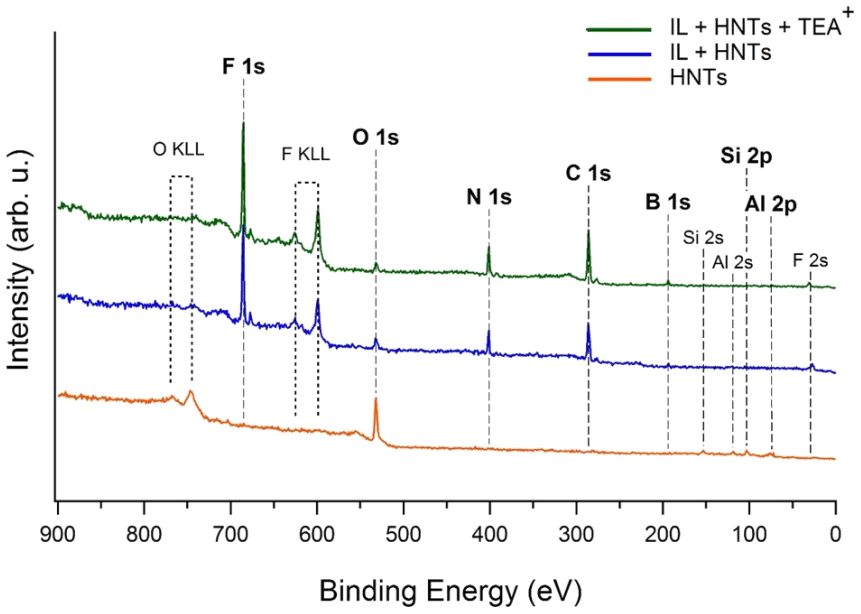

Figure 35. XPS wide spectra of HNC and HNC precipitates after immersion in EmimBF4 and EmimBF4 in the presence of TEA^+.

In Figure 36 and Figure 37, the O1s and Si2p edges are shown respectively. In both cases, the spectra were normalized. The O1s peak of the HNC (Halloysite nanoclays) was deconvolved in three features, related to different bonds of oxygen in the halloysite, namely OH^-, O^- and O_2. The areas of the fitted peaks are compliant with the content of the different oxygen chemical bonds. In both the samples treated with EmimBF4 the O1s peak shows a shoulder at lower binding energies, indicating a reduction of the oxygen ascribable to an interaction with the ionic liquid. This metallization of the silicon can be again imputable to the interaction between the ionic liquid and the outer surface of the HNC (Halloysite nanoclays), which appears to be favorably promoted by the presence of TEA^+.

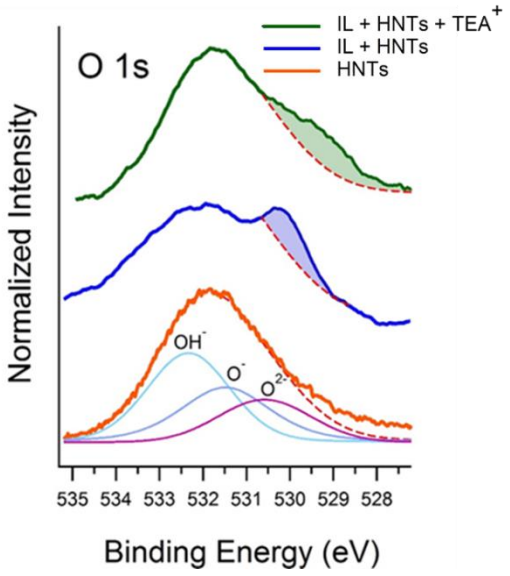

Figure 36. XPS wide spectra O1s of HNC and HNC precipitates after immersion in $EmimBF_4$ and $EmimBF_4$ in the presence of TEA^+.

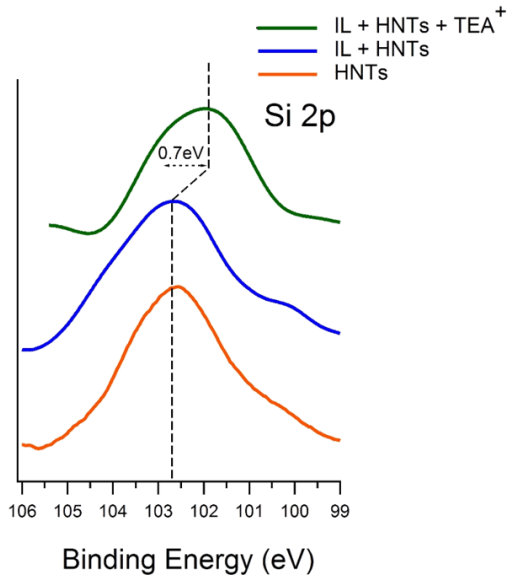

Figure 37. XPS wide spectra Si 2p of HNC and HNC precipitates after immersion in $EmimBF_4$ and $EmimBF_4$ in the presence of TEA^+.

The peaks related to the ionic liquid, namely carbon, nitrogen in Emim cation and boron, fluorine in tetrafluoroborate anion, do not show any evident feature attributable to interactions between EmimBF4 and HNC (Halloysite nanoclays). This lack could be due to the ionic liquid that fully coats the HNC (Halloysite nanoclays), which consequently remain deeply buried. It follows that the

photoemission signal, sensitive to the first atomic layers, is dominated by the surface not-interacting atoms. On the contrary, even if the signals coming from the elements of the HNC (Halloysite nanoclays) are very weak, chemical shifts imputable to the interaction between the surface siloxanes and the EmimBF4 are evident.

7.1.5 XRD

The interaction between HNC (Halloysite nanoclays) and ionic liquid was also confirmed by analyzing the same samples using XRD. The spectra profiles (Figure 38) showed that EmimBF4 could be partially intercalated in the nanotubes after the mixing process, as revealed by the presence of an absorption band at 10 Å.

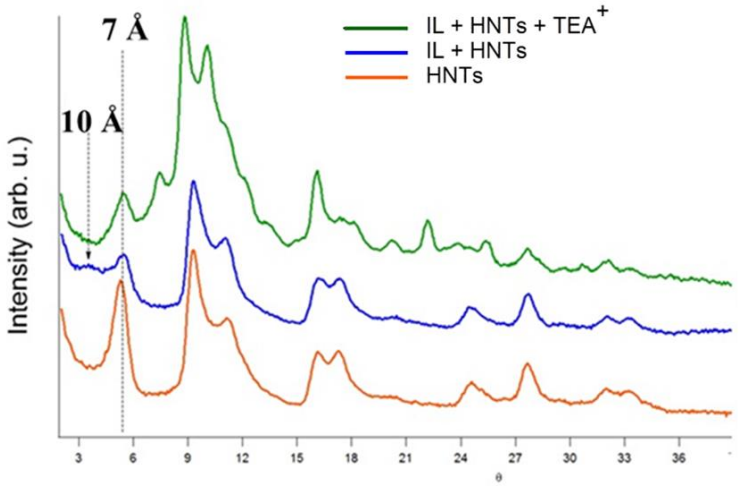

Figure 38. XRD spectra of HNC and HNC precipitates after immersion in $EmimBF_4$ and $EmimBF_4$ in the presence of TEA^+.

7.1.6 Electrical properties of the IGMNs

Figure 39 shows a photograph of the iongel implanted by the gold clusters. The homogeneous

surface quality of the iongel before and after SCBI was also proved by optical microscopy, which suggests that SCBI is a feasible reproducible technology for the fabrication of high-surface quality nanocomposites (Figure 40).

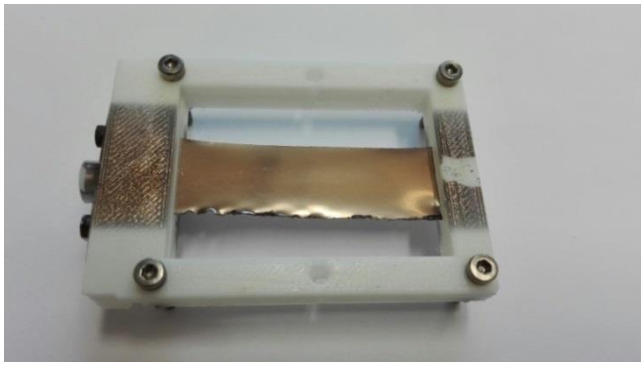

Figure 39. A picture of the produced IGMN after fabrication.

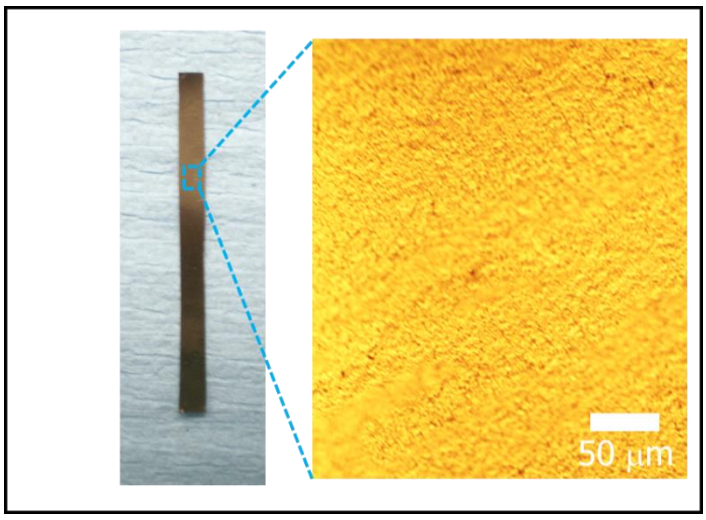

Figure 40. Photograph of an IGMN-based actuator. The inset shows an optical microscope image of the metallized surface of the actuator.

7.1.7 Electrical properties of the IGMNs

The electrical resistance of the IGMNs was measure in real time during SCBI. The sample preparation setup for the electrical resistance measurements during SCBI and an example of a

specimen tested for this purpose is reported in Figure 41.

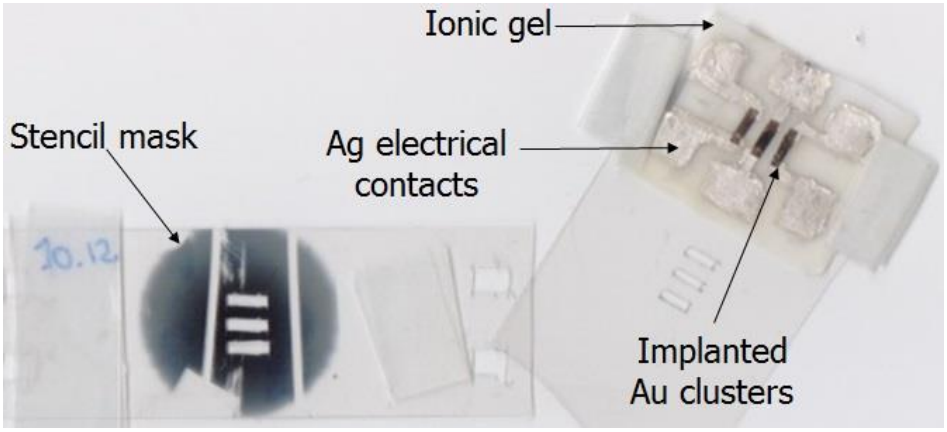

Figure 41. A picture of the sample preparation setup for the electrical resistance measurements during SCBI and an example of a fabricated specimen.

As long as the implantation proceeds, the actuator resistance decreases in time. In Figure 42 the sample resistance evolution during the implantation is reported.

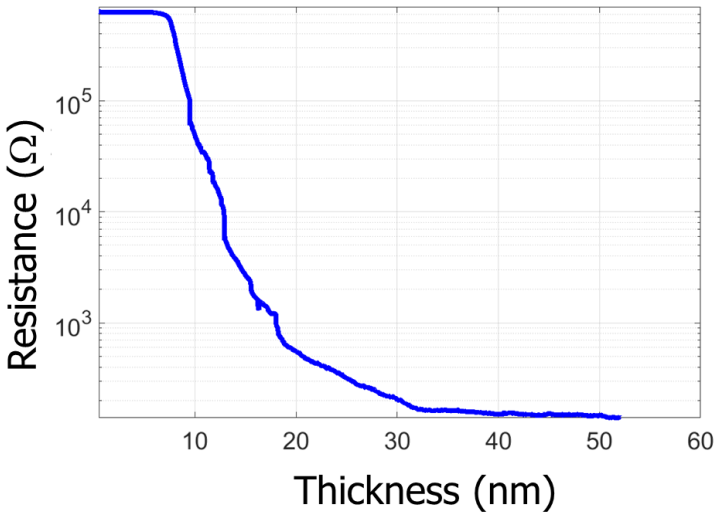

Figure 42. Resistance evolution of the IGMN during SCBI.

It can be observed that the polymer has an intrinsic conductivity of about 10^6 Ohm, probably due to the free ions contribution. By continuously increasing the amount of nanoparticles, three different regimes can be observed. In the first region, between 0 and 6 nm, the sample resistance is that of the

ionic gel (about 6 x 10^5 Ω), and this is because the amount of implanted nanoparticles is not enough to create conductive paths between them. A conduction onset is observed after the implantation of 6 nm; at this stage, a path of gold nanoparticles spanning the entire gap between the electrodes is instored. The addition of further nanoparticles reinforces the conductive path and the resistance decreases from 6 x 10^5 Ω to 10^2 Ω after the deposition of 27 nm. Once the polymer is saturated with clusters, the addiction of further nanoparticles does not affect the sample conductivity. In fact in the thickness range between 33 to 52 nm no significant changes in the resistance are recorded. After the metallization of the actuators is completed (100 nm), the electrodes surface resistance was measured using a multimeter and resulted to be 95 Ω /cm^2.

7.2 Electrochemical and electromechanical characterization of IGMNs

7.2.1 Electrochemical charactericzaion

To investigate on the effects of the presence of HNC (Halloysite nanoclays) and TEA^+ (tetraethylammonium) cation on the electrochemical properties and actuation performance of the IGMNs, ionic gel samples without the embedded nanoclays (IGMN-WNC) and without TEA^+ (IGMN-WTEA+) were molded as 100 µm thick layers and subsequently processed using supersonic cluster bean implantation (SCBI, Figure 43).

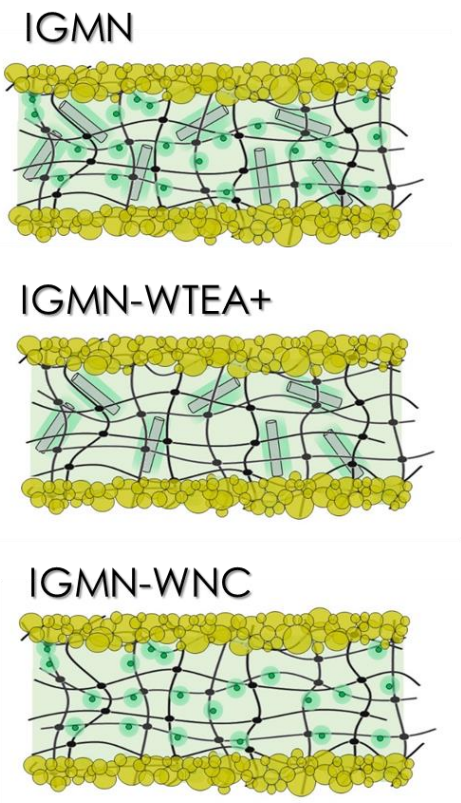

Figure 43. Schematic of the samples produced:the IGMN standard formulation (top), IGMN without the presence of TEA+ (IGMN-WTEA+, middle) and without the embedded nanoclays (IGMN-WNC, bottom).

The electrochemical characteristics of the produced nanocomposites were monitored using EIS. The Nyquist plot for the three formulations is reported in Figure 44 and shows that all samples have a capacitive behavior due to the formation of an electric double layer at the Au electrode interface.

The high-frequency intercept with the real impedance axis represents the equivalent series resistance (ESR) of the actuator. For the IGMN-WNC and IGMN-WTEA+ samples, the conductivity decreases to 0.18 mS/cm and 0.16 mS/cm respectively.

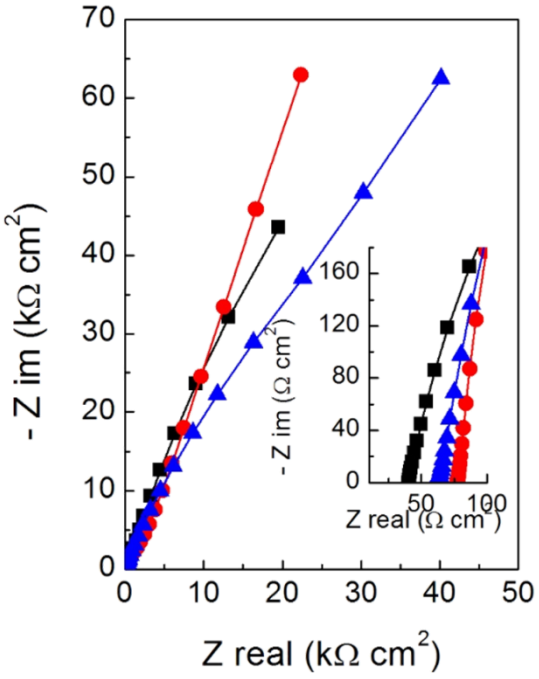

Figure 44. Impedance spectrum of the three type of nanocomposites.

The inset shows a magnification of the high frequency intercept with the real impedance axis.

Electric double layer capacitances of the IGMNs were calculated from the impedance spectra and reported in Figure 45. At 0.1 Hz, the specific capacitance of the standard IGMN was measured as C=30 μF/cm^2.

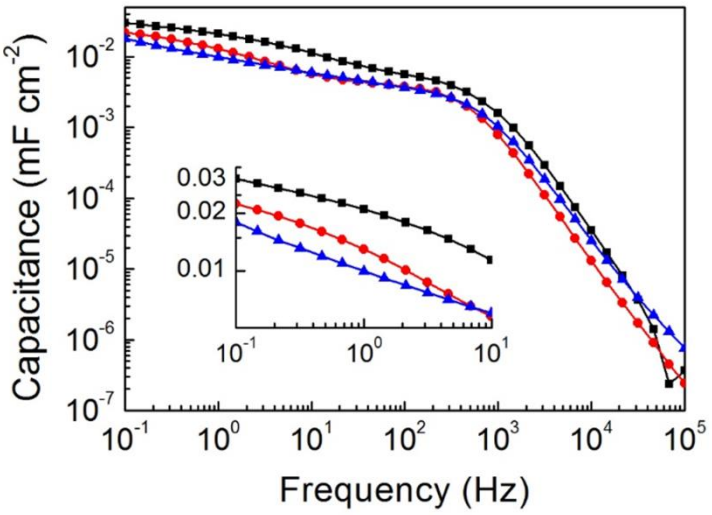

Figure 45. Specific electrochemical capacitance of the samples produced. A magnification of the low frequency region is reported in the inset.

Cyclic voltammetry was also carried out on the standard IGMN formulation, showing that the electrochemical window of the composite was ±3 V. (shown in Figure 46)

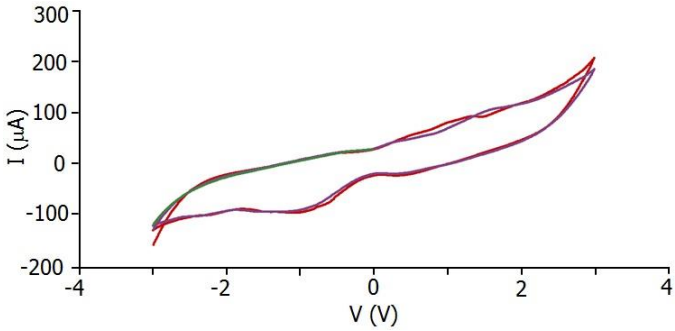

Figure 46. Cyclic voltammetry of the standard IGMN actuator.

7.2.2 Electro-mechanical performance of the IGMNs

The electro-mechanical performance of the IGMN samples was monitored using a custom-made setup where samples were fixed in a classical cantilever configuration and underwent electrical stimulation. A square wave voltage of variable amplitude and frequency was applied to the actuators and their response was recorded by acquiring video sequences, from which captures could be collected and analyzed using an image processing software. For the standard material formulation (100 μm thick), the response to the electric field was observed to take place at 0.1 V and exhibited relatively low tip displacement values (around 0.06 mm) and reached values up to 0.25 mm at 1 V. As expected, the tip displacement and the generated net strain increased with increasing voltages and showed their maximum values at 5 V (31.5 mm and 0.36% respectively), achieved 30 seconds after the electric field was applied. Examples of the system bending actuation are reported in Figure 47 and Figure 48.

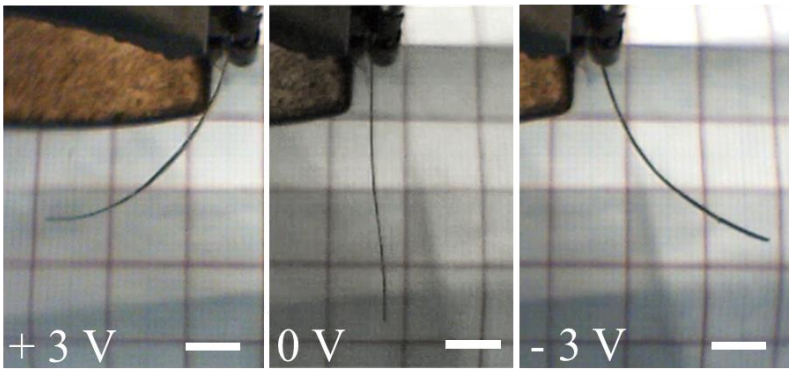

Figure 47. Example of bending for the IGMN standard formulation at 3 V and 0.02 Hz.

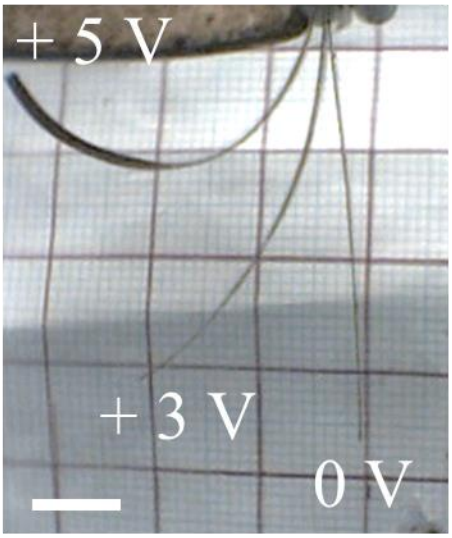

Figure 48. Example of bending for the IGMN standard formulation at 3 V and 5 V.

At 3 V and 5 V, the maximum tip displacement and bending speed showed a linear behavior as a function of the inverse of the sample thickness (Figure 49 and Figure 50).

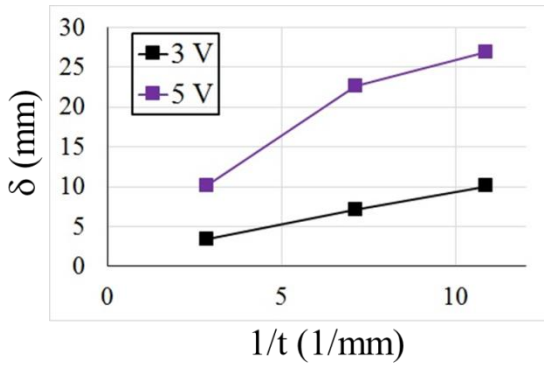

Figure 49. Actuation performance of the IGMNs in tip displacement

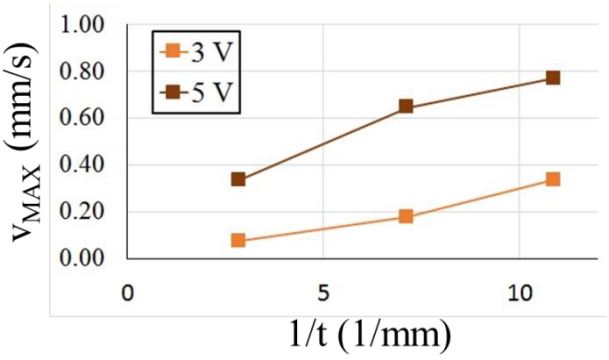

Figure 50. Maximum speed as a function of the inverse of the actuator thickness for the standard IGMN formulation.

The maximum net strain of 1.04% was achieved by the 350 µm thick sample under the application of 5 V for 30 seconds. The specimen demonstrated a stable frequency response for frequency values up to 10 Hz for all the thickness tested and the generated strain showed a decreasing profile when the frequency of the driving signal was increased(shown in Figure 51). For the 100 µm thick actuator, the tip displacement decreased from 17.1 mm at 0.05 Hz to 2.9 mm at 0.5 Hz (the signal amplitude was 3 V).

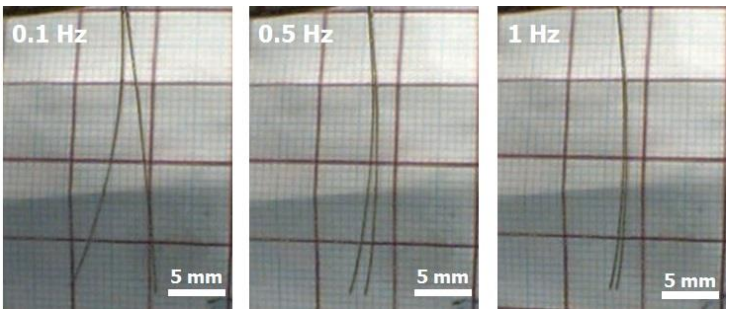

Figure 51. Frequency dependent displacement of IGMN actuator.

Cyclic measurements were also carried out at 2 V and 1 Hz for 76000 cycles. No fatigue effects or decrease of performance were registered in more than 20 hours of observation, which proved high

working durability of the produced actuators (As shown in Figure 52).

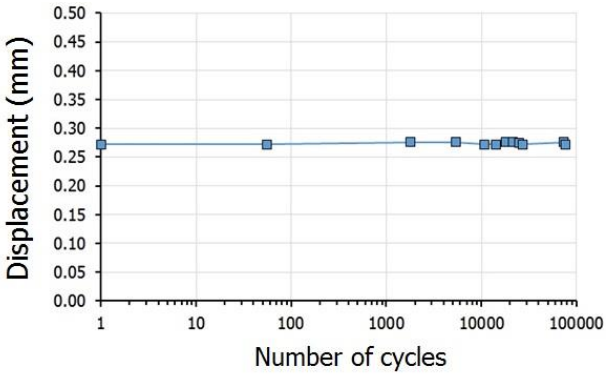

Figure 52. Durability of performance of IGMN actuator.

The electro-mechanical performance of the IGMN-WNC and IGMN-WTEA+ samples was analyzed using the same setup and compared with the standard IGMN at 0.02 Hz in the voltage range going from 1 V to 5 V (all samples were 100 µm thick). A decrease in the generated peak-to-peak strain with respect to the standard IGMN actuator was observed for both samples, reflecting the decrease in the measured electrochemical capacitance for the two material formulations.

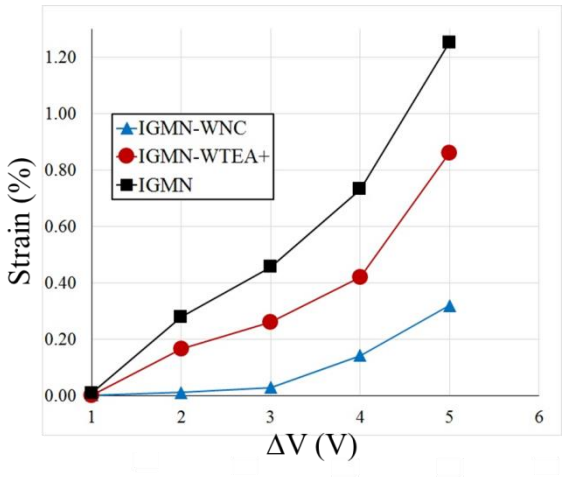

Figure 53. Peak-to-peak strain profile as a function of the applied voltage for all the IGMN formulations in actuator performance.

In the low voltage regime, the peak-to-peak strain value for the standard IGMN at 1 V decreased from 0.019% to around 0.003% and 0.002% for the IGMN-WNC and IGMN-WTEA+ respectively. This significant difference of around one order of magnitude was preserved for voltages up to 3 V, while for higher voltage values a decrease of about 50% was observed. A comparison between the peak-to-peak strain values for all the samples formulation is reported in Figure 53.

The actuation behavior of the IGMNs can be considered highly relevant in the framework of electroactive ionic polymers, as reported by the most recent literature on in-air working IPMCs, bucky-gels and other electroactive ionic polymers and blends, such as engineered PSS block co-polymers provided with ionic nano-channels and poly (ethylene oxide)-based electrolytes with chemically modified graphene electrodes.

8.Discussions

A summary of the main features of the SCBI technique and of the properties of the fabricated IGMNs is reported here below.

SCBI has already proven to be an enabling technology for the development of elastomeric polymer/metal functional nanocomposites provided with flexible and stretchable electrodes with thickness from few tenths to few hundreds of nanometers, firmly anchored to the polymeric substrate. This metallization approach consists of directing a highly collimated beam of neutral metal clusters onto a polymeric target [1, 29].

The mix of gas and clusters produced in a cluster source attached to the expansion chamber is accelerated and collimated by the aerodynamic focuser. Nanoparticles then enter the deposition chamber and are implanted into the polymeric substrate, which is fixed on a movable sample holder, enabling the metallization on large areas though a rastering technique. The mechanical and electrical properties of the produced materials can be finely tuned by controlling the amount of clusters implanted into the polymer[2]. Therefore, this implantation technique is feasible to control the electrical resistance of the electrodes and the composites elasticity, minimizing the interfacial stresses between the metallic and the polymeric layers when deformation of the material takes place. By using SCBI to process highly ionic conductive PAA-co-PAN gels, having Young's modulus in the range of elastomeric materials, a novel family of IGMN blended with HNC were produced, this system exhibited high-strain electro-mechanical actuation performance in a low voltage regime (from 0.1 V to 5 V) and robust stability up to 76,000 cycles. The actuation behavior of the IGMN presented in this thesis work is due both to the intrinsic features of the PAA-co-PAN-based electrolyte (elasticity, ionic transport capability) and to the electrical and morphological features of the electrodes. In fact, the low thickness of the cluster-assembled metal layers (~100 nm) do not significantly alter the mechanical properties of

the bulk material, while their nanostructured nature simultaneously implies low electrical resistance values (< 100 Ω/cm2) and large surface area to operate as double layer capacitors for an effective ions storage (electrochemical capacitance ~ mF/g). The fabrication of these novel nanocomposites is cost-effective and involves processes that are suitable for scale up manufacturing.

According to the material structure and to the experimental data on its electrochemical and electro-mechanical properties, the actuation mechanism of the IGMNs can be considered to be intermediate between that of IPMCs and bucky-gels. In IPMCs, the ionic liquid absorbed by the polymer plays the role of the transport medium, while the counter-cations (such as alkali metals or organic compounds), coordinated to the fixed anionic sites, constitute the active mobile specie that migrates across the polymer thickness when the electric field is applied. These positive charges, dragging ionic liquid ion pairs along with their drift, accumulate at the polymer/metal composite region, where a double layer capacitance is established. The unbalance in ionic liquid concentration at the anode and cathode causes a differential swelling of the material at the two opposite regions, which in turn results in a bending deformation. In bucky-gels, ionic liquid has a direct and active role in the actuation, since it is intercalated into the solid phase in a dissociated form, and therefore its anions and cations constitute themselves the mobile species drifting across the material and accumulating at the electrodes under the effect of the applied electric field. In fact, depending on their surface chemistry and surface area, the carbon-based nanostructures present in the electrolyte interact with imidazolium-based ionic liquids during the mixing stage (mainly through π-π interaction), causing the solvent polarization and ion-pair dissociation. These phenomena, which are particularly favored for single-walled carbon nanotubes (SWNTs) with respect to other carbonaceous structures, are strongly dependent on the dispersion degree of the nanomaterials in the liquid phase. The generated strain of such actuators is proportional to the net electric charge accumulated at the electrodes, which is in turn

proportional to the density of the nanostructures in the composite layer and to the dissociation degree of the ionic liquid.

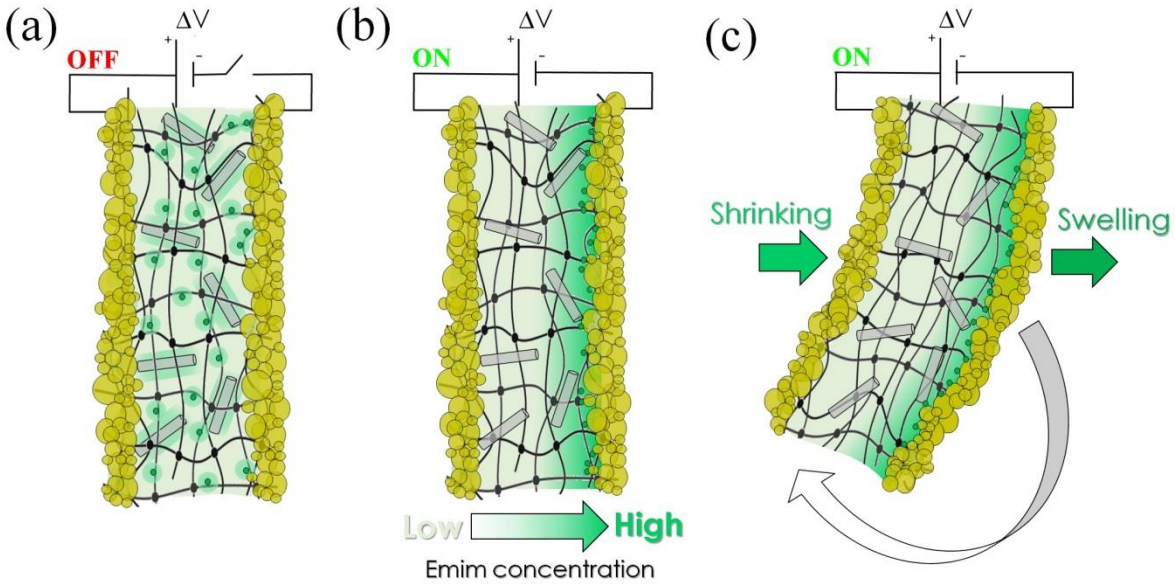

Figure 54. Actuation mechanism of the IGMN.

a) IGMN-based actuator. b) When the electrical stimulus is applied, both the TEA+ and Emim cations migrate towards the cathode. c) The differential swelling at the anodic and cathodic side of the IGMN induces the bending of the actuator towards the anode.

In the IGMN network (Figure.54a), both the mobile TEA+ cations and the partially dissociated EmimBF4 contribute to trigger the actuation of the system under electrical stimulation. EmimBF4 can be absorbed by the composite through the interaction with the acidic PAA groups (in the same framework as it takes place in the carboxyl groups-rich phase of Flemion) and orientate to form a hydration region around the mobile organic counter-ion. Furthermore, the imidazolium cation interacts with the surface siloxanes of the HNC. The minerals, which are homogeneously dispersed in the ionic gel matrix, induce a partial dissociation of the ionic liquid through an oxygen reduction reaction, which therefore promote the Emim cations migration towards the cathode when the electric field is applied (Figure.54b). In this sense, HNC has the same function of the carbonaceous nanostructures in

bucky-gel actuators, i.e. interacting with the imidazolium cations, but through a different molecular mechanism, and being present in the bulk of the electrolyte rather than in the electrode layers. Along with the Emim accumulation at the cluster-assembled gold electrode, TEA+ also migrates at the cathodic side of the actuator in the same framework as it takes place in IPMCs[30-32]. The contribution of both the positive charged species that accumulates at the nanostructured electrode in a double layer capacitance regime generates a differential swelling at the opposite sides of the actuator, which bends towards the anode.

To get insights on the EmimBF4 interaction with the nanostructured silicates, we used XPS on pure HNC powders and on HNC precipitates, recovered after being soaked under stirring overnight in pure EmimBF4 and in a 0.17 mM ionic liquid solution containing the quaternary ammonium cation (HNC are 20% in weight with respect to the ionic liquid). Figure.35 shows the wide spectra of the analyzed samples. From this picture, it could be concluded that the peaks could only be contributed from oxygen, silicon and aluminum and an almost negligible carbon. In Figure.36 and Figure.37, the O1s and Si2p edges appeared respectively and whose spectra were normalized. The O1s peak of the HNC was deconvolved and appears three features which is related to different bonds of oxygen in the halloysite in the form of OH-, O- and O^2. The areas of the fitted peaks are compliant with the content of the different oxygen chemical bonds. A shoulder at lower binding energies in both the samples treated with EmimBF4 the O1s peak suggests a reduction of the oxygen ascribable to an interaction with the ionic liquid. This shift is even more remarkable when TEA+ is present, probably due to the polarization induced by the quaternary ammonium on the surrounding EmimBF4, which in turns enable the Emim cation to interact more effectively with the nanotubes. This behavior is mirrored by the silicon profiles, where a manifest shift towards a lower binding energy is well evident in the sample containing the TEA+ and can be quantified in 0.7 eV, in agreement with was is reported in the literature[33, 34]. This

metallization of the silicon can be concluded to be contributed from the interaction between the ionic liquid and the outer surface of the HNC, which appears to be favorably promoted by the presence of TEA^+.

The interaction between HNC and ionic liquid was also confirmed by using XRD in analyzing the same samples. The spectra profiles above (Figure 38) showed that EmimBF4 could be partially intercalated in the nanotubes after the mixing process, due to the fact that the absorption band attained at 10 Å. According to the literature, this change in the HNC spectrum can be relied on larger lattice interspacing in nanoclays domains, which resulted from the ionic liquid partially intercalation in the nanostructures[35].

The electrochemical properties of the IGMNs, unveiled by EIS and correlated to the actuation performance of samples without the nanostructures and the organic cation, showed the fundamental role of both the HNC and the TEA+.

ESR of the standard IGMN resulted to be ESR= 40 Ohm/cm^2. By considering the ESR to be dominated by the bulk ionic resistance of the IGMN, the ionic conductivity of the actuator can be calculated as $\sigma = t/(A * ESR)$, where t and A are the thickness and surface area of the IGMN respectively[36]. For the standard formulation, $\sigma = 0.35$ mS/cm. This value is one order of magnitude higher with respect to the ionic conductivity of Nafion membranes swollen with imidazolium-based ionic liquids, having solvent uptake values comparable with the IGMN (around 40% mol/mol) and TEA+ incorporated as the mobile cation, as well as with respect to Multi-Walled Carbon Nanotubes (MWCNTs)-based bucky-gels[12, 37]. Furthermore, the measured ionic conductivity is comparable with that of SWCNTs/PVDF-based bucky-gels having higher solvent uptake values of a variety of ionic liquids with different viscosity and transport properties[38]. For the IGMN-WNC and IGMN-WTEA+ samples, the conductivity decreases to 0.18 mS/cm and 0.16 mS/cm respectively i.e. about 50% of the σ value

measured for the standard IGMN formulation. These results suggest that both the presence of HNC and TEA+ have a significant influence on the electrolyte transport properties due to their interaction with EmimBF4 and that the contributions of the nano-filler and mobile cation have an important role in determining these characteristics.

Also, by taking into account the small amount of gold employed for the fabrication of the electrodes (around two μg, corresponding to an overall thickness of the interpenetrating metal layer of about 100 nm), the measured C value can be considered significantly high and it proves the presence of a large electrode interface area for charge storage. In fact, for IPMCs actuators swollen with ionic liquid, the specific electrochemical capacitance ranges from 0.1 mF/cm^2 to 100 mF/cm^2. When an organic counter-ion is included into the polymers as the active specie, the capacitance range typically goes from 0.3 mF/cm^2 to 10 mF/cm^2. However, for these systems, the inter-penetrating electrodes consist of a 10 to 20 μm deep platinum/polymer composite region, provided with an additional 1 to 5 μm thick surface layer of pure noble metal (usually platinum or gold) as the electrical signal collector. Therefore, the double-layer capacitance in IPMCs is established in an effective layer that is two to four orders of magnitude thicker than the thin IGMN gold electrodes fabricated by mean of SCBI. The specific electrochemical capacitance of the IGMN-WNC and IGMN-WTEA+ also dropped to lower values with respect to the one measured for the standard IGMN, being equal to 18 $\mu F/cm^2$ and 23 $\mu F/cm^2$ respectively. This result confirms the active role of both the nanoclays and the quaternary ammonium cation in the charge accumulation process, which is of primary importance for the actuators strain generation. Cyclic voltammetry was also carried out on the standard IGMN formulation, showing that the electrochemical window of the composite was ±3 V (shown in Figure.46) and the result of impedance spectra confirms the active role of both the nanoclays and the quaternary ammonium cation in the charge accumulation process, which is of primary importance for the

actuators strain generation as schematized in Figure 55.

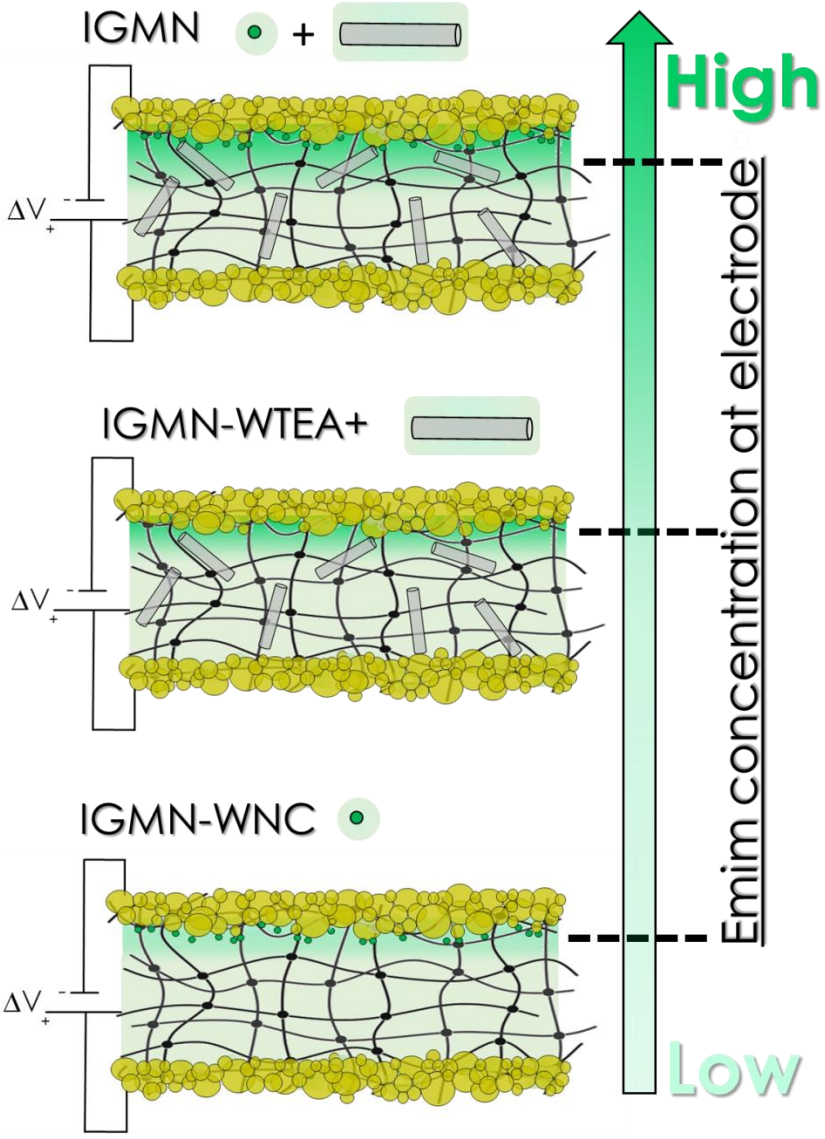

Figure 55. Schematic of the different samples produced, having increasing Emim cation concentration at the cathodic side after the application of the electric field.

From electro-mechanical performance, a decrease in the generated peak-to-peak strain with respect to the standard IGMN actuator was observed for both samples, reflecting the decrease in the measured electrochemical capacitance for the two material formulations. This trend is confirming the effect that both the nano-filler and the organic cation have on the dissociation of the ionic liquid and therefore on the electrochemical capacitance and electro-mechanical performance of the composites.

In the low voltage regime, the peak-to-peak strain value for the standard IGMN at 1 V decreased from 0.019% to around 0.003% and 0.002% for the IGMN-WNC and IGMN-WTEA+ respectively. This significant difference of around one order of magnitude was preserved for voltages up to 3 V, while for higher voltage values a decrease of about 50% was observed. A comparison between the peak-to-peak strain values for all the samples formulation is reported in Figure 53.

The actuation behavior of the IGMNs can be considered highly relevant in the framework of electroactive ionic polymers, as reported by the most recent literature on in-air working IPMCs, bucky-gels and other electroactive ionic polymers and blends, such as engineered PSS block co-polymers provided with ionic nano-channels and poly (ethylene oxide)-based electrolytes with chemically modified graphene electrodes[23, 24]. For example, PSS block co-polymers synthesized by Kim's group proved that incresing the amount of $–SO_3H$ groups could provide the dissociation of ionic liquids, which in turns offer the capability to improve the actuator performance by facilitating ion transport in the polymer layer. Moreover, the block-copolymer poly(styrenesulphonate-b-methylbutylene) (PSS-b-PMB) will create self-assembled morphology through the thermodynamic immiscibility between the ionic PSS and non-ionic PMB phases, which offers short ion diffusion pathways along the nanoscale ionic channels. Comparing with such structure, the IGMNs actuator shows a structure similar to the (PSS-b-PMB) block-copolymer based actuator. In the IGMNs, Both PAA and HNC provide the dissociation of ionic liquids like the role of PSS part in block-copolymer. However, unlike the) (PSS-b-PMB) which requires the thermodynamic immiscibility process to form self-assembled morphology, IGMNs has a porous structure, characterized by an average mesh size, generated by the chemical crosslinking of the network and, what's more, HNC also create physical channels to facilitate the transport of ions, since they are able to intercalate the ionic liquid in their lumen. In another representative example of state-of-the-art electro-active actuators,

Graphitic carbon nitride nanosheet electrode-based ionic actuator introduced an interpenetrating polymer network based on poly(ethylene oxide) and PEO-NBR, which structure is similar to the IGMNs i.e. both of them provide sufficient ions for rapid migrating and shows higher ion uptake, ionic conductivity and ion transportation. By incorporating the particle of hierarchically porous g-CN inside, the actuator will form a very high capacitance electrode on both side and perform actuation as a supercapacitor.

Although the similarity in structures from both updated actuators, the actuation schemes are not the same. During the overall formation process, both typical actuators highly depended on the CNTs which not only enhanced the mechanical strength and but also increase the electrical conductivity through π–π interaction between layers of the carbon. However, in these IGMN actuators, the dissociation of ions is contributed from the interaction between the ionic liquid and the outer surface of the HNC, which appears to be favorably promoted by the presence of TEA+. Apart from that, both cases all required hot-pressing and interpenetrating electrodes fabrication process, which hinders their applications for further mass production and scale up. Due the fact of one step synthesis approach, the IGMN actuators showed its advantages for future industrial work.

9.Conclusions

In conclusion, I demonstrated the fabrication of electroactive IGMNs based on ionic conductive PAA-co-PAN network with embedded HNC by mean of SCBI. The production of cluster-assembled gold thin films (100 nm thick), inter-penetrating with the quasi-solid state electrolyte, enabled the manufacturing of elastic soft actuators provided with flexible electrodes having low surface electric resistance and large surface area for an effective charge storage. The electro-responsive properties of the materials are intermediate between that of IPMCs and bucky-gels. This feature is due to the synergistic effect of the quaternary ammonium TEA^+ counter-ion and HNC on the transport ability and electrochemical characteristics of the functional nanocomposites. Both the organic cation and the inorganic nanostructures confer high ionic conductivity (0.35 mS/cm) and large double layer capacitance (30 $\mu F/cm^2$) to the composites, by favoring the partial dissociation of the EmimBF4 ionic liquid incorporated in the structure (solvent molar uptake is 37%). The materials showed sensitivity to the applied electric field starting at 0.1 V and exhibited high-performance actuation in response to electrical stimuli at low voltages (up to 1.04% net strain at 5 V) and good durability in their frequency response (up to 76000 cycles at 2 V and 1 Hz).

There are several key aspects which constitute novelty in terms of both the material intrinsic features and the actuator fabrication process. These can be summarized as follows:

i. The dissociation of ions is attributed to the interaction between the ionic liquid and the outer surface of the HNC, which appears to be favorably promoted by the presence of TEA+ rather than the π–π interaction between the layers of the carbon nanotubes and ionic liquid, characteristic of bucky gel based actuators. By introducing HNC as the fillers instead of carbonaceous materials, the nanostructures can be properly dispersed, avoiding stacking and entanglements typical of carbon nanotubes in traditional bucky gel actuator, which hinder the performance of the

actuation and the stability of their electro-active properties.

Since the majority of electro-active actuators fabrication technologies highly rely on tenths of μm depth electrodes interpenetrating with the polymers for absorption of ions which will promote the bending motion of the actuator. These are fabrication procedures are expensive and time-consuming, and this makes the industrial manufacture approach not easy for a convenient scale-up. In the IGMN production, SCBI proved to be a feasible enabling technology to fabricate conductive gold electrodes interpenetrating with the polymeric structure by implantation of the metal clusters after the one-pot step of synthesis and molding of the iongel. These nanostructures electrodes provide large surface for ions storage in a double layer capacitance regime and, due to their low thickness (around 100 nm), preserve the flexibility of the system and minimize the mechanical stresses at the metal/polymer composite interface upon deformation. The coupling of these properties of the electrodes enables the IGMNs to generate high-performance actuation without having the electrochemical characteristics of the supercapacitor-based electroactive polymers (capacitance tenths to hundreds of F/g). Furthermore, the IGMNs elementary structure (compliant thin metal electrodes sandwiching the polymeric electrolyte) is achieved with a simple deposition-based process, which is advantageous with respect to the relatively complex layer-by-layer fabrication of bucky gels.

ii. The one-step synthesis approach and the SBI metallization technique renders the IGMN manufacturing cost-effective and suitable for industrial production scale up.

iii. As proved by the IGMNs based actuators, the design principles and working mechanism of such structure has potential to be introduced as a guidance scheme for the production of a new family of actuators, merging the properties of IPMCs and bucky gel based actuators.

In summary, I believe that the novel IGMNs presented here represent a forefront technological

solution for the development of smart flexible components suitable for the manufacturing of soft bio-mimetic robots, deformable electronic and haptic systems, and wearable biomedical devices.

10.Appendix A

10.1 SWNTs based iongel actuator

10.1.1.Introduction

As previously reported in section, SWNTs loaded bucky gel could acted as a promising actuator which attracted a lot of interest[39]. In these systems, the ionic liquid is known to interact with the p-electronic surface of the SWNTs by means of cation–π and/or π–π interactions that will produce the gelation by using a ultra-sound generator or by grinding the suspension in an agate mortar with a pestle. In this Appendix, I will report and discuss the introduction of SWNTS as the fillers of the PAA-co-PAN ionic gel based actuators. The materials employed for the polymer synthesis and the thin films manufacturing methodologies are the same as the one reported in Section materials and methods and SWCNTS filled ionic gels/metal nanocomposites were produced by mean of SCBI. Beside the use of SWCNTs as the fillers instead of HNC, the only difference with respect to the standard formulation of the ionic gel is the use of tetrabutylammonium fluoride hydrate (TBAF) instead of TEAF to operate as the mobile ions candidate. PVP, was used again to promote the dispersion of the fillers in the mother mixture. PVP is a physiologic inert component; extensively used in medicine due to its water affinity and its capacity of confer elasticity to films and membranes with potential applications in skin grafts. To examine the effect of both PVP and TBAF on the structure and actuation properties of the ionic gels, three polymers were synthesized following the procedure below:

10.1.2.Materials and Methods

10.1.2.1 Sample preparation

1) PAA-PAN IONGEL(P1): in this formulation, no PVP and no TBAF are included. 547.5 µl (8 mmol)

acrylic acid and 130 µl (2 mmol) acrylonitrile are mixed together, then Emim/H_2O 651 µl (7:3 V/V) solution was added with EGDMA 19 µl (0.1 mmol). Then the solution was stirred 5 mins, and 6 mg Single Wall Carbon Nanotube (SWNTs) was added and the mixture stirred overnight. After that, 30 µl DMAP solution (15% W/V) was mixed into the solution and the whole solution was injected into a hollow silicone spacer, sandwiched between two glasses. Finally, the mold was exposed to UV (365nm wavelength) radiation for one hour.

2) PAA-PAN IONGEL(PP1): in this formulation TBAF is included, but no PVP is present. 547.5 µl (8 mmol) acrylic acid and 130 µl (2 mmol) acrylonitrile are mixed together, then Emim/H2O 651 µl (7:3 V/V) solution was added with EGDMA 19 ul (0.1 mmol). Then the solution was stirred 5 mins, and 160 mg TBAF as well as 6 mg Single Wall Carbon Nanotube (SWNTs) were added and the mixture stirred overnight. After that, 30 µl DMAP solution (15% W/V) was mixed into the solution and the whole solution was injected into the silicone mold between two glasses. Finally, the mold was exposed by 365nm wavelength and the solution was initiated by UV lamp.

3) PAA-PAN with PVP IONGEL(PPW1): in this formulation, both PVP and TBAF are included. 547.5 µl (8 mmol) acrylic acid and 130 µl (2 mmol) acrylonitrile are mixed together, then Emim/H2O 651 µl (7:3 V/V) solution was added with EGDMA 19 µl (0.1 mmol). Then the solution was stirred 5 mins, and 160 mg TBAF, 100mg PVP as well as 6 mg Single Wall Carbon Nanotube (SWNTs) were added and the mixture stirred overnight. After that, 30 µl DMAP solution (15% W/V) was mixed into the solution and the whole solution was injected into the silicone mold between two glasses. Finally, the mold was exposed by 365nm wavelength and the solution was initiated by UV lamp.

10.1.2.2 FT-IR spectroscopy

To confirm the chemical structure of the three ionic gel formulations, FT-IR was used for characterization, in the attenuated transmitted reflectance (ATR) mode. First, film PAA-PAN hydrogel (P1-H) which has no ionic liquid, mobile ions TBAF and PVP was synthesized as the standard sample for FT-IR test.

The procedures to fabricate P1-H layers are as following: 547.5 µl (8 mmol) acrylic acid and 130 µl (2 mmol) acrylonitrile are mixed together, added with H_2O 651 µl solution and EGDMA 19 µl (0.1 mmol). Then the solution was stirred 5 mins, adding 30 µl DMAP solution (15% W/V) into the solution and put the solution directly exposed by 365nm wavelength and initiated by UV lamp.

Then, the film of P1, PP1 and PPW1 were synthesized following the procedures above. The dried films were peeled off the glass support and, after drying, they were placed onto the crystal of the spectrometer. The instrument used was a FT-IR spectrometer (Bruker IFS 88) equipped with a temperature chamber. The resolution was 4 cm^{-1}.

10.1.2.3 Electromechanical Characterizations

To investigate the actuation behavior of P1, PPW1 and PP1, the iongel with implanted electrodes were characterized for their electromechanical transduction behavior as actuators. For the actuation testing, the actuators were clamped in a cantilevered configuration and allowed to bend freely. A schematic of the test setup is shown in Figure.27. The membranes were 2 mm wide and 3.5 cm in length, with a free length of 3 cm when positioned in the clamp, and all the films are fixed in 300 um thick. Then the displacement and the geometry of the benders were measured by input different voltages and frequency.

10.1.3.Result and Discussion

10.1.3.1 Iongel and Fabrication of actuators

As shown in Figure 56, PP1 and PPW1 are all successfully synthesized. Apparently, PPW1 shows better dispersion than PP1. That may be because the PVP shows excellent stabilize ability for SWNTs inside iongel and makes the SWNTs perfectly dispersed after synthesized. However, even under the stirring for a long time, PP1 without PVP still shows worse dispersed SWNTS inside iongel.

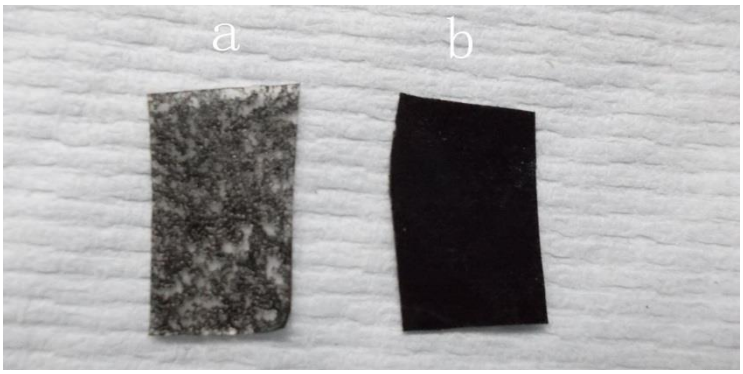

Figure 56. the picture of iongel after synthesis samples (a) the PAA-PAN iongel without PVP, (b) the PAA-PAN iongel with PVP (10% W/V).

10.1.3.2 FT-IR

To identify the ion associations within ionic liquid-swollen actuators, the Fourier transform infrared spectroscopy was used. Several researchers have performed FTIR studies of PAA polymer which have concluded that the peak that is observed near 1733 and 1710 cm^{-1} in the spectrum corresponds to the non-bonded and hydrogen-bonded carbonyl group in the acrylic acid segment (shown in Figure 57). Following the theory of Marek, whose experiment performed a detailed analysis of one peak between water and acrylic acid group. They observed that the carbonyl band at 1733 and 1710 cm^{-1} are absent and instead the two new bands at 1407 and 1547 cm^{-1} appear. In Figure 4, it could see the peak of 1691

cm^{-1} which related to hydrogen-bonded carbonyl group of acrylic acid group of P1-H polymer. While, after swollen ionic liquid of Emim, the two new bands at 1446 and 1569 cm^{-1} appear which suggest the association between acrylic acid and Emim solvent inside iongel. As shown in Figure 57. Also, I could find out that the peak of 1643 cm^{-1} proves the existence of PVP inside the film. What is more, the shift of 1643 cm^{-1} peak from 1680 cm^{-1} show that PVP has the hydrogen bonding with acrylic acid group in the polymer as well.

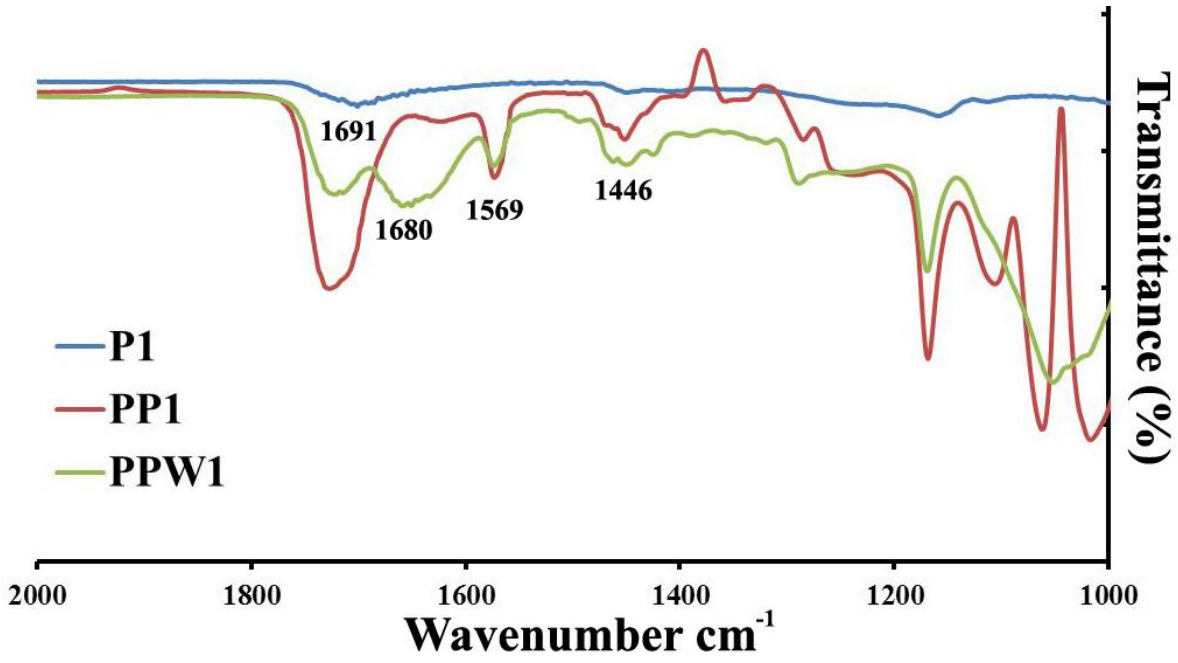

Figure 57. FTIR spectra of P1, PP1 and PPW1.

10.1.3.3 Electromechanical Characterization

Prior the fabrication of the actuators by supersonic cluster deposition, for the first electromechanical characterization, I used a thin silver layer painted onto the polymer surfaces using a commercial silver paint (silver conductive paint, RS company) to first test the materials on a basic level. The objective of this preliminary tests was to check if the materials exhibited actuation and to which extent, and contextually to spot out the main differences between the different material formulations. As seen

from Figure 58, the bending response of the actuators based on the PPW1, and PP1 films are performed at alternating square wave voltages of ±5V and frequencies of 0.5 Hz and 0.05 Hz. The displacement (d) was measured from the position of the actuator tip and a negative sign in the d-value indicates that –5V was applied to the actuator to yield the bending motion in the opposite direction. Figure.66 also shows that the largest displacement exceeding 4.2mm was achieved by the film of PPW1 with a cycle time of 20s, whereas 1.2 mm was were obtained with the use of PP1. Comparing with those two films, P1 shows no bending ability in the whole test. Apparently, the cation of TBA plays an important role during the actuation of the iongel as the active ions, while [EMIM][BF_4] is just the solvent inside of gel. When applying the voltage, TBA^+ ions will move from one side to another side of the gel which will result in imbalance of osmotic pressure of Emim and make the [EmIm][BF4] solvent accumulate to one side and shows physical bending behavior. Also, the larger performance from PPW1 than PP1 may suggest that PVP could remarkably improve actuation behavior of actuators by enhancing the mechanical properties of the iongel and better dispersion of SWNTs inside iongel.

Furthermore, table 7 also shows the strain-frequency dependency of the actuator compared with the values reported in the literatures. The actuation properties distinctly deviated from the trend line, that is, large displacement were recorded at ±5V in the frequency range of 0.05 Hz, while, smaller displacement was in 0.5 Hz. For example, for PPW1, at 5V the actuator strip moved 4.7 mm in 0.05 Hz and then reached to a displacement of 1.5 mm in 0.5 Hz, suggesting that the actuator could be successfully operated with a small battery and in controlled movement by tuning the frequency. Considering the uncertainty related to the nature and fabrication procedure of the silver electrodes, this actuation behavior constitutes a remarkable and promising result. The use of SCBI as the electroding technique is expected to improve the performance of the actuators, due to the nano-structured morphology of the implanted metal layer, which can enhance the electrode

capacitance.

It should be noted that, comparing with iongel which loaded with HNC, the SWNTs loaded iongel with silver paste as the electrodes did not show any better actuation performance, but instead, the displacement is smaller than HNC loaded actuators which suggests that the dissociation resulted from HNC/ionic liquid is better than π-π interaction between the carbon layer with ionic liquid.

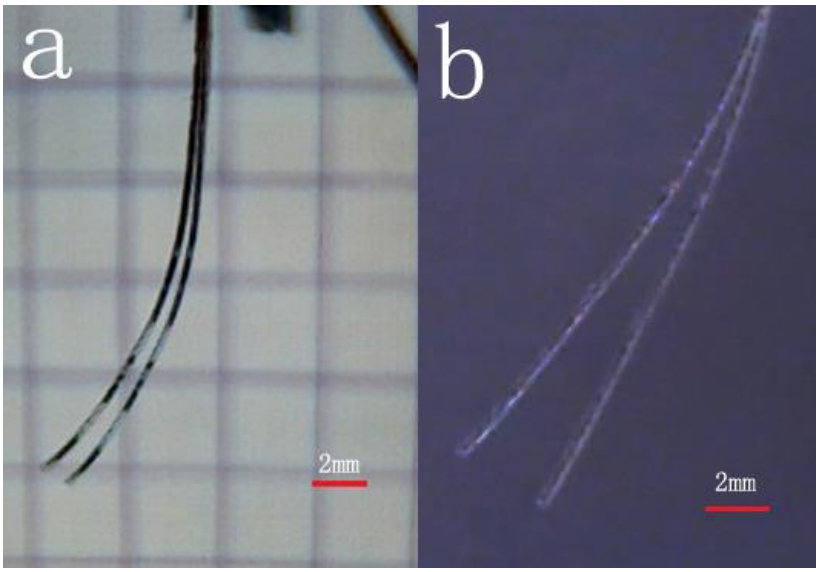

Figure 58. bending performance of actuators (a) the performance of actuator based on PP1 (b) the performance of actuator based on PPW1.

Frequency	0.05 Hz		0.5 Hz	
Polymer	Bending angle(º)	Dispalcement (mm)	Bending angle(º)	Dispalcement (mm)
P1	0	0	0	0
PP1	3	1.25	0.7	0.2
PPW1	10	2.8	2	1.3

Table 7. the actuation ability of actuators.

10.1.3.4 Supersonic cluster beam implantation: ionogel/gold nanocomposites and electro-mechanical behavior.

As seen from Figure 59, the electrodes assembled on the surface of iongel proves that SCBD technology here is an wonderful tool for fabricating the flexible electrodes of actuators which potentially support the mass production of actuators in the future. And, I also did the test for PPW1 which is fabricated by supersonic cluster deposition technology (gold electrodes has nominal thickness of 150 nm). A shorter cantilever (10 mm long, 1.5 mm wide) was used and the results obtained seem particularly promising (Figure.67b and Table 8), considering the relatively small length of the actuator.

Figure 59. bending performance of actuators (a) the picture of actuators based on PPW1 after implanted with gold.

(b) Bending behavior of the actuator.

Frequency	0.05 Hz		0.5 Hz	
Polymer	Bending angle(º)	Dispalcement (mm)	Bending angle(º)	Dispalcement (mm)
PPW1 (silver paste)	10	2.8	2	1.3
PPW1 (SCBD)	10	2.6	1	0.2

Table 8. the actuation ability of actuators.

10.2 Iongel actuator performance test influenced by different fillers

10.2.1.Methods and Materials

10.2.1.1 Synthesis Iongel actuator with different filler

In this section, the effects of different fillers on the electromechanical response of the ionic gell are reported. The filler used were (Poly(3,4-ethylenedioxythiophene)) PEDOT, MWCNT, Silver Nanoparticles (100nm), graphene oxide powders, Ruthenium(IV) oxide, silica, sodium, Y zeolite, hydrophilic bentonite, kaolinite. All the fillers I choose are because of the reported electro-properties like π-π interaction, and dyes loading ability. And all chemicals were purchased from Sigma Aldrich. The one-pot synthesis was carried out at room temperature, mixing the reagents in a 4 ml glass test tube. 547.5 µl of AA were mixed with 130 µl of AN and subsequently added in a 650 µl solution containing $EmimBF_4$ and H_2O ($EmimBF_4$: H_2O = 7 : 3 v/v), in which 26 mg of tetraethylammonium fluoride (TEAF) were previously dissolved under stirring for 3 hours. Then, EGDMA (19 µl) was added in the solution. After manually stirring the tube for 10 minutes, 30 mg of the filler were dispersed in the mixture respectively. Poly vinyl pirrolidone (PVP) was again used to facilitate the dispersion of the nanostructures (100 mg). The solution was then stirred overnight at 900 rpm using a magnetic stirrer. After stirring, the initiator was added to the test tube. 30 µl of a dimethyl sulfoxide solution containing 2,2-Dimethoxy-2-phenylacetophenone (0.15 w/w) was added to the test tube. The polymerizing solution was then vigorously stirred and injected in a silicone frame, positioned on a glass slide (2 mm thick). A second glass layer was used as a lid to spread the liquid into the frame and after the molding system was clamped, the apparatus was exposed to UV light for 1 hour. The equipment used to induce the photo-cross-linking was a UVLS-24 EL series (UVP) lamp, endowed with a 4 W light bulb. After polymerization, the formed ionic gel film was peeled off the glass, fixed into a 3D printed poly lactic

acid (PLA) frame, and positioned into a dryer overnight to remove water residuals.

10.2.1.2 Synthesis Iongel actuator with different salt

The one-pot synthesis was carried out at room temperature like normal IGMN synthesis described above, the difference is that each tube is added 26 mg of tetraethylammonium fluoride (TEAF), Tetrabutylammonium fluoride(TBAF), tetraethylammonium hydroxide(TEA.OH), Tetrabutylammonium hydroxide (TBA.OH), tetraethylammonium tetrafluoroborate ($TEA.BF_4$) respectively. After synthesis, al the samples are fixed with PLA frame and keep them in vacuum for 2 days before the fabrication.

10.2.1.3 Synthesis Iongel actuator with different amount of PVP

The one-pot synthesis was carried out at room temperature like normal IGMN synthesis described above, the difference is that each tube is added 50 mg of PVP, 100mg PVP, 150mg PVP and 300mg PVP respectively. After synthesis, al the samples are fixed with PLA frame and keep them in vaccum for 2 days before the fabrication.

10.2.1.4 Synthesis Iongel actuator with different amount of nanoclays

The one-pot synthesis was carried out at room temperature like normal IGMN synthesis described above, the difference is that each tube is added 10 mg of HNC, 30mg HNC and 60mg HNC respectively. After synthesis, al the samples are fixed with PLA frame and keep them in vacuum for 2 days before the fabrication.

10.2.1.5 Electro-mechanical performance

After the treatment of the vacuum, the iongel film is taken out. Then, silver conductive paint (RS Company) was used to paste the iongel surface to fabricate the simple electrodes on both side. After be kept in vacuum for 30 mins, the actuators were successfully fabricated for electro-mechanical performance tests, which could be used as systematic probes to find out the best composition of iongel and may influence the performance of actuator. Although such tests could not be highly reliable due to the rough surface of electrodes resulted from silver conductive paint, the results from the performance of such actuator based on different composition could still be a reference to test the different iongel actuators.

For the actuation testing, the actuators were clamped in a cantilevered configuration and allowed to bend freely. A schematic of the test setup is shown in Figure.61. The membranes were 2 mm wide and 3.5 cm in length, with a free length of 3 cm when positioned in the clamp, and all the films are fixed in 300 um thick. Then the displacement and the geometry of the benders were measured by input different voltages.

10.2.2. electro-mechanical behavior of actuators

The result in table 9 proves that only carbon based materials as the filler rather than inorganic particles could confer the iongel ability to become the actuator and offer the reasonable bending performance. The reason why these particles could not affect the iongel and form gel based actuator is maybe because this new kind of iongel is highly relying on the ion distribution between the network of carbon based materials and ionic liquid which resulted high ratio of ion dissociation of ionic liquid, however, the inorganic nanoparticle may influence the electronic conductivity rather than ion

conductivity. Furthermore, from the result I also found out that the structure of clays influence the bending performance a lot. In the test, in the same working condition, the displacement of actuator is as following: SWNTs>MWNTs>PEDOT (data not shown). It apparently proves that the carbon in well structure will have a better ion dissociation property and single layer structure is better than multiple structure.

Type of gel	Type of fillers	Whether the actuators work(Y/N)
PAA-PAN iongel	PEDOT	Yes
PAA-PAN iongel	SWNT	Yes
PAA-PAN iongel	MWNT	YES
PAA-PAN iongel	Silver Nanoparticle	No
PAA-PAN iongel	Graphene oxide	No
PAA-PAN iongel	Gold nanoparticle	No
PAA-PAN iongel	RuO2	No

Table 9. the actuator performance with different filler.

Type of gel	Type of salt	Maxium displacement at 5V	Time to achieve the Max bending
PAA-PAN iongel	TEAF	17.32mm	28s
PAA-PAN iongel	TEA.OH	12.95mm	17s
PAA-PAN iongel	TEA.BF4	6.82mm	11s
PAA-PAN iongel	TBAF	13.12mm	73s
PAA-PAN iongel	TBA.OH	3.15mm	17s

Table 10. the actuator performance at 5V with different salt.

Type of gel	Type of salt	Displacement at 0.5Hz	Displacement at 0.05Hz
PAA-PAN iongel	TEAF	0.53mm	2.45mm
PAA-PAN iongel	TEA.OH	0.70mm	6.30mm
PAA-PAN iongel	TEA.BF4	0.53mm	2.45mm
PAA-PAN iongel	TBAF	0.35mm	0.35mm
PAA-PAN iongel	TBA.OH	0.35mm	2.63mm

Table 11. the actuator performance in different frequency with different salt.

Apart from the effect of the different fillers, salts also influence the bending behavior for the iongel actuators. From the table 10, it was found out that the TEA^+ (tetraethylammonium) salt has better actuator performance than TBA+, which could be the result from the radius of the salt. Also, even the salt shares the cation, if the anion is too large, the actuator performance will also decrease. However, from the table 11, it shows out that the OH- has better improvement in the frequency performance, it may suggest that higher pH may provide better frequency actuation.

Type of gel	Amount of PVP	Max displacement at 5V	Time to achieve the Max bending
PAA-PAN iongel	50mg	2.80mm	20s
PAA-PAN iongel	100mg	17.32mm	28s
PAA-PAN iongel	150mg	4.38mm	10s
PAA-PAN iongel	300mg	0.70mm	3s

Table 12. the actuator performance at 5V with different amount PVP.

Type of gel	Amount of PVP	Displacement at 0.5Hz	Displacement at 0.05Hz
PAA-PAN iongel	50mg	0.35mm	2.28mm
PAA-PAN iongel	100mg	0.53mm	2.45mm
PAA-PAN iongel	150mg	0.35mm	6.13mm
PAA-PAN iongel	300mg	0.18mm	0.53mm

Table 13. the actuator performance in different frequency with different amount PVP.

Also, from the table 12, the different amount of PVP influences the actuation performance as well. In the table, it apparently proves that 100mg PVP works better than 150mg, 300mg, and 50mg PVP in maximum bending ability. It may be due to the fact that PVP could confer the actuator a certain mechanical property which helps the actuator performance in the test. However, after the PVP amount attains a certain level (100mg) the overloaded mechanical property restricts the actuator performance instead. So, the reasonable amount of PVP is quite necessary for the actuator system in max bending.

From the table 13, it found out that only the 150mg PVP loaded iongel plays a better actuator frequency performance than others. It may suggest that the reasonable amount of PVP is quite necessary for the actuator system in frequency work.

Type of gel	Amount of clays	Max displacement at 5V	Time to achieve the Max bending
PAA-PAN iongel	10mg	21.7mm	22s
PAA-PAN iongel	30mg	17.32mm	28s
PAA-PAN iongel	60mg	7.75mm	28s

Table 14. the actuator performance at 5V with different amount PVP.

Type of gel	Amount of clays	Displacement at 0.5Hz	Displacement at 0.05Hz
PAA-PAN iongel	10mg	0.35mm	2.28mm
PAA-PAN iongel	30mg	0.53mm	2.45mm
PAA-PAN iongel	60mg	0.35mm	2.10mm

Table.15. the actuator performance in different frequency with different amount PVP.

By increasing the amount of the loaded nanoclays from 10 to 60mg, the max bending performance decreased from 21.7 mm to 7.75 mm. Even the nanoclays loaded iongel actuator is far better than the SWNTs loaded iongel, the reasonable amount of nanocalys imbedded into the iongel are still quite necessary for actuation. I think this is because the ionic liquid could only dissociated with certain amount of nanoclays with certain ratio, when increasing more nanoclays, the inogel mechanical properties are changed, and could become blocking force and limit the further actuation. However, from the result of table 15, the nanoclays seems like not be the effect to change the frequency work of the actuator at all.

11. Appendix B

Low-voltage electrically driven homeostatic hydrogel-based actuators for underwater soft robotics

Yunsong Yan[a,b] et.al

a) Centro Interdisciplinare Materiali e Interfacce Nanostrutturati (CIMaINa), University of Milan, Via Celoria, 16, 20133 Milan, Italy. b) European School of Molecular Medicine (SEMM), Campus IFOM-IEO, Via Adamello 16, 20139 Milan, Italy.

This chapter has been published.

Yunsong Yan;Lorenzo Migliorini;Tommaso Santaniello;Cristina Lenardi;Paolo Milani. "Low-voltage electrically driven homeostatic hydrogel-based actuatorsfor underwater soft robotics". Sensors and Actuators B: Chemical. 2016.

11. 1. Introduction

Synthetic ionic hydrogels able to change their shape in response to an applied electrical stimulus in aqueous environments are of strategic importance for the development of remotely controlled soft underwater actuators and robots [40-42]. These materials have the ability to absorb and retain large water amounts, still maintaining their solid state, and they present ionic groups covalently bonded to the main backbone, to which a mobile counter-ion specie is stably coordinated[43]. The embedded intelligence of this family of polymers dwells in their capability to undergo controllable swelling-shrinking cycles in the presence of an electric field, eventually leading to a bending deformation of the hydrogel, as a result of the mobile ions migration across the polymer[44-47].

This actuation mechanism strongly depends on the inter-play between a variety of factors, such as the material inner chemical and physical structure (e.g. monomers type and cross-linking degree), the ionic concentration difference between the polymeric matrix and the outside environment and the field intensity[48-50]. More specifically, the choice of the ambient solution ionic specie, the electrode geometry and configuration, as well as the actuator distance from the same, are all key elements to enable a fine control over the electro-mechanical performance of this class of responsive polymers[51]. Furthermore, having fixed both the material properties and working conditions, the electrically induced deformation and actuation speed of the components scale according to their dimensions i.e. faster response time (up to the order of few hundred of milliseconds) and larger bending angles (above 90°) are favored at the micro-scale, as demonstrated by the production of artificial micro-swimmers and miniaturized aquabots[52, 53]. Although the protocols and setups employed for the electro-mechanical characterization of hydrogel-based materials are extremely broad[53], it is possible to identify several common features related to the actuation properties of this class of polymers and to highlight their main limitations.

Despite the low electrochemical window of water (1.23 V), the actuation of electro-responsive hydrogels shaped as macroscopic bending cantilevers or freestanding cylinders in saline aqueous solutions is restricted to the use of relatively high voltages as the triggering stimulus (3 V to 30 V)[54-58]. At this working condition, water electrolysis and perturbation phenomena connected to the generation of gases, such as bubbling at the electrodes, inevitably take place in the ambient solution, therefore limiting the life time and application area of the actuators[59-61]. Moreover the characteristic bending speed observed for the most performing electro-active hydrogels, such as poly (acrylic acid), poly vinyl alcohol or poly styrene sulfonate based polymers, has showed to reach values up to 5 °/s[62-65]. However, a dynamic bending behavior that could resemble the angular speed

exhibited by micro-cantilevers (from 10 to 20 °/s) at larger spatial length scales would be highly relevant for a variety of applications, such as the production of propulsive biomimetic subaqueous soft robots and for the integration of smart stirring systems in bioreactors[66-68].

Examples of electro-active hydrogels working at the sub-Volt regime have only been reported for micro and mesoscale sized hydrogel strips, which could be operated as bending micro-actuators or smart valves and mixing pumps in microfluidic devices[69-71]. To our knowledge, no evidence of electro-responsive hydrogel-based materials that can function at the macroscale level as high-performance bending actuators at working voltages below 1 V has been reported so far.

Here we report the synthesis, fabrication and characterization of a novel electro-responsive hydrogel based on Na-4-vinylbenzenesulfonate (Na-4-VBS), which operates as a fast response soft actuator in the voltage range between 0.2 V and 5 V in NaCl aqueous solutions, with concentration going from the milli-molar to the molar range. The produced polymer showed similar performance in environments of biological interest, such as Phosphate Buffer Solution (PBS) and Dulbecco's Modified Eagle's Medium (DMEM). The manufactured polymeric actuators are Uv photo-polymerized freestanding layers, having macroscopic dimensions in their length and width and variable thickness of 0.1 and 0.3 mm. The results obtained in terms of electro-mechanical actuation are correlated to the swelling properties of the materials in the different aqueous environments, which are experimentally determined with the blot and weigh method[72].

11.2. Materials and method

11.2.1. Hydrogel preparation and swelling

The material is a three-component co-polymer, comprising also hydroxyl ethyl methacrylate

(HEMA) and poly acrylonitrile (AN). The presence of the hydroxyl side groups characteristic of the HEMA monomer confers high hydrophilicity to the hydrogel and also offers potential to its further functionalization (e.g. with bioactive molecules coating), while AN provides mechanical toughness and elasticity to the structure.

I synthesized samples using three different formulations of the material, by varying the amount and the relative ratio of the co-monomers Na-4-VBS/HEMA/AN as follows: 0.5/6.5/3.0 mmol (PSS5%), 1.0/6.5/2.5 mmol (PSS10%), 2.0/6.0/2.0 mmol (PSS20%). This approach was chosen to investigate on the effect that the amount of Na-4-VBS has on the electro-active properties of the hydrogel. The HEMA quantity was always kept at least at 60% of the total co-monomers amount to ensure a high degree of hydrophilicity to the polymers, while the AN percentage was varied accordingly. The synthesis and manufacturing procedure of the polymeric layers can be described as reported below. The UV initiator solution was prepared using 2,2-dimethoxy-2-phenylacetophenone (DMPA), 0.7 M, in dimethylsulfoxyde (DMSO). The three monomers, Na-4-VBS, HEMA and AN, were sequentially dissolved in 1.3 mL of pure water (MilliQ type) in a glass test tube. The cross-linker, ethylene glycol diacrylate (EGDA), 0.053 mmol, and the catalyst, N,N,N'N-tetramethylethylendiamine (TEMED), 0.15 mmol, were then added to the mixture. Finally, 30 µL of the initiator solution were injected and the preparation tube was vigorously stirred for 1 min. The resulting low viscosity liquid was a completely transparent solution. A three-components mold was used to shape the hydrogel layers. This comprised a square silicon spacer (80x80x0.3 mm^3 or 80x80x0.1 mm^3), having a 40x40 mm^2 wide hollow region for the injection of the polymerizing solution, which was positioned on a 2 mm thick glass slide. After injection of the liquid, the mold was sealed by a second identical glass component and the system was appropriately clamped. The molding apparatus was then exposed to UV radiation (λ= 365 nm) for one hour, to ensure homogeneous and full cross-linking of the hydrogel. The equipment used was a

UVLS-24 EL series (UVP) lamp, endowed with a 4 W light bulb; this relatively low power does not produce any significant heating of the samples during the irradiation process. This simple yet effective fabrication protocol enabled to achieve PSS-co-PHEMA-co-PAN co-polymer based freestanding layers. The chemical structure and synthesis scheme of the co-polymer are represented in Figure 60. As firstly evaluated on a qualitatively level, the resulting product was a transparent, elastic and dull film. After removing the hydrogel from the mold, the material was immediately soaked in pure water, in order to wash out the unreacted compounds. During this process, which lasted 24 hours, hydrogels underwent a volumetric increase due to water absorption. After hydration, each sample was cut in four pieces and then immersed for 24 hours in three NaCl aqueous solutions with different concentration (0.005 M, 0.05 M, 0.5 M) and in PBS whose Na+ concentration was 0.137 M). To have quantitative information on the swelling phenomenon, we used the blot and weigh method and calculated the Swelling Ratio (Sr) as the ratio between the samples weight after and before immersion in the aqueous solutions.

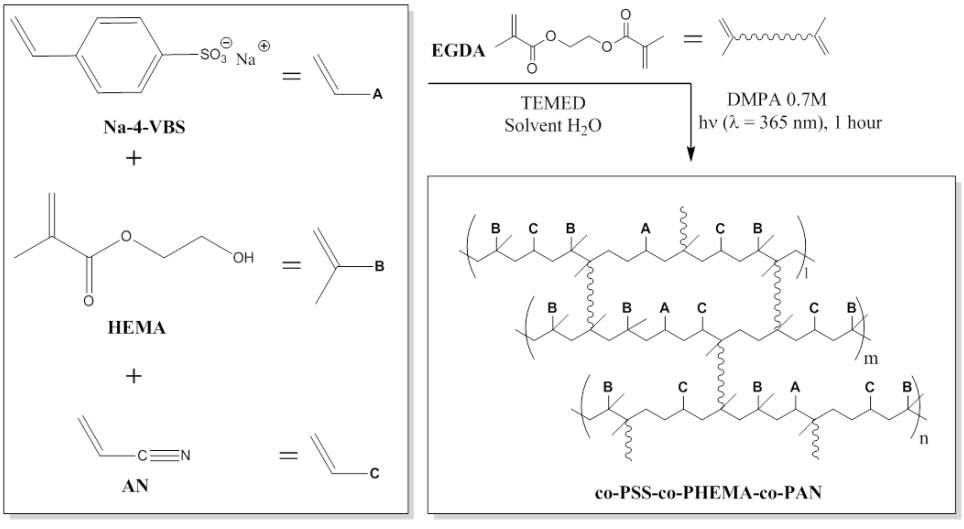

Figure 60. Synthesis schematic and chemical structure of the PSS-co-PHEMA-co-PAN hydrogel.

11.2.2. Electro-mechanical characterization

Once the samples PSS5%, PSS10% and PSS20% have reached the swelling equilibrium in solution A (NaCl 0.005 M), B (NaCl 0.05 M) and C (PBS, Na^+ 0.137 M), electro-mechanical actuation tests were carried out in the same environments. Solution A and B were chosen because their concentration is significantly inferior to the expected Na^+ concentration inside the gel, while PBS constitutes a solution of biological interest. For the latter reason, DMEM (High Glucose type) cell medium was also used in the actuation tests (Na^+ concentration is about 0.154 M). Bending characterization took place in a 10 cm diameter Petri dish positioned above a millimeter grid. Each swollen sample was cut as a cantilever (15x2x0.3 mm^3 and 15x2x0.1 mm^3), having a larger square basis to be fastened (5x5 mm^2). The electrodes employed were two Platinum wires (0.25 mm diameter), each of them positioned 10 mm apart from the free end of the hydrogel. Both samples and electrodes were clamped and then fixed in a custom-designed Teflon apparatus (Figure.61). In each test, a potential difference (ΔV) going from 0.2 to 9 V was applied between the electrodes, in order to explore both low (0.2 to 5 V) and high (6 to 9 V) voltages. The frequency response of all samples was also tested by applying a square wave of variable amplitude (1 to 5 V) at the electrodes, with frequency ranging from 0.5 to 2 Hertz, in order to assess the materials suitability to operate as resonating soft structures in liquid (e.g. soft smart stirrers, fast response valves or propulsive motion generators). To ensure a high degree of homogeneity of the electric field along the full width of the cantilever, two gold electrodes having surface area of 35x10 mm^2 were coated on a 0.3 mm brass-based foil using physical evaporation and then employed in the characterization setup (Figure 61). The equipment used for the metal deposition was an Edwards Coating System (model E306A). By using a camera connected to a personal computer, videos were captured for each test and then analyzed to calculate the angular speed w (°/s) of the cantilevers, using an image processing software (ImageJ). All the

experiments were conducted at room temperature, as regularly measured by immersing a thermometer in the solutions.

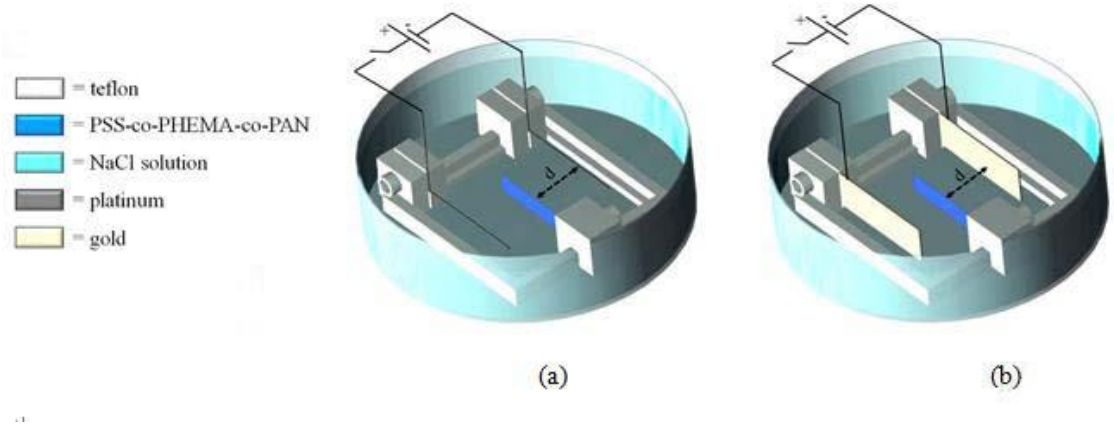

Figure 61. 3D modeling of the setups employed for the hydrogels electro-mechanical characterization.a) Configuration 1: the electrodes were thin platinum wires (diameter is 0.25 mm). b) Configuration 2: gold plated layers were used as the electrodes. In both cases, the distance d between the sample and the electrodes is fixed as 10 mm.

11.3. Results and Discussion

11.3.1. Swelling behavior in saline aqueous solutions

Hydrogels swelling was monitored in pure water and in all the saline solutions A, B, C and D (NaCl 0.5 M). The estimated concentration of Na+ after polymerization (Cg,0) was 0.38 M, 0.77 M and 1.54 M for PSS5%, PSS10% and PSS20% respectively. Once swelled in pure water, the hydrogels were weighted and we calculated that the samples absorbed 1.4 mL, 4.0 mL and 4.8 mL of solvent respectively and the related Na+ concentrations inside the gels (Cg) were then estimated to be 0.17 M, 0.18 M and 0.24 M. On a qualitative level, we observed that the swelling in pure water was more pronounced for larger Na-4-VBS amounts incorporated in the polymer. After soaking the materials in the saline solutions directly from the water bath, all hydrogels underwent shrinking, which extent was increasingly larger

for larger values of Cs. In Figure 62, the swelling ratio Sr of PSS5%, PSS10% and PSS20% is reported as a function of the concentration of solution A, B, C and D, expressed in the logarithmic scale (pC = - logCs). It can be seen how the swelling of the samples increases for higher values of Cg,0 (i.e. higher Na-4-VBS amounts), while decreases for higher values of Cs.

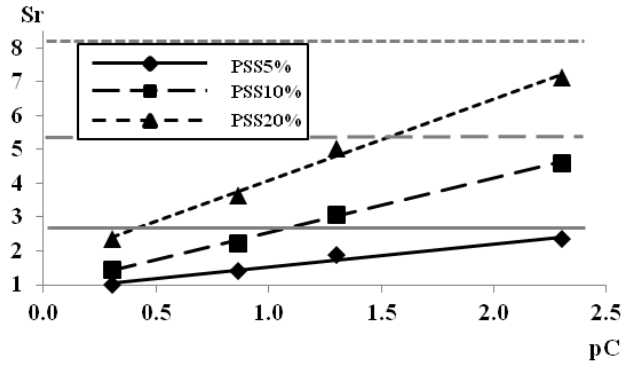

Figure 62. Swelling ratio Sr of the produced hydrogels as a function of the NaCl concentration of solutions A, B, C and D(the x-axis is reported in the logarithmic scale). The reference state for calculating Sr was the weight of the hydrogels in their relaxed state immediately after synthesis. The straight lines represent the equilibrium value Sr,max of the materials in pure water.

From the general point of view, the volumetric increase of the films in water is due to the osmotic pressure Δπ and its extent results larger for larger hydrogel hydrophilicity and porosity. The osmotic contribution is strongly dependent on the amount of mobile Na+ cations conjugated with the fixed anionic sulfonate groups bonded to the co-polymer backbone. In fact, Δπ spontaneously originates in the attempt to minimize the cations concentration difference (ΔCgs) between the permeable gel film (Cg) and the ambient solution (Cs, which is equal to zero for pure water), therefore promoting the penetration of H_2O molecules into the material inner structure. The water flux into the matrix stops whenΔπ is balanced by the mechanical stress of the polymer chains and equilibrium is reached. Since Δπ is proportional to ΔCgs, varying saline concentration in the swelling liquid environment and the amount of Na-4-VBS used for the synthesis permits to modulate the entity of the samples volumetric

increase. This behavior was confirmed by experimental data. In the the graph of Figure 3, the three horizontal lines represent the maximum swelling ratio (Sr,max) reached in pure water for each sample. It is interesting to notice how the value of Sr plotted against the saline solutions concentration in the logarithmic scale could be interpolated by straight lines, described by the linear equation Sr = σ (pCs) + Sr,0, where Sr,0 is the virtual value that Sr would have in a 1 M NaCl solution, while σ can be defined as the Swelling Coefficient. The parameters describing the swelling characteristics of PSS5%, PSS10% and PSS20% were calculated and reported in Table 16. As can be seen, both Sr,max and σ seemed to increase with Cg,0.

	PSS5%	**PSS10%**	**PSS20%**
$C_{g,0}$ **(M)**	0.38	0.77	1.54
$S_{r,max}$	2.66	5.30	8.15
σ	0.68	1.60	2.42
$S_{r,0}$	0.86	0.93	1.67

Table 16. Parametrization of the swelling characteristics for the PSS-co-PHEMA-co-PAN samples.

Beside their responsive behavior when electrically stimulated, the ability of the materials to change size according to the outside concentration renders them good candidates to be used as purely homeostatic actuators, which have potential applications in microfluidic systems (e.g. as ionic strength sensitive valves) or as drug delivery vectors responsive to specific solute concentrations in biological media. However, in the framework of the proposed work, what is of primary interest is that the swelling characteristics of the PSS-co-PHEMA-co-PAN co-polymers and their related homeostatic features strongly affect their electro-mechanical behavior.

11.3.2. Actuators performance

The electro-mechanical actuation of PSS5%, PSS10% and PSS20% was initially tested using 0.3 mm thick samples positioned between two Platinum electrodes in solution A, B and C. After the application of the electric field, all samples showed bending towards the cathode. This deformation behavior, which was not expected a priori, has already been reported for anionic electro-responsive hydrogels actuated in low concentrated saline solutions and it strongly depends on the value of ΔCgs[73, 74]. By inverting the bias the actuation resulted to be reversible. All samples responded to the applied electric field above 3 V, except PSS5%, which was sensitive to the stimulus starting at 2 V in solution A. For increasing values of the voltage, bending angle and actuation speed increased as expected. The bending angle α showed to increase almost linearly with the applied voltage for each material formulation, while for fixed values of ΔV it showed to decrease for increasing Na-4-VBS content and outside solution concentration. At 3V, α did not exceed 11°, at 5V it was equal to 20°, while for higher voltages the maximum angle that could be reached, according to the electrodes spatial configuration, was about 30°. Results concerning the bending speed are reported in Figure 63, where w is plotted as a function of ΔV for PSS5%, PSS10% and PSS20% in the three saline solutions.

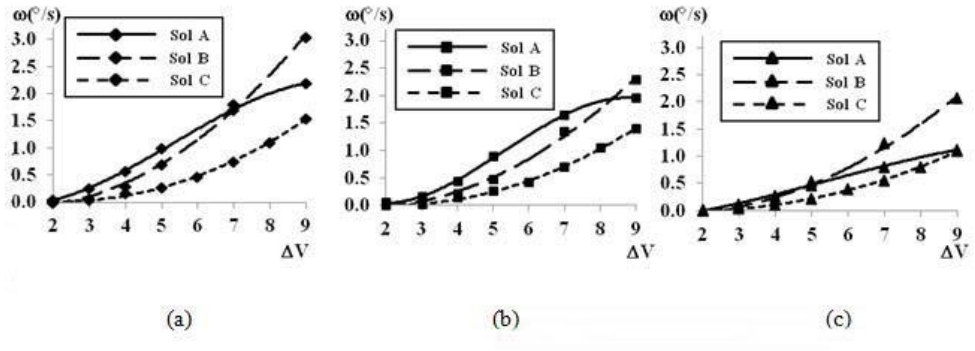

Figure 63. Bending speed w for the three PSS-co-PHEMA-co-PAN formulations in solution A, B and C plotted against the applied voltage.a) PSS5%. b) PSS10%. c) PSS20%.

It is possible to distinguish two different behaviors: a low-voltage regime (ΔV < 5V), where w~ ΔV2 and faster bending is reached in solution A, and a high-voltage regime (ΔV > 5V), where the parabolic profile of w is progressively lost and faster bending is reached in solution B. The w values obtained in solution C are the lowest at any applied voltage and regardless the Na-4-VBS amount incorporated in the polymer. By focusing on the voltage-regime of main interest (2 to 5 V), the overall results can be summarized as follows. i) The bending speed resulted to be larger for lower saline concentrations of the outside solution, regardless of the specific hydrogel formulation. ii) PSS5% showed faster bending with respect to PSS10% and PSS20% in all the environments. This behavior was particularly emphasized in solution A (Figure 64a), where w reached the value of 1°/s at 5 V. This constitutes a remarkable result, which is further valued by the fact that the electrodes employed have a width of about ten times smaller than the one of the actuators (0.25 mm versus 2 mm) and therefore the intensity of the generated electric field is not homogeneously distributed along the cantilevers body. iii) Although provided with the largest amount of the electro-active monomer, PSS20% showed to be the less performing actuator in all the experimental conditions tested. In Figure 64b, the values of w at 5 V are plotted against pCs for each sample, in order to give insights on the bending speed dependency on the Na-4-VBS amount and the outside concentration.

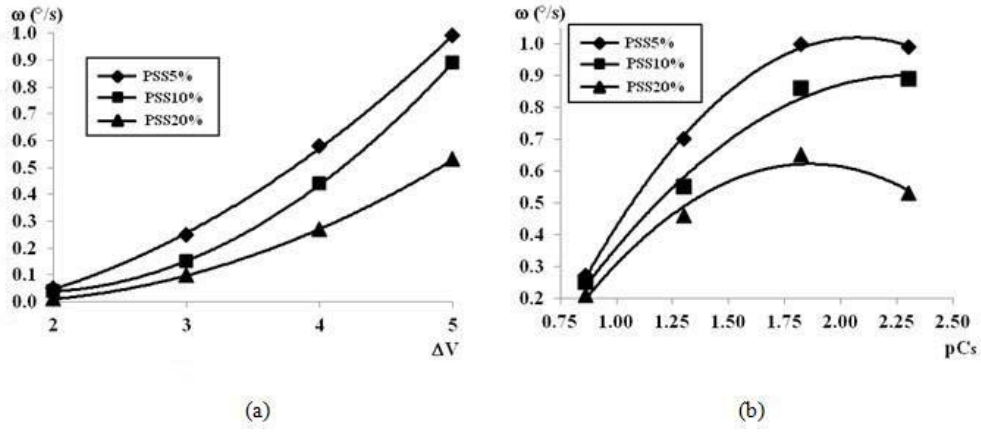

Figure 64. Actuation speed of different actuators. a) Actuation speed for PSS5%, PSS10% and PSS20% in solution A in the low-voltage regime. b) Actuation speed for PSS5%, PSS10%, PSS20% at 5V as a function of the NaCl

concentration (x-axis is express in the logarithmic scale). W values at Cs = 0.015 M were also measured at 5 V to increase the number of data points.

For what concerns the actuators frequency response, all the specimen were able to symmetrically bend at 5 V for frequency up to 1 Hz in all the saline solutions and the bending angle decreased as the driving frequency was increased. Moreover, PSS5% showed to stably oscillate for frequencies up to 2 Hertz in solution A and B. For this hydrogel formulation, the bending angle was measured as 1° (tip displacement = 0.3 mm) at 1 Hz and as 0.48° (tip displacement = 0.1 mm) at 2 Hz in solution A. No systematic tests to investigate on possible fatigue effects on the materials induced by multiple bending cycles was carried out for this bunch of samples.

Since PSS5% showed to be the most performing actuator in the low-voltage regime in all of the solutions tested, samples having the same material formulation, but thickness of 0.1 mm (namely PSS5%-01), were produced and their electro-mechanical response characterized. We conducted this new group of experiments in order to investigate on the effect that the material thickness has on the actuation, but still using benders with macroscopic dimensions in their length and width. Despite their relatively small thickness, the produced PSS5%-01 benders could be easily handled as freestanding components. Using the same experimental setup and conditions, the new actuator was firstly tested in solution A and a dramatic increase in the bending angle and speed of actuation was observed. More interestingly, PSS5%-01 showed high responsiveness, starting its deformation at 1 V, with a bending angle of 1.4° (w = 0.70 °/s). At 5V, α reached the value of 30° (maximum angle achievable according to the setup configuration), with a bending speed of 9.3 °/s, i.e. about ten times the speed of the 0.3 mm thick sample having the same material formulation.

In order to provide a more homogeneous electric field along the hydrogels width, we then carried

out a systematic characterization of the PSS5%-01 samples in solution A, B and C, using the gold plated electrodes and by varying the voltage from 0.2 to 3.0 Volt. Using the same experimental setup and voltage range, we also tested PSS5%-01 in DMEM (High Glucose type). This cellular medium is widely used for in vitro cell culture and therefore it represents a model environment for the application of PSS-co-PHEMA-co-PAN in biological solutions. The results of all these tests on PSS5%-01 are shown in Figure 65.

As shown in Figure.65b, PSS5%-01samples tested with gold electrodes demonstrated responsiveness starting at 0.2 V and the observed values of w went through a dramatic increase in all the voltage range employed, still maintaining the actuation profile characteristic of the first group of hydrogels tested. The bending angle also showed a remarkable increase, reaching 30° at 1.5V in all of the solutions tested; in particular, α was equal to 12° at 0.4V and equal to 25° at 1V in solution A. The actuation performance of PSS05%-01 at 1 V can also be observed in the video reported in the Supplementary Content.

Once again, it is possible to distinguish between two voltage regimes. In the high-voltage one (ΔV > 1.7V) faster bending is reached in solution B (α=30°and w = 22°/s at 3V). In the low-voltage regime, below the potential of water electrolysis, PSS5%-01 showed an excellent performance, considering also the macroscopic size of the cantilever (Figure.65d), reaching faster bending in solution A, with α= 29° and an angular speed w = 3.6°/s at 1.2 V. Although the bending speed observed in solution C is still relatively small in both low- and high-voltage regime, in this environment PSS05%-01 showed high responsiveness (starting from 0.2V) and values of w three hundred times higher than those obtained with the 0.3 mm-thick PSS5% (for which α=9º and w= 1.1°/s at 1.2V and α=30°and w = = 12°/s at 3V). The overall actuation profile and values recorded for PSS5%-01 in DMEM are almost comparable to those obtained in PBS, because of the similar concentration of NaCl present in both

media. The frequency response of PSS5%-01 was also tested in solution A with the gold electrodes. At 1.2 V it showed a bending angle of 3.6° (tip displacement of 0.9 mm) at 1 Hz and of 1.8° (tip displacement of 0.5 mm) at 2 Hz, while at 3 V α was equal to 16.3° (tip displacement of 4.4 mm) at 1 Hz and equal to 8.2° (tip displacement of 2.2 mm) at 2 Hz.

In Figure 66, PSS5%-01 bending speed at 1, 2 and 3V, measured using the gold electrodes, is plotted against pCs. At 1 V (under the potential of water electrolysis) w increased monotonically with pCs. Considering higher voltages, the bending speed profile shifted to larger values and showed a characteristic curvature, which led to the maximum value w_{max} at an intermidiate concentration between 0.05 M and 0.005 M.

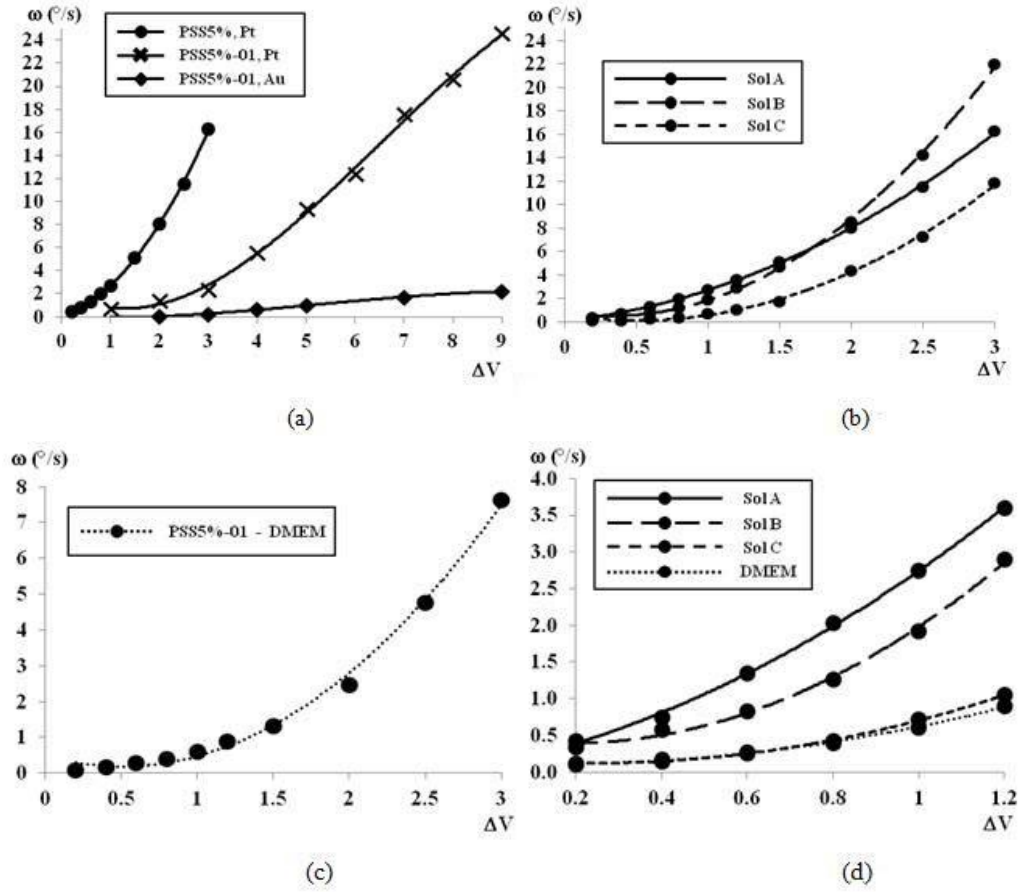

Figure 65. Bending speed plotted against the applied voltage for different actuators: a)PSS5% and PSS5%-01 tested using the platinum electrodes, compared with PSS5%-01 tested using the gold electrodes, in solution A. b)

PSS5%-01 tested with gold electrodes in solution A, B and C (ΔV from 0.2 to 3.0 V). c) PSS5%-01 tested with gold electrodes in DMEM (ΔV from 0.2 to 3.0 V). d) PSS5%-01 tested with gold electrodes in solution A, B, C and DMEM (ΔV from 0.2 to 1.2 V).

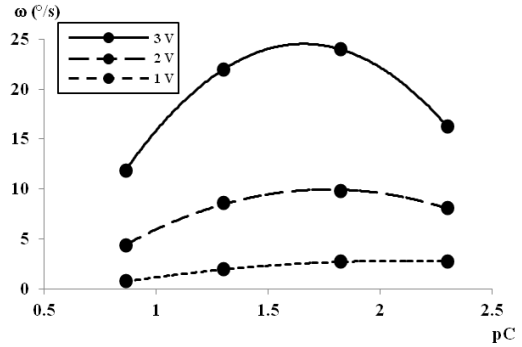

Figure 66. Actuation speed of PSS5%-01 at 1V, 2V and 3V as a function of NaCl concentrations(x-axis is express in the logarithmic scale). W values at Cs = 0.015 M were also measured to increase the number of data points.

Considering the experimental setup and the electrodes configuration employed, the observed actuation features of this novel copolymer are particularly interesting for the design of hybrid materials soft robotic systems able to provide finely controlled and complex motion in liquid environments. The production of tightly anchored gold layers on soft stretchable substrates, such as gold nanoclusters implanted in poly dimethyl siloxane (PDMS), has been reported in the literature, while in our previous work we demonstrated that PHEMA-based hydrogels has potential to be interfaced with surface modified elastomeric components[2, 75]. Therefore, merging the actuation performance of the PSS-co-PHEMA-co-PAN hydrogels with the geometrical flexibility and electrical stability of deformable PDMS/gold nanocomposite-based electrodes in a single architecture constitutes a promising solution for the realization of a new class of controllable self-regulating bio-inspired artifacts.

11.3.4. Electro-mechanical actuation model

From the general point of view, the total osmotic pressure acting on the hydrogels swollen in the saline solutions ($\Delta\pi_{Tot}$) can be expressed in terms of three contributions, which are related to the affinity of the polymer matrix with the swelling solvent ($\Delta\pi_{Mix}$), the elasticity of the cross-linked macromolecules ($\Delta\pi_{Elas}$) and the mobile ionic species concentration inside and outside the gel ($\Delta\pi_{Ions}$)[76]. According to Flory's theory, which is applicable for neutral gels, the mixing contribution can be written as:

$$\Delta\pi_{\text{Mix}} = (\ln(1-v) + v + \chi v^2)\frac{RT}{V_M} \quad [1]$$

where v is the polymer volume fraction in the swollen hydrogel, χ is the polymer-solvent interaction parameter, VM is the molar volume of the hydrogel, R is the gas constant and T is the temperature. The elastic term can be expressed as:

$$\Delta\pi_{\text{Elas}} = (v^{1/3} + \frac{v}{2})\frac{RTv_c}{V_0} \quad [2]$$

where vc is the number of cross-linked polymer chains and V0 is the volume of the hydrogel in the reference relaxed state. The ionic contribution depends from the values of Cg and Cs, and can be written as:

$$\Delta\pi_{\text{Ions}} = RT\sum_i(c_{g,i} - c_{s,i}) \quad [3]$$

where the index i refers to the mobile ionic species present in the system. Therefore, the total osmotic pressure is:

$$\Delta\pi_{Tot} = \Delta\pi_{Mix} + \Delta\pi_{Elas} + \Delta\pi_{Ions} \quad [4]$$

$\Delta\pi_{Mix}$ can be considered negligible with respect to $\Delta\pi_{Ions}$ for highly swollen polyelectrolyte gels, and therefore in the case of the electro-responsive hydrogels presented here, it can be reasonably assumed that ΔπTot = ΔπElas + ΔπIons. At equilibrium, ΔπTot = 0[77]. When an electric field is applied, the movement of the ions across the hydrogel layer induces changes in the local ionic concentration, leading to a variation of ΔπIons. The actuators bending results from the balance between this contribution and the elastic term, which is known to depend from the material swelling and the related chain stretchability[78].

Different models have been proposed to explain the behavior of electro-responsive hydrogels in saline aqueous solutions[57]. Due to the intrinsic complexity of the system, the reversible bending towards the cathode or anode is due to a superposition of effects, electrostatic and homeostatic, over which there is a dominating driving mechanism[79]. The bending behavior towards the cathode of the PSS-co-PHEMA-co-PAN hydrogels can be interpreted in the framework of the Dynamic Enrichment/Depletion model, which has already been used to describe the actuation mechanism of ionic polyelectrolytic gels in diluted saline solutions where Cg is higher than Cs[80]. According to the model, the bending motion is due to the anisotropic distribution of charged ions inside the polymer, caused by the application of an external electric field. Without the application of the electric field, the hydrogel is at rest and equilibrated in the saline solution (Figure 8-a). When the electric field is applied, in the boundary region between the anodic side of the gel and the solution, the cationic concentration goes through a dynamic and gradual decrease because of the mobile cations drifting (Figure 8-b). Since Cs is lower than Cg, the number of cations entering the boundary region from the solution is lower

than the number of cations leaving the same while migrating towards the cathodic side of the gel. This depletion takes place at a characteristic speed depending on the value of ΔV applied and ΔCgs. Several explanations have been proposed to get insights on the correlation between the interface depletion and the swelling of the anodic side. The decrease of solute concentration at the solution/hydrogel interface causes an increase of the osmotic pressure between the boundary and the contiguous anodic side of the gel, leading to a flux of solvent which induces the material swelling localized at its anodic side [10]. Moreover, compatibly with this, the osmotic pressure difference across the interface is known to be a decreasing function of the salt concentration in the surrounding solution, which decreases at the anodic side when the electric field is applied [26]. The inverse phenomenon takes place at the cathodic side of the gel (Figure 64c), leading to a localized shrinking instead. This asymmetric dynamic enrichment/depletion of solute, associated with an asymmetric swelling/shrinking of the hydrogel, causes the bending towards the cathode (Figure 8-d).

The speed of actuation of the PSS-co-PHEMA-co-PAN hydrogels is strongly connected both to the homeostatic mechanism described and to the equilibrium swelling properties of each material. The progressive depletion of cations at the anodic side of the gel is faster for higher values of ΔCgs: this explains why at low voltages the values of w for all the hydrogels tested were higher in solution A (the most diluted) rather than in solutions B and C. Nevertheless, the Dynamic Enrichment/Depletion model does not explain why the samples with lower amounts of Na-4-VBS (lower Cg, then lower ΔCgs) were more performant than those having higher amounts of the electro-active monomer. This behavior can be interpreted by considering the entity of the samples swelling in the different solutions. Because of the higher Na+ concentration present in the polymer, PSS20% exhibited a larger swelling than PSS10% and PSS5% i.e. it incorporated a dramatically larger amount of water (around 7 times its

own weight after synthesis). Because of this, it is reasonable to speculate that the polymeric chains of the matrix experienced a higher mechanical stress in response to the severe osmotic pressure that it underwent and so the whole structure was then more resistant to further swelling on the anodic side. In this sense, the cross-linked macromolecules of co-polymers having higher amount of Na-4-VBS can be considered closer to their limit of stretching finite extensibility (i.e. the maximum extension of the polymer chains, [43]) and therefore a decrease in the cross-linking amount could be beneficial to further increase its swelling capability and its related actuation performance.

Higher swelling degrees also imply an increase in the samples thickness, which dampens the bending speed, as previously demonstrated. As a consequence, hydrogels with larger swelling ratio are those displaying slower bending. The characteristic swelling behavior is also probably correlated to the high w values reached in solutions B in the high-voltage regime. This speculation was supported by the experimental data on both the swelling characteristics and the actuation performance of the samples. In fact, comparing the graphs in Figure.64b (electro-mechanical actuation in terms of w as a function of pCs) and in Figure 62 (swelling ratio as a function of pCs) it can be noticed how w values increase inversely with Cs and that lower values of the swelling ratio and lower value of w correspond to faster bending and to a steeper slope of the actuation curve in Figure 64b.

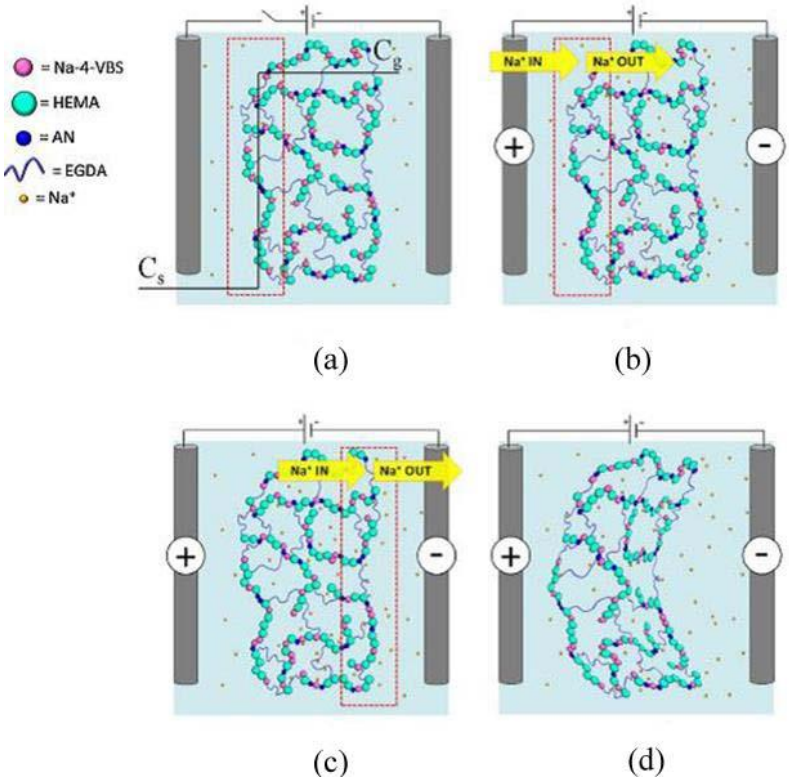

Figure 67. Schematic of the Dynamic Enrichment/Depletion model.a) A PSS-co-PHEMA-co-PAN hydrogel having internal Na+ concentration equal to Cg is equilibrated in a NaCl solution of concentration Cs. b) After the application of the electric field, the number of Na+ entering the boundary region (dashed red line) at the anodic side is lower than the number of Na+ leaving the same (depletion). c) The opposite phenomenon is taking place at the cathodic side (enrichment). d) The differential swelling at the boundary region on both anodic and cathodic sides leads to the bending of the material.

All of the actuation tests have been conducted in neutral solutions, thanks to the high pKa value of benzensulfonic acids (about -2.8), which prevented Na-4-VBS protonation by water. The pH of the ambient solution is known to affect both the swelling and responsive behavior of smart electrically driven hydrogel-based systems [45]. In the present case, if the pH would be alkaline, there would be no significant differences in the electromechanical actuation, as far as OH- concentration is lower than the concentration of the salt in the ambient solution. On the other hand, if tests would be conducted in moderately acidic pH, the fixed sulfonate groups could undergo partial protonation, resulting in a decrease of Cg [45]. Only extreme pH values (strongly acidic or alkaline) could dramatically change the

actuation mechanism and the electro-responsive behavior of the hydrogel. However, to have exhaustive information on the materials electro-mechanical behavior as a function of the pH of the ambient solutions, tailored investigations should be carried out.

11.4. Conclusions

I synthesized a novel electro-responsive hydrogel, based on Na-4-VBS, HEMA and AN (co-PSS-co-PHEMA-co-PAN), able to generate low-voltage electro-mechanical actuation at the macroscale in NaCl aqueous solutions of different concentration (from 5 mmol to the molar range) with a reversible bending towards the cathode. We investigated on the bending speed dependency on sample thickness, electrodes configuration, concentration of the outside solution and amount of Na-4-VBS used. We observed that the fabricated polymeric components displayed faster bending for low amounts of Na-4-VBS in highly diluted solutions. In particular, samples provided with 5% of Na-VBS and having thickness of 0.1 mm showed responsiveness to the electrical stimulus starting at 0.2 V, and actuated with a bending speed of almost 3°/s under the standard potential of water electrolysis, while reached w values up to 22 °/s at 3 V.

The results on the responsiveness characterization were also correlated to the swelling behavior of the hydrogels in the same saline solutions, which were experimentally determined. According to the set of data collected, we speculate that the actuation mechanism can be interpreted as a dynamic osmotic equilibrium effect, induced by the ions migration throughout the polymeric network and by an anisotropic charge density distribution, as described by the enrichment/depletion model reported by Doi et al [42]. We also conducted the electro-mechanical characterization of the most performant actuator in PBS and in a standard cellular medium (DMEM) and observed similar bending trends.

Due to the highly performing actuation features of the hydrogels, we believe that the developed materials have potential to be employed in the design and prototyping of smart soft underwater systems, such as remotely controllable bio-inspired robotic artifacts, which can operate in a low-voltage regime in liquid environments of biological interest.

12. Appendix C

A room temperature bonding technique for the packaging of hydrogel-based hybrid microfluidic devices

Yunsong Yan[a,b] et.al

a) Centro Interdisciplinare Materiali e Interfacce Nanostrutturati (CIMaINa), University of Milan, Via Celoria, 16, 20133 Milan, Italy. b) European School of Molecular Medicine (SEMM), Campus IFOM-IEO, Via Adamello 16, 20139 Milan, Italy.

This chapter has been published.

Yunsong Yan;Tommaso Santaniello; Alessandro Tocchio;Federico Martello;Paolo Milani;Cristina Lenardi. "A room-temperature bonding technique for the packaging of hydrogel-based hybrid microfluidic devices". Microfluid Nanofluid. 2015.

12.1 Introduction

Hydrogels are natural and synthetic hydrophilic polymeric networks, able to absorb and retain a high water content, maintaining their solid state after their swelling process[81]. They are suitable materials to be implemented in cells-based Lab-on-a-chip (LOC) systems, mainly due to their biocompatibility, permeability to biomolecules and metabolites, low production costs and ease to be microfabricated [82-84]. Furthermore, their biocompatible character can be enhanced during the synthesis step, by incorporating bioactive co-monomers in the polymer matrix and by tuning their mechanical properties in order to generate a tissue analogue for the specific cell type involved [85]. The microfabrication techniques developed to engineer and mould soft polymers, such as laser

processing, photolithography, printing and replication, are important tools for producing surface microstructured hydrogels provided with microchannels networks that can be potentially used as microfluidic biomimetic components for on-chip cell culture and different LOC applications [86-88].

Despite the relatively simple manufacturing schemes developed to microfabricate this family of polymers, their implementation in sealed multi-components LOC systems is still challenging [89]. This is predominantly due to the lack of surface chemical affinity between the water-swollen hydrogels and the traditional hydrophobic polymeric materials employed in microdevices production, such as thermoplastics (e.g. poly methyl methacrylate, PMMA) and elastomers (e.g. poly dimethyl siloxane, PDMS), which hinders a direct assembly of the platforms via conformational contact [90, 91]. As a consequence, the use of a supplementary interface material acting as an adhesive has been employed to promote the bonding between the components, however the risk of clogging the microchannels during the packaging process substantially affects the applicability of this procedure [92, 93].

Grafting of photopolymerized microstructured hydrogels onto supporting surfaces was also tested as an integration approach, but the in-plane mechanical constraint induced by the interaction between the substrate and the formed hydrogel confines the swelling of the grafted polymer to the azimuthal direction only, therefore causing a deformation of the microstructures along the hydration process[94, 95]. On the other hand, traditional packaging routes like thermal bonding and laser welding are not applicable to water-swollen hydrogels because of the tendency of the materials to degrade at relatively low temperatures [96].

Other bonding strategies adopted to produce hydrogel thin films tightly anchored to thermoplastic or elastomeric platforms relied on the use of surface topography and chemical modification of the components prior the cross-linking of the hydrogel precursor, e.g. 3-(trimethoxysilyl)propyl methacrylates functionalized nano-pillars arrays fabricated on PDMS, as

reported by Zhang et al[97]. In this framework, the swelling of the sealed hydrophilic polymer after the packaging process is still confined in only one direction, and therefore the technique is not applicable to produce microstructured hydrogel layers based devices [98].

Here we demonstrated a room temperature packaging technique to seal fully hydrated micromoulded poly(hydroxy ethyl methacrylate) (PHEMA) based hydrogel platforms and thin films to PMMA and PDMS components, which can be employed for the rapid prototyping of a broad class of hybrid materials microfluidic stacking systems, such as perfusion microbioreactors and diffusion-based controlled release microsystems [99, 100].

PHEMA is a cross-linked synthetic polymer widely used in the biological fields, e.g. ophthalmology, because of its biocompatibility, biodegradability and nontoxicity [101-103]. The characteristic of being optically transparent also makes PHEMA a suitable substrate for screening cells biological activity over time by means of optical microscopy, whether culture takes place [104, 105].

12.2 Materials and methods

12.2.1 Hydrogel synthesis and micromoulding

A synthesis protocol was developed for producing pure PHEMA hydrogels which exhibit good elasticity and high resistance to compressive stresses. The determined reaction sequence was: i) 2-Hydroxyethyl methacrylate (HEMA, monomer); ii) MilliQ or de-ionized water (H2O, solvent); iii) Ethylene glycol dimethacrylate (EGDMA, cross-linker,); iv) N,N,N,N-Tetramethylethylenediamine (TEMED, catalyzer); v) 20% w/w Ammonium persulfate (APS) aqueous solution (initiator). All chemicals were purchased from Sigma Aldrich. To obtain the material with the desired properties, the monomer to cross-linker and monomer to initiator ratios were set as 1 : 0.06 and 1 : 0.01 (mol/mol) respectively. After complete cross-linking (1 hour), hydrogels having hyperelastic properties are obtained, as already

investigated in our previous work by mean of compressive tests and numerical simulations (Zhao et al. 2013). The molecular unit of PHEMA is shown in Figure 68.

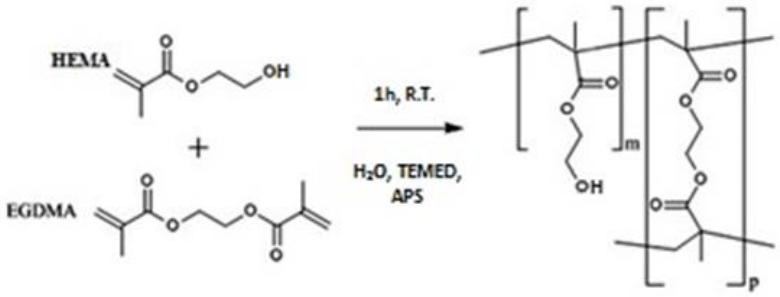

Figure 68. Scheme of the cross-linking reaction leading to the PHEMA molecular unit.

The PHEMA micromoulding protocol can be described as follows. A PMMA master was micro-milled to produce the microstructures to be transferred to the hydrogel surface. With the specific computer numerical control machine employed, the surface of the thermoplastic can be processed achieving features with the minimum characteristic linear dimensions of 100 μm and a maximum lateral resolution of about 2 μm. In this work, 500 μm diameter mills were used to manufacture a fluidic structure replicating a single channel 2D perfusion microbioreactor [106]. This choice was made because of the general applicability of this class of systems in a variety of perfusion microfluidic-based cell culture assays; from a micro-fluidic point of view, the design was conceived to obtain the proper culture media residence time and low shear stress in the cylindrical chambers [107-109].

More specifically, a 35 mm long 0.5 x 0.5 mm2 rectangular cross section channel was milled at the center of a 3 mm deep recess manufactured on a 80 x 40 mm2 PMMA slab. A 3 mm diameter cylindrical chamber (2 mm deep) was then milled at the centre of the microchannel. Two fluidic ports (3 mm diameter, 2 mm deep) were fabricated as well on the terminal regions of the channel. A PDMS negative cast of the microstructures is obtained by curing the elastomer directly on the

microfabricated PMMA at room temperature (elastomer to curing agent ratio is kept as 10 : 1 w/w). The resulting PDMS replica is then rig up into a custom made PMMA apparatus to become the new master mould onto which the hydrogel pre-polymer is cross-linked, to therefore achieve the microstructured platform to be implemented in the stacking microfluidic chip. A schematic illustration of the replication process used is shown in Figure 69. In the insets, microscope images of the obtained microstructures are shown. The fluidic circuits are perfectly transferred from the PMMA master to the PHEMA through PDMS replication; the micro-milling circular features characteristic of this micromachining technique is still present in the hydrogel.

300 µm flat PHEMA films were produced by injecting the hydrogel cross-linking solution at room temperature onto a Teflon substrate, in a rectangular hollow region defined by a silicone spacer mould. After injection, the system was closed and hold in compression by using a second Teflon lid and a 3 Kg weight. After reaction completion, the formed film was weakly bound to the supporting platform, so that its removal can be easily carried out by peeling off the hydrogel.

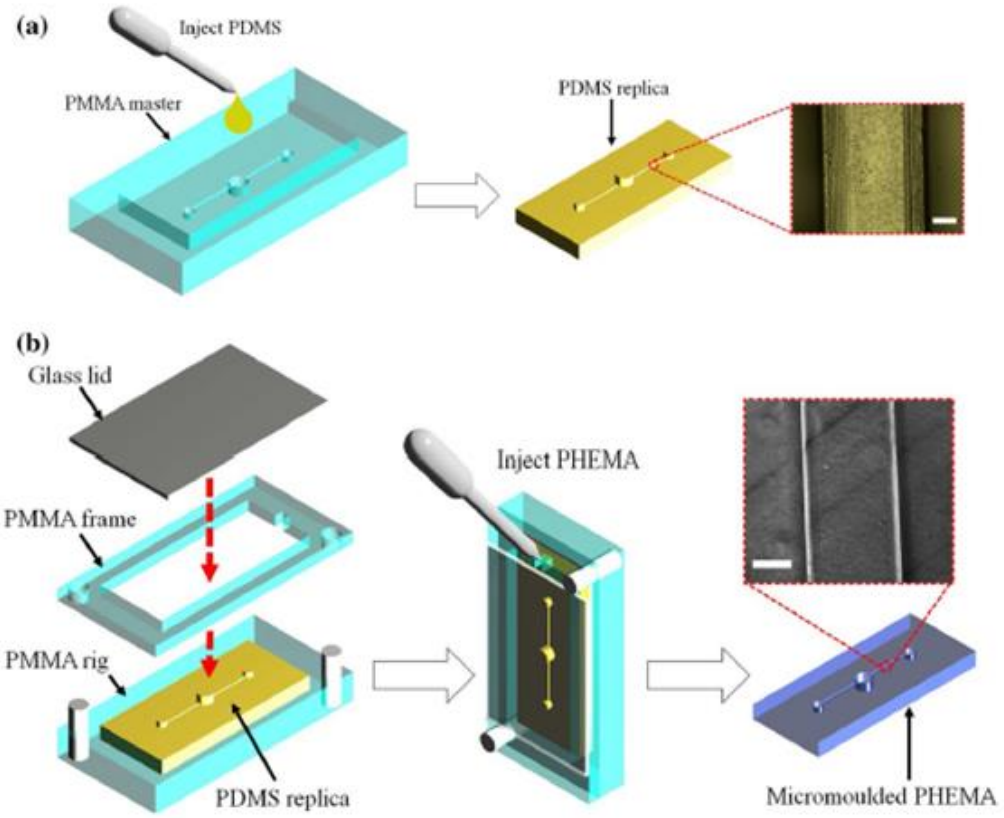

Figure 69. 3D schematic representation of the replication process to achieve micromoulded hydrogels; a) The PDMS pre-polymer is injected over the PMMA master and then cured at room temperature to obtain the negative replica of the microstructures. Scale bar in the inset is 100 µm; b) The obtained negative cast is assembled in a supporting PMMA rig and employed as a new master for PHEMA hydrogel micromoulding. After one hour, the microfluidic hydrogel is obtained. The inset shows a microscope image of the fabricated microchannel in the PHEMA water-swollen state (scale bar is 200 µm).

Prior to hydration, both the produced micromoulded and flat PHEMA layers were washed to remove the non-reacted impurities using a water/ethanol mixture, according to a swelling procedure already reported in Zhao et al[110]. The hydrogel volumetric swelling ratio was evaluated by measuring the dimensions of the components before and after hydration and resulted to be 1.3[111]. The determination of this parameter was necessary to have information on the fully hydrated layers

dimensions, so that the relative PMMA and PDMS interconnection modules could be fabricated accordingly to provide the appropriate alignment of the components to be bonded.

12.2.2 Fabrication of PDMS and PMMA microstructured components and world-to-chip interfaces

The PDMS and PMMA world-to-chip interface layers to be assembled with the microfluidic moulded hydrogels were fabricated using casting and milling respectively. The components were 50 x 20 mm^2, 3 mm thick slabs, provided with through-holes for tubing interconnections. In the case of PDMS, 3 mm diameter holes were punched in the appropriate locations after casting and polyurethane tubes were fitted to the ports and sealed using a silicone paste. On the other hand, threaded 3 mm diameter through-holes were drilled on the PMMA slab so that fluidic connectors (SMC) could be screwed to the fluidic inlet and outlet ports and could host 2 mm outer diameter polyurethane tubes.
The microstructured platforms to be assembled with the flat PHEMA membranes were produced with a similar fabrication route. A PDMS microfluidic platform having the same perfusion microbiorector design employed for the PHEMA hydrogel components micromoulding was obtained by room temperature direct casting of the elastomer over a 4 mm recess milled on a PMMA master, where the protruding negative fluidic structure was micro-milled (Figure 70a). The PMMA fluidic module was manufactured by mean of numerical control micro-milling and consisted of a 45 x 30 mm2 and 3 mm thick slab, having a central cylindrical recess (10 mm diameter, 1 mm height) and two 2.5 mm long straight rectangular cross-section channels (height x width = 1 x 0.5 mm^2) that operated as inlet and outlet for the fluid flow across the chamber (Figure 70b).

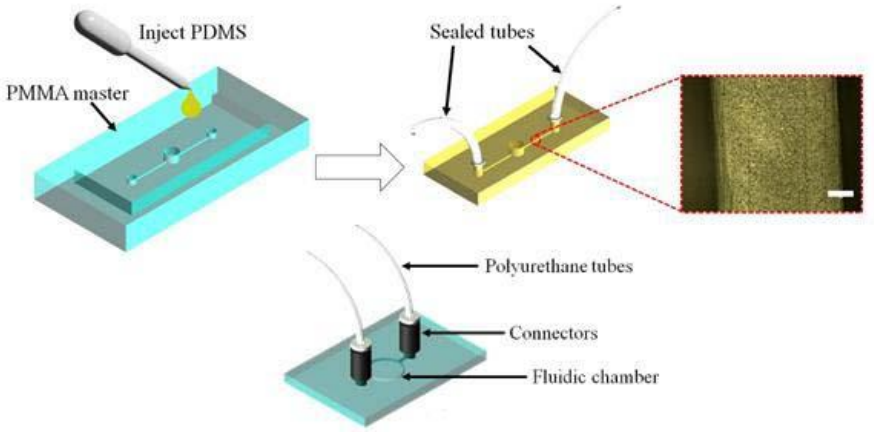

Figure 70. Microfluidic PDMS and PMMA components fabrication.The PDMS module is obtained by casting the curing elastomer on a PMMA master, provided with micro-milled protruding fluidic features (top). The PMMA layer is obtained by direct micro-milling of the thermoplastic (bottom).

12.2.3 Hybrid materials microdevices bonding technique

The core idea of the developed bonding technique is that to take advantage of the surface reactivity of water-swollen PHEMA hydrogels, due to the presence of pendant hydroxyl groups, in conjunction with physical and chemical surface functionalization techniques of both PDMS and PMMA. The exposure to plasma oxygen fluxes combined with chemical treatments using silanizing agents, such as 3-(trimethoxysilyl)propyl methacrylates (TMSPMA) and (3-amino)propyl triethoxysilane (APTES), are known to be suitable tools to confer hydrophilic character to thermoplastics and PDMS-based hydrophobic materials. According to the literature, hybrid microdevices having functionalized PMMA and PDMS components bonded together after direct contact were produced and tested using these approaches[112-115].

In our work, plasma oxygen treatments and low temperature silanization processes using diluted APTES aqueous solutions were empirically optimized in order to confer specific chemical surface

functionalities to the produced thermoplastic and elastomeric platforms. All the PMMA and PDMS components were thoroughly washed using isopropanol and dried using compressed air prior insertion in the instrument chamber. After the first plasma treatment, the formation of hydroxyl groups on the exposed surfaces is promoted and the layers turned to be hydrophilic, as qualitatively observed by pipetting a drop of pure water on them. Immediately after the modification, the samples were immersed in an APTES solution, which was prepared in a 500 ml glass beaker, by keeping the concentration constant at 5% (v/v), and heated up at 80° C. The PDMS and PMMA components immersion time was set as 1 hour, according to the protocol described by Vlachopoulou et al [116].. This procedure resulted in the formation of a surface monolayer of the silanizing agent, which conferred NH_2 amine functionalities to the polymer surfaces, dramatically increasing their hydrophilic character. After removal of the materials from the mixture, a second plasma oxygen processing was carried out; this last step enabled the generation of hydroxyl groups at the terminal side of the formed APTES chain.

A schematization of the functionalization protocol for a flat PDMS component is reported in Figure 71 the representation is equivalent for the PMMA platforms.

In order to assess the best set of conditions to maximize the hydrophilicity of both materials prior and after the silanization of the layers, a set of plasma oxygen functionalization tests in which the power and exposure time were varied from 50 to 150 W and 10 to 90 seconds respectively were carried out by keeping the chamber pressure fixed at 700 mTorr and the oxygen flux at 20 ccm and the static contact angle of the layers was subsequently measured using a FTA1000 Modular Optical Contact Angle System. More specifically, the measurement system is equipped with a syringe fluid delivery apparatus which enables a direct drop of the probe liquid (MilliQ water in our case) onto the polymeric surfaces to be tested. The drop profile is then imaged and recorded using an integrated camera and

fine focus optics (magnification up to 20x) and the corresponding contact angle value is recorded via the embedded image processing software (the accuracy is ± 5%).

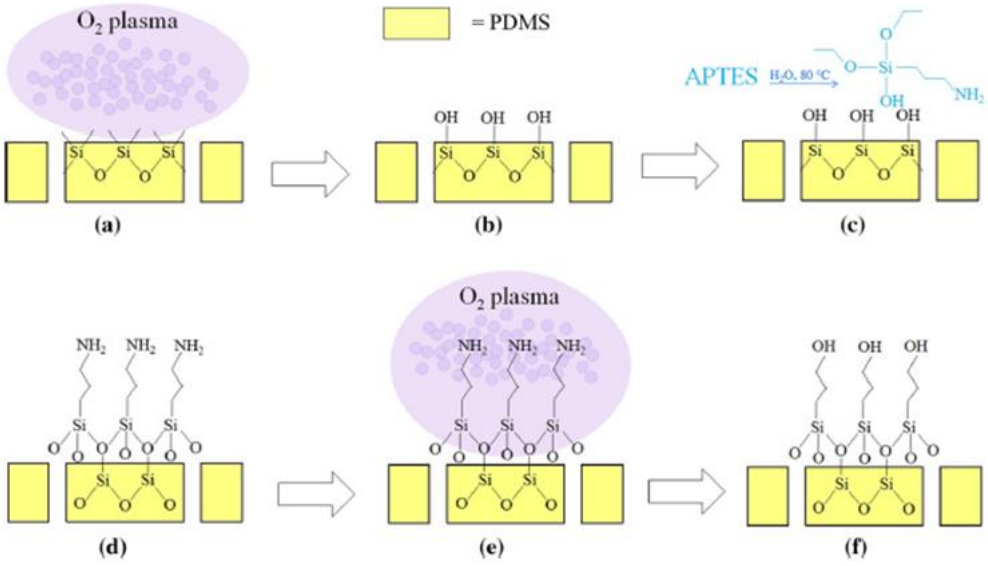

Figure 71. Functionalization procedure of the PDMS component. a) A first plasma oxygen treatment is carried out on the surface of the elastomer; b) Hydroxyl groups are formed after plasma treatment; c) The functionalized platform reacts with the free hydroxyl obtained from APTES hydrolysis (H2O, 80°C); d) Amine groups are formed on the PDMS surface; e) The component undergoes a second plasma oxygen treatment; f) Stable OH-terminated organic chains are present on the elastomer surface after the complete functionalization.

The surface modification of the layers using the optimized set of parameters determined by mean of the performed contact angle measurements offered the possibility to seal the water swollen micromoulded PHEMA hydrogels or thin films to the treated PDMS and PMMA platforms, by simply contacting the two components together using a mild compression in a water environment to favor the formation of hydrogen bonds between the materials. The modified PMMA and PDMS components were manually aligned with the hydrated PHEMA hydrogels, which were positioned on a 2 mm thick

Teflon support leaning at the bottom of a Petri dish, and contact was promoted by pressing the platforms together, using parafilm coated 1 Kg brass weights. According to the geometry of the components, the corresponding pressure exercised on the contacted layers is 4.5 kPa. Still keeping the compression active, water was then added at the bottom of the Petri dish, so that the hydrogel was soaked in liquid for half of its thickness. The assemblies were then left in contact overnight, being covered by a parafilm capping, to prevent water evaporation. After the packaging process, the devices were endowed with the appropriate interconnections and tubing and stored in a 15 ml water filled Petri dish.

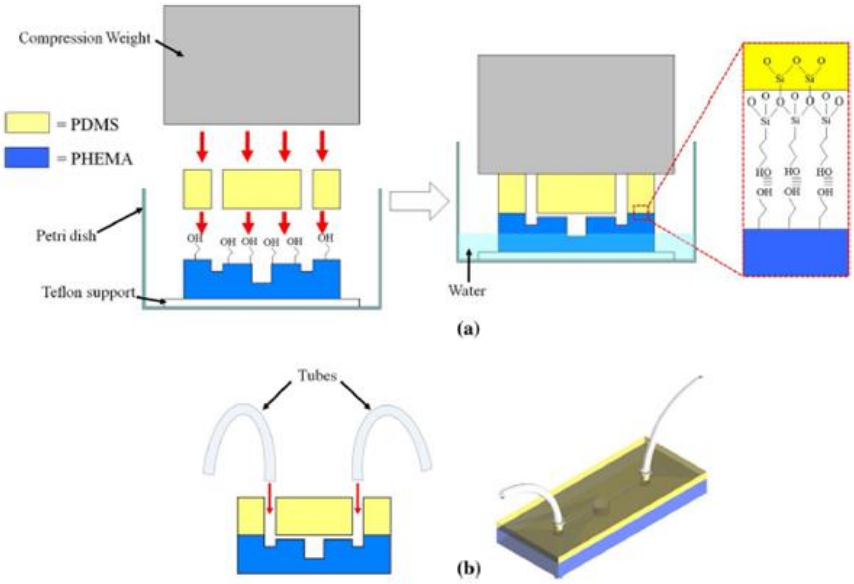

Figure 72. Schematic of the developed bonding technique. a) A surface modified PDMS component is contacted with a water-swollen PHEMA microfluidic layers and hold in compression in an aqueous environment. Hydrogen bonds are forming between the two materials (inset). b) The sealed hybrid microsystems is provided with tubes.

Four types of devices were produced, according to the combination of the designed microfluidic components reported: i) micromoulded PHEMA bonded with flat PDMS provided with fluidic ports; ii) micromoulded PHEMA bonded with PMMA provided with fluidic ports; iii) 300 µm PHEMA thin film bonded with micromoulded PDMS; iv) 300 µm PHEMA thin film bonded with micro-milled PMMA. A functionalized PDMS world-to-chip component sealing to a microstructured hydrogel using the

described bonding technique is reported in Figure 72; the representation is equivalent for all of the hybrid materials systems produced.

12.3 Results & discussion

12.3.1 Contact angle measurements

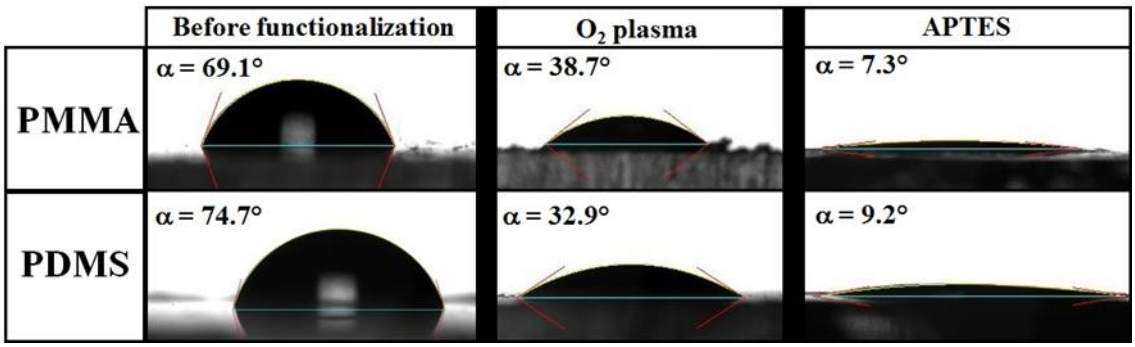

Figure 73. Contact angle measurements of the PMMA and PDMS platforms, showing an increase in the materials hydrophilicity along the surface modification process. The average values are reported only.

Figure 73 shows contact angle images of pure water on both PMMA and PDMS prior and after functionalization. For both materials, three measurements were taken at each step and the averaged values and relative standard deviations were then calculated. All the errors were found to be below 15% of the corresponding average static contact angle, therefore reflecting a good homogeneity of the modification over the surfaces tested. Using a plasma power value of 150 W and exposure time of 30 seconds, the average contact angle decreased from 69.1°±3.1° to 7.3°±1.0° (being 38.7°±4.0° after the first plasma modification) and from 74.7°±3.7° to 9.2°±1.3° (being 32.9°±3.8° after the first plasma modification) for PMMA and PDMS respectively. This can be considered as the best conditions

determined for increasing the layers hydrophilic character, according to the specific type of thermoplastic and elastomer employed.

The modified components were then assembled with PHEMA hydrogel-based layers using the procedure previously described and the bonding degree was initially evaluated by manually peeling off the hydrogels. Although the minimum contact angle was obtained for both materials with this set of parameters, it was observed that hybrid PMMA-PHEMA bi-layer systems did not show good sealing properties, while hybrid PDMS-PHEMA stacks were found to be tightly bonded, as evaluated on this largely qualitative level. By lowering the plasma power to 100 W and by increasing the exposure time to 60 seconds, PMMA and PHEMA exhibited a far better bonding degree, so this new set of conditions were employed for producing thermoplastic-hydrogel hybrid systems. With this new set of parameters, the PMMA water contact angle was measured to be 47.1°±4.1° after the plasma oxygen treatment and did not exhibited significant variation after the APTES coating with respect to the previous case (the contact angle was measured as 13.6°±1.1°).

The need of tuning the functionalization recipe for the PMMA components is probably due to a substantial difference in terms of the final surface quality that the plasma oxygen treatment generates on the thermoplastic with respect to the elastomeric material. According to the literature, it is reasonable to believe that the surface of the PMMA was partially degraded after the plasma modification, so the appropriate conformational adhesion between the thermoplastic and the hydrogel is hindered and the resulting sealing is therefore wakened[117-119]. On the other hand PDMS is less prone to be affected by relatively high power plasma attacks; furthermore the elastomeric material is softer and more compliant than PMMA, so that the conformational adhesion with the hyperelastic PHEMA is favored in any case with respect to thermoplastic-hydrogel case[120]. Preliminary bonding tests were also carried out using a single plasma oxygen treatment of the PDMS modules, but the

resulting hybrid systems showed a weak bonding of the layers. On the other hand, after the APTES coating of the elastomer surface and a second plasma attack, the formation of a tighter sealing between the components was observed. This difference is probably due to two main factors. First, the silanization procedure could confer a more stable functionalization to the surface after the second plasma oxygen attack with respect to the single plasma treatment because of the presence of long organic OH-terminated chains, so that the components could keep their reactivity when exposed to air for the time required to handle and assembly the components. Moreover, the bonding is favored due to the high wettability of the surface after the APTES modification, which dramatically decreases the surface energy mismatch between the highly hydrophilic hydrogel and the treated PDMS. The goodness of the sealing for all the families of the produced microdevices was then validated in a quantitative way by liquid leakage tests.

12.3.2 Leakage tests and bonding validation

Liquid leakage tests can be considered as a reliable way to prove the bonding degree of stacking sealed microdevices in the LOC systems framework [121]. We conducted a set of experiments by keeping each of the produced device in a water-filled Petri dish, using a red colored dye aqueous solution (E122-Azorubine, 30 mmol) to perfuse the fluidic structures at a flow rate ranging from 15 to 100 ml/h (maximum flow rate achievable) using a syringe pump (KD Scientific, model KDS100). After perfusion, the microsystems were analyzed using an inverted optical microscope to assess the presence of leakage at the component interfaces. Each test had a duration of 40 minutes and each flow rate value was set for 10 minutes; the chosen values were 15, 50, 75 and 100 ml/h. According to the flow rate values imposed, the hybrid systems were perfused with liquid amounts going from 5 to 30

times of the total volume of the fluidic structures per minute, except for the flat PHEMA-microfluidic PMMA system for which the flow rate ranged from from 3 to 20 times of the perfused structures volume. The pressure differences ΔP, corresponding to the maximum volumetric flow rate value employed Qmax = 100 ml/h, which are expected to be developed in the channels with respect to the atmospheric pressure in the static configuration, could be estimated by considering the fluidic resistances of each microstructures for the developed hybrid systems (Bruus 2008). More specifically, the overall resistance R of each device was calculated as the equivalent series connected fluidic resistors consisting of the inlet and outlet microchannels and central chamber, by assuming no-slip boundary conditions and Hagen-Poiseuille flow[122, 123]. In order to estimate the pressure difference, the chamber was considered as a rectangular cross-sectional channel having the width and length equal to the cylinder radius. Hence, the hydraulic resistance of the i-th structure of each device could be calculated as:

$$R_i = \frac{{h_i}^3 w_i}{12\eta L_i}\left[1 - 0.630\ \frac{h_i}{w_i}\right] \qquad [1]$$

where hi,wi and Li are the height, width and length of the in series channel respectively and η is the viscosity of the dye solution (considered equal to the water viscosity at room temperature i.e. 0.89 mPas). Using this approximation and considering that h = w for all of the micro-structures, the error of each fluidic resistance Ri is about 13% of the value derived from the Navier-Stokes exact solution. By applying the Ohm's law to fluidic circuits , the pressure difference is given by[123]:

$$\Delta P = RQ_{max} \qquad [2]$$

For the 2D bioreactor-like devices, ΔP = 0.5 kPa, which can be considered as a relatively large pressure for perfusion cell culture microsystems and as a physiologically relevant value in terms of the generated shear stresses[124, 125]. On the other hand, for the largest fluidic network present on the PMMA component bonded to the flat PHEMA layer, ΔP was calculated to be equal to 7 Pa, which corresponds to the maximum value tested achievable with the setup employed. In Figure 74, microscope images of the perfused structures are shown. No leakage was observed to take place at the materials interface, both around the microchannels and the fluidic ports, reflecting the good sealing properties of the microdevices.

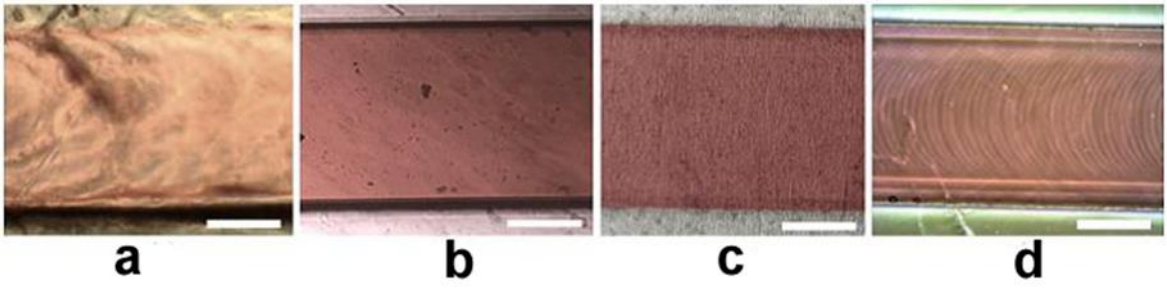

Figure 74. Microscope images of the devices microchannels after perfusion (scale bar is 200 μm). a) Fluidic PHEMA sealed to PDMS; b) Fluidic PHEMA sealed to PMMA; c) PHEMA thin film sealed to fluidic PDMS; d) PHEMA thin film sealed to fluidic PMMA.

A further validation of the bonding quality was carried out by drying the systems in air and by conducting a second set of leakage tests in this new configuration. In Figure 75a, a dried microfluidic PHEMA bonded to the relative PDMS world-to-chip interface is shown. After the drying process, due the force exercised by the in-plane constrained hydrogel shrinking process the PDMS layer resulted to be bended, but still adhering to the PHEMA. The leakage tests conducted on the deformed system showed how the bi-layer device could preserve its operational behavior during perfusion i.e. the no-leakage regime was confirmed and a smooth flow for all the flow rate values tested was observed

(Figure 75b-c); this constitutes a further proof that the sealing of the layers is stable and tight. Furthermore the PHEMA-PDMS system could be reversibly dried and swollen in water, periodically in time. Six drying-swelling cycles were carried out for three months after the bonding and the functional behavior of the system during perfusion was checked to be invariant both in the hydrogel hydrated and dried conditions. On the contrary, for the PHEMA-PMMA bonded stacking devices, the drying of the hydrogel layers did not cause any deformation of the thermoplastic component, due to the higher stiffness of the material with respect to PDMS. In this case, the periodically shrinking and swelling of the constrained hydrogel ended up to generate in-plane stresses which eventually overcame the work of adhesion between the components in time, so that the drying-swelling cycles could be carried out only two times before the platforms separations.

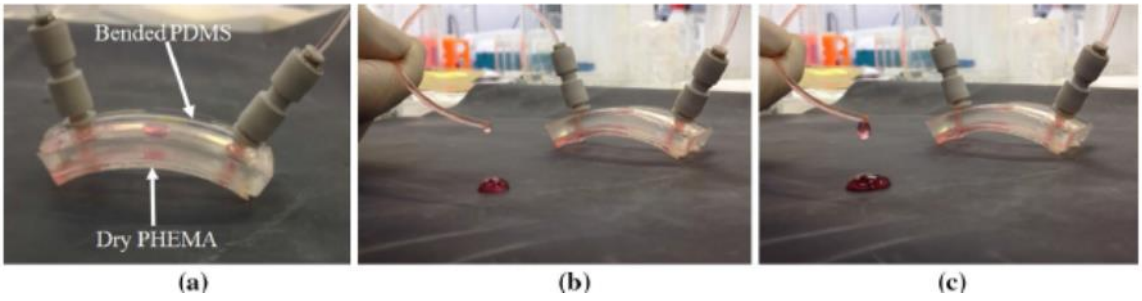

Figure 75. Microfluidic PHEMA bonded to the chip-to-the-world PDMS platform after dehydration of the hydrogel.a) The bi-layer system is bended due to the in-plane stresses generated by the PHEMA shrinking process; b) and c) Images of the perfused device at 100 ml/h, showing a smooth liquid flow.

Based on these results, a second route was adopted to give insight on the bonding strength between the sealed PHEMA and PMMA components in the assembled microsystems. This approach relied on monitoring the diffusion of a dye molecule through the hydrogel matrix, which was initially dispersed in the batch solution hydrating the device. For this purpose, a three-layer system having a

hydrated 300 µm thick PHEMA film sandwiched between the microfluidic PMMA component and an APTES functionalized glass slide was produced (Figure 76). The modification of the glass platform was carried out employing the same set of parameters used for the PDMS functionalization, since it has been shown how plasma treatments of the two materials led to very similar results in terms of surface reactivity, due to their chemical affinity [126].

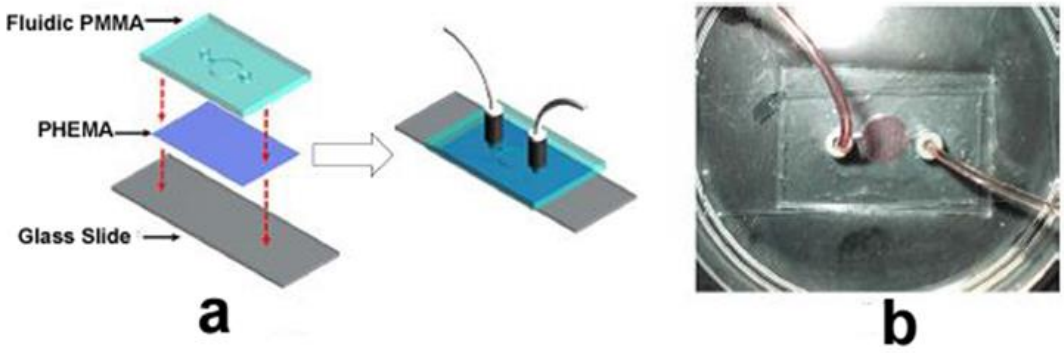

Figure 76. Hybrid glass-PHEMA-PMMA system. a) Schematic of the device assembly. b) Photo of the perfused microsystem partially immersed in pure water.

The objective of this test was to assess whether the diffusion of the dye in the hydrogel was limited to the lateral direction only when the soft polymer integrated in the stacking system was exposed to the liquid bulk. A 10 mmol methylene blue aqueous solution was prepared in a Petri dish and the produced microdevice was then positioned in the container, so that the liquid level could reach half of the PMMA thickness, therefore guaranteeing that the PHEMA layer was completely immersed in the solution. The system was then connected to the syringe pump and perfused with the red E122-Azorubine aqueous solution for 40 minutes at the flow rate of 15 ml/h. A freestanding water-swollen PHEMA layer (still 300 µm thick) was soaked in the same blue methylene solution, in order to compare the diffusion rate of the blue dye into the polymeric matrix when completely exposed to the liquid with respect to the one taking place when the hydrogel is integrated in the

three-layer stacking system.

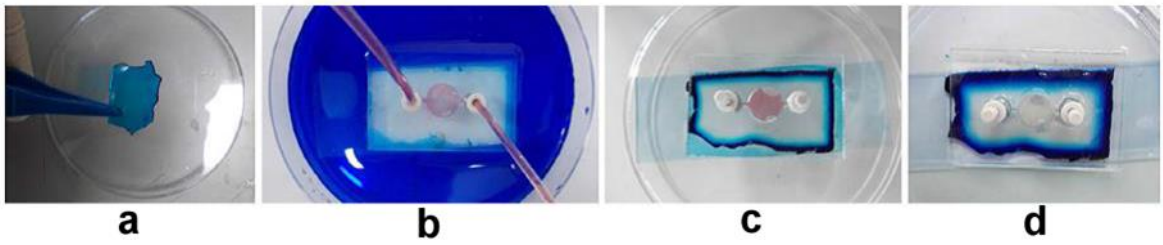

Figure 77. Validation of the sealing degree for the hybrid glass-PHEMA-PMMA system using methylene blue diffusion in the hydrogel matrix. a) Freestanding PHEMA after being exposed for 10 seconds to the dye solution; b) Image of the perfused hybrid system soaked in the colored mixture for 2 hours. c) Methylene blue diffusion in the hydrogel after the device was soaked in the solution for 4 days; d) Image of the device after 10 days of exposure to the mixture.

As shown in Figure 77a, the free hydrogel film exhibited a marked blue color after 10 seconds, indicating that the dye permeated in to the structure. Figure 77b to d shows the evolution over time of the methylene blue diffusion into the PHEMA layer implemented in the sealed glass-PHEMA-PMMA microsystem instead. After 2 hours, a thin blue region (approximatively 0.2 mm wide) was observed to spread from the outside borders of the layer toward the center of the hydrogel (Figure 77b). After 4 days (Figure 77c), a net gradient showing the progressing of the dye diffusion appeared and after 10 days (Figure 77d) the phenomenon showed even more marked features, having the dye approaching the central region of the device, but still limited to the periphery of the hydrogel film. This behavior indicates that for the sealed PHEMA, the methylene blue diffusion only takes places in the lateral direction i.e. perpendicularly to the hydrogel thickness, therefore confirming the tight sealing of the components.

Taken all together, these results validate the bonding technique employed to produce hybrid

materials microdevices as a suitable packaging approach for the rapid prototyping of PHEMA hydrogel-based LOC systems, which could offer the possibility of carrying out molecule controlled release in 2D cell culture perfusion-based miniaturized environments. The present packaging approach is also currently exploited in the development of a polymeric microdevice designed by the authors for on-chip single cell isolation, which relies on the use of a freestanding PHEMA based layer implemented as an interface between two microfluidic PMMA components. The sealing of the modules for this specific stacking system showed to preserve its robustness when perfusion was carried out in the thermoplastic platforms over the integrated hydrogel layer.

12.4 Conclusions

I proposed a room temperature bonding technique to seal water-swollen microstructured PHEMA hydrogel platforms and thin films to PMMA and PDMS chip-to-the-world and microfluidic components respectively. Physico-chemical functionalization procedures based on plasma oxygen treatments and silanization processes with APTES were empirically optimize and monitored using contact angle measurements to confer surface reactivity to the thermoplastic and elastomeric layers, which enabled the formation of hydrogen bonds with the superficial hydroxyl groups of the hydrated hydrogels at the materials interface when contacted. Using this integration strategy, the freestanding hydrogels can be bonded with the modified modules after their full three-dimensional swelling in pure water, therefore preserving the shape of the manufactured microfeatures.

The technique provides the tight sealing of the layers, as demonstrated by leakage tests. After being equipped with an external displacement pump to perfuse the systems, the produced sealed microdevices are kept immersed in a pure water-based liquid environment (wet microfluidics), which

guarantees the constant hydrogel hydration during operation. The possibility of conducting continuous perfusion of the microstructured biocompatible hydrogels in a liquid environment mingled with their intrinsic permeability to biomolecules and metabolites render this class of hybrid microsystems potentially feasible for dynamic 2D cell culture in miniaturized environments, where different fluidic phenomena such as convective flow and diffusion can be simultaneously controlled in the same polymeric platform.

I believe that the presented method retains a significant importance in the framework of hydrogel-based hybrid materials microfluidic devices rapid prototyping and manufacturing for cells-on-chip applications.

13. References

1. Borghi, F., et al., *Stretchable nanocomposite electrodes with tunable mechanical properties by supersonic cluster beam implantation in elastomers.* Applied Physics Letters, 2015. **106**(12): p. 121902.
2. Corbelli, G., et al., *Highly Deformable Nanostructured Elastomeric Electrodes With Improving Conductivity Upon Cyclical Stretching.* Advanced Materials, 2011. **23**(39): p. 4504-4508.
3. Hunt, A., et al., *An integrated electroactive polymer sensor–actuator: design, model-based control, and performance characterization.* Smart Materials and Structures, 2016. **25**(3): p. 035016.
4. Bhandari, B., G.-Y. Lee, and S.-H. Ahn, *A review on IPMC material as actuators and sensors: Fabrications, characteristics and applications.* International Journal of Precision Engineering and Manufacturing, 2012. **13**(1): p. 141-163.
5. Mojarrad, M. and M. Shahinpoor. *Ion-exchange-metal composite sensor films*. 1997.
6. Bahramzadeh, Y. and M. Shahinpoor, *A Review of Ionic Polymeric Soft Actuators and Sensors.* Soft Robotics, 2013. **1**(1): p. 38-52.
7. Dong, B., et al., *Super Proton Conductive High-Purity Nafion Nanofibers.* Nano Letters, 2010. **10**(9): p. 3785-3790.
8. Kwok, M.Y.F., et al., *Micro Nafion Actuators for Cellular Motion Control and Underwater Manipulation*, in *Experimental Robotics VII*, D. Rus and S. Singh, Editors. 2001, Springer Berlin Heidelberg: Berlin, Heidelberg. p. 471-480.
9. Shi, W. and L.A. Baker, *Imaging heterogeneity and transport of degraded Nafion membranes.* RSC Advances, 2015. **5**(120): p. 99284-99290.

10. Bar-Cohen, Y., et al. *Challenges to the application of IPMC as actuators of planetary mechanisms*. 2000.

11. Bennett, M.D. and D.J. Leo, *Ionic liquids as stable solvents for ionic polymer transducers.* Sensors and Actuators A: Physical, 2004. **115**(1): p. 79-90.

12. Bennett, M.D., et al., *A model of charge transport and electromechanical transduction in ionic liquid-swollen Nafion membranes.* Polymer, 2006. **47**(19): p. 6782-6796.

13. Shahinpoor, M. and K.J. Kim, *Novel ionic polymer–metal composites equipped with physically loaded particulate electrodes as biomimetic sensors, actuators and artificial muscles.* Sensors and Actuators A: Physical, 2002. **96**(2–3): p. 125-132.

14. Kim, B., et al. *Analysis of mechanical characteristics of the ionic polymer metal composite (IPMC) actuator using cast ion-exchange film*. 2003.

15. Zickgraf, B., G.A. Schneider, and F. Aldinger. *Fatigue behaviour of multilayer piezoelectric actuators*. in *Applications of Ferroelectrics, 1994.ISAF '94., Proceedings of the Ninth IEEE International Symposium on*. 1994.

16. Lee, J.-W. and Y.-T. Yoo, *Preparation and performance of IPMC actuators with electrospun Nafion®–MWNT composite electrodes.* Sensors and Actuators B: Chemical, 2011. **159**(1): p. 103-111.

17. Katakabe, T., et al., *Electric Double-Layer Capacitors Using "Bucky Gels" Consisting of an Ionic Liquid and Carbon Nanotubes.* Journal of The Electrochemical Society, 2005. **152**(10): p. A1913-A1916.

18. Usui, H., et al., *Improved dye-sensitized solar cells using ionic nanocomposite gel electrolytes.* Journal of Photochemistry and Photobiology A: Chemistry, 2004. **164**(1–3): p. 97-101.

19. Fukushima, T., et al., *Fully Plastic Actuator through Layer-by-Layer Casting with Ionic-Liquid-Based Bucky Gel.* Angewandte Chemie International Edition, 2005. **44**(16): p. 2410-2413.

20. Baughman, R.H., et al., *Carbon Nanotube Actuators.* Science, 1999. **284**(5418): p. 1340-1344.

21. Mirfakhrai, T., J.D.W. Madden, and R.H. Baughman, *Polymer artificial muscles.* Materials Today, 2007. **10**(4): p. 30-38.

22. Gao, R., et al., *Imidazolium sulfonate-containing pentablock copolymer-ionic liquid membranes for electroactive actuators.* Journal of Materials Chemistry, 2012. **22**(27): p. 13473-13476.

23. Kim, O., T.J. Shin, and M.J. Park, *Fast low-voltage electroactive actuators using nanostructured polymer electrolytes.* Nat Commun, 2013. **4**: p. 2208.

24. Wu, G., et al., *Graphitic carbon nitride nanosheet electrode-based high-performance ionic actuator.* Nat Commun, 2015. **6**: p. 7258.

25. Abdullayev, E. and Y. Lvov, *Halloysite clay nanotubes as a ceramic "skeleton" for functional biopolymer composites with sustained drug release.* Journal of Materials Chemistry B, 2013. **1**(23): p. 2894-2903.

26. Ghisleri, C., et al., *Patterning of gold–polydimethylsiloxane (Au–PDMS) nanocomposites by supersonic cluster beam implantation.* Journal of Physics D: Applied Physics, 2014. **47**(1): p. 015301.

27. Pravin, K. and K. Ravindranath, *Current Research Trends in Modification / Interaction of Halloysite Nanotube Filled Polymer Blends and Its Composites: A Review.* International Journal of Science and Research, 2013. **4**(12): p. 1766-1772.

28. Mohsen, S. and J.K. Kwang, *The effect of surface-electrode resistance on the performance of ionic polymer-metal composite (IPMC) artificial muscles.* Smart Materials and Structures, 2000. **9**(4): p. 543.

29. Mattia, M., et al., *Flexible and biocompatible microelectrode arrays fabricated by supersonic cluster beam deposition on.* Journal of Micromechanics and Microengineering, 2011. **21**(4): p. 045013.

30. Hayyan, M., et al., *Investigating the electrochemical windows of ionic liquids.* Journal of Industrial and Engineering Chemistry, 2013. **19**(1): p. 106-112.

31. Fan, X.-H., Y.-P. Chen, and C.-S. Su, *Density and Viscosity Measurements for Binary Mixtures of 1-Ethyl-3-methylimidazolium Tetrafluoroborate ([Emim][BF4]) with Dimethylacetamide, Dimethylformamide, and Dimethyl Sulfoxide.* Journal of Chemical & Engineering Data, 2016. **61**(2): p. 920-927.

32. Takagi, K., N. Tomita, and K. Asaka, *A simple method for obtaining large deformation of IPMC actuators utilizing copper tape.* Advanced Robotics, 2014. **28**(7): p. 513-521.

33. Bretti, C., et al., *Thermodynamics of Proton Binding of Halloysite Nanotubes.* The Journal of Physical Chemistry C, 2016. **120**(14): p. 7849-7859.

34. Kim, O., et al., *Ion Transport Properties of Self-Assembled Polymer Electrolytes: The Role of Confinement and Interface.* The Journal of Physical Chemistry Letters, 2013. **4**(13): p. 2111-2117.

35. Horváth, E., et al., *Hydrazine-hydrate intercalated halloysite under controlled-rate thermal analysis conditions.* Journal of Thermal Analysis and Calorimetry, 2003. **71**(3): p. 707-714.

36. Shi, B., et al., *Tuning the performance of anion exchange membranes by embedding multifunctional nanotubes into a polymer matrix.* Journal of Membrane Science, 2016. **498**:

p. 242-253.

37. Chen, Y., et al., *Polyetherimide/Bucky Gels Nanocomposites with Superior Conductivity and Thermal Stability.* ACS Applied Materials & Interfaces, 2013. **5**(15): p. 7478-7484.

38. Terasawa, N. and K. Asaka, *High performance polymer actuators based on single-walled carbon nanotube gel using ionic liquid with quaternary ammonium or phosphonium cations and with electrochemical window of 6 V.* Sensors and Actuators B: Chemical, 2014. **193**: p. 851-856.

39. Fukushima, T. and T. Aida, *Ionic liquids for soft functional materials with carbon nanotubes.* Chemistry, 2007. **13**(18): p. 5048-58.

40. Ionov, L., *Biomimetic Hydrogel-Based Actuating Systems.* Advanced Functional Materials, 2013. **23**(36): p. 4555-4570.

41. Calvert, P., *Hydrogels for Soft Machines.* Advanced Materials, 2009. **21**(7): p. 743-756.

42. Morales, D., et al., *Electro-actuated hydrogel walkers with dual responsive legs.* Soft Matter, 2014. **10**(9): p. 1337-1348.

43. Esmaiel, J., T. Javad, and S.S. Alireza, *Swelling characteristics of acrylic acid polyelectrolyte hydrogel in a dc electric field.* Smart Materials and Structures, 2007. **16**(5): p. 1614.

44. O'Grady, M.L., P.-l. Kuo, and K.K. Parker, *Optimization of Electroactive Hydrogel Actuators.* ACS Applied Materials & Interfaces, 2010. **2**(2): p. 343-346.

45. Bassil, M., J. Davenas, and M. El Tahchi, *Electrochemical properties and actuation mechanisms of polyacrylamide hydrogel for artificial muscle application.* Sensors and Actuators B: Chemical, 2008. **134**(2): p. 496-501.

46. Ionov, L., *Hydrogel-based actuators: possibilities and limitations.* Materials Today, 2014. **17**(10): p. 494-503.

47. Abdolhamid, A., B. Jörg, and W. Thomas, *Modeling and simulation of the bending behavior of electrically-stimulated cantilevered hydrogels.* Smart Materials and Structures, 2015. **24**(3): p. 035021.

48. Seon Jeong, K., et al., *Behavior in electric fields of smart hydrogels with potential application as bio-inspired actuators.* Smart Materials and Structures, 2005. **14**(4): p. 511.

49. Homma, M., Y. Seida, and Y. Nakano, *Effect of ions on the dynamic behavior of an electrodriven ionic polymer hydrogel membrane.* Journal of Applied Polymer Science, 2001. **82**(1): p. 76-80.

50. Wallmersperger, T., B. Kröplin, and R.W. Gülch, *Coupled chemo-electro-mechanical formulation for ionic polymer gels—numerical and experimental investigations.* Mechanics of Materials, 2004. **36**(5–6): p. 411-420.

51. Homma, M., Y. Seida, and Y. Nakano, *Evaluation of optimum condition for designing high-performance electro-driven polymer hydrogel systems.* Journal of Applied Polymer Science, 2000. **75**(1): p. 111-118.

52. Ionov, L., *Polymeric Actuators.* Langmuir, 2015. **31**(18): p. 5015-5024.

53. Kwon, G.H., et al., *Biomimetic Soft Multifunctional Miniature Aquabots.* Small, 2008. **4**(12): p. 2148-2153.

54. Rossmeisl, J., A. Logadottir, and J.K. Nørskov, *Electrolysis of water on (oxidized) metal surfaces.* Chemical Physics, 2005. **319**(1–3): p. 178-184.

55. Engel, L., et al., *Actuation of a novel Pluronic-based hydrogel: Electromechanical response and the role of applied current.* Sensors and Actuators B: Chemical, 2014. **191**: p. 650-658.

56. Jin, S., et al., *Preparation and electrical sensitive behavior of poly (N-vinylpyrrolidone-co-acrylic acid) hydrogel with flexible chain nature.* European Polymer

Journal, 2013. **49**(7): p. 1871-1880.

57. Glazer, P.J., et al., *Role of pH gradients in the actuation of electro-responsive polyelectrolyte gels.* Soft Matter, 2012. **8**(16): p. 4421-4426.

58. Yu, X., et al., *Sulfoacetic acid modifying poly(vinyl alcohol) hydrogel and its electroresponsive behavior under DC electric field.* Smart Materials and Structures, 2013. **22**(1): p. 014009.

59. Carmo, M., et al., *A comprehensive review on PEM water electrolysis.* International Journal of Hydrogen Energy, 2013. **38**(12): p. 4901-4934.

60. Elshaer, S.E. and W.A. Moussa, *Comparative study of chemo-electro-mechanical transport models for an electrically stimulated hydrogel.* Smart Materials and Structures, 2014. **23**(7): p. 075022.

61. Rahimi, N., et al., *Electrosensitive Polyacrylic Acid/Fibrin Hydrogel Facilitates Cell Seeding and Alignment.* Biomacromolecules, 2012. **13**(5): p. 1448-1457.

62. Lin, S.-B., et al., *Electrical response characterization of PVA–P(AA/AMPS) IPN hydrogels in aqueous Na2SO4 solution.* Sensors and Actuators B: Chemical, 2008. **134**(1): p. 281-286.

63. Tai, Z., et al., *Synthesis of a graphene oxide-polyacrylic acid nanocomposite hydrogel and its swelling and electroresponsive properties.* RSC Advances, 2013. **3**(31): p. 12751-12757.

64. Kim, S.J., et al., *Electrical sensitive behavior of poly(vinyl alcohol)/poly (diallyldimethylammonium chloride) IPN hydrogel.* Sensors and Actuators B: Chemical, 2003. **88**(3): p. 286-291.

65. Yao, L. and S. Krause, *Electromechanical Responses of Strong Acid Polymer Gels in DC Electric Fields.* Macromolecules, 2003. **36**(6): p. 2055-2065.

66. Bassil, M., M. Ibrahim, and M. El Tahchi, *Artificial muscular microfibers: hydrogel with high*

speed tunable electroactivity. Soft Matter, 2011. **7**(10): p. 4833-4838.

67. Stefano, P., et al., *Propulsion of swimming microrobots inspired by metachronal waves in ciliates: from biology to material specifications.* Bioinspiration & Biomimetics, 2013. **8**(4): p. 046004.

68. Lim, H.L., et al., *Dynamic Electromechanical Hydrogel Matrices for Stem Cell Culture.* Advanced Functional Materials, 2011. **21**(1): p. 55-63.

69. Moschou, E.A., et al., *Artificial Muscle Material with Fast Electroactuation under Neutral pH Conditions.* Chemistry of Materials, 2004. **16**(12): p. 2499-2502.

70. Kwon, G.H., et al., *Electrically-driven hydrogel actuators in microfluidic channels: fabrication, characterization, and biological application.* Lab on a Chip, 2010. **10**(12): p. 1604-1610.

71. Kwon, G.H., et al., *A low-energy-consumption electroactive valveless hydrogel micropump for long-term biomedical applications.* Lab on a Chip, 2011. **11**(17): p. 2910-2915.

72. Kato, N. and S.H. Gehrke, *Microporous, fast response cellulose ether hydrogel prepared by freeze-drying.* Colloids and Surfaces B: Biointerfaces, 2004. **38**(3–4): p. 191-196.

73. Luo, R., et al., *Modeling of electric-stimulus-responsive hydrogels immersed in different bathing solutions.* Journal of Biomedical Materials Research Part A, 2008. **85A**(1): p. 248-257.

74. Bekin, S., et al., *Synthesis, characterization and bending behavior of electroresponsive sodium alginate/poly(acrylic acid) interpenetrating network films under an electric field stimulus.* Sensors and Actuators B: Chemical, 2014. **202**: p. 878-892.

75. Santaniello, T., et al., *A room-temperature bonding technique for the packaging of hydrogel-based hybrid microfluidic devices.* Microfluidics and Nanofluidics, 2015. **19**(1): p.

31-41.

76. Lin, J., et al., *Electric field sensitivity of conducting hydrogels with interpenetrating polymer network structure.* Colloids and Surfaces A: Physicochemical and Engineering Aspects, 2009. **346**(1–3): p. 177-183.

77. Korpe, S., et al., *Crosslinked DADMAC polymers as cationic super absorbents.* Reactive and Functional Polymers, 2009. **69**(9): p. 660-665.

78. Miao, B., et al., *Effect of Finite Extensibility on the Equilibrium Chain Size.* Macromolecular Theory and Simulations, 2010. **19**(7): p. 414-420.

79. Glazer, P.J., et al., *Electro-actuation of biocompatible Pluronic/methacrylic acid hydrogel in blood-plasma and in blood-mimicking buffers.* RSC Advances, 2014. **4**(4): p. 1890-1894.

80. Doi, M., M. Matsumoto, and Y. Hirose, *Deformation of ionic polymer gels by electric fields.* Macromolecules, 1992. **25**(20): p. 5504-5511.

81. Cushing, M.C. and K.S. Anseth, *Hydrogel Cell Cultures.* Science, 2007. **316**(5828): p. 1133-1134.

82. Yeo, Y., et al., *Photocrosslinkable hydrogel for myocyte cell culture and injection.* Journal of Biomedical Materials Research Part B: Applied Biomaterials, 2007. **81B**(2): p. 312-322.

83. Lin, C.-C. and A.T. Metters, *Hydrogels in controlled release formulations: Network design and mathematical modeling.* Advanced Drug Delivery Reviews, 2006. **58**(12–13): p. 1379-1408.

84. Deligkaris, K., et al., *Hydrogel-based devices for biomedical applications.* Sensors and Actuators B: Chemical, 2010. **147**(2): p. 765-774.

85. Shin, H., et al., *Attachment, proliferation, and migration of marrow stromal osteoblasts cultured on biomimetic hydrogels modified with an osteopontin-derived peptide.*

Biomaterials, 2004. **25**(5): p. 895-906.

86. Gupta, K., et al., *Lab-on-a-chip devices as an emerging platform for stem cell biology.* Lab on a Chip, 2010. **10**(16): p. 2019-2031.

87. Khademhosseini, A. and R. Langer, *Microengineered hydrogels for tissue engineering.* Biomaterials, 2007. **28**(34): p. 5087-5092.

88. Chung, B.G., et al., *Microfluidic fabrication of microengineered hydrogels and their application in tissue engineering.* Lab on a Chip, 2012. **12**(1): p. 45-59.

89. Ren, K., J. Zhou, and H. Wu, *Materials for Microfluidic Chip Fabrication.* Accounts of Chemical Research, 2013. **46**(11): p. 2396-2406.

90. Cha, C., et al., *Tailoring Hydrogel Adhesion to Polydimethylsiloxane Substrates Using Polysaccharide Glue.* Angewandte Chemie International Edition, 2013. **52**(27): p. 6949-6952.

91. Greiner, A.M., et al., *Stable Biochemically Micro-patterned Hydrogel Layers Control Specific Cell Adhesion and Allow Long Term Cyclic Tensile Strain Experiments.* Macromolecular Bioscience, 2014. **14**(11): p. 1547-1555.

92. Gan, Z., L. Zhang, and G. Chen, *Solvent bonding of poly(methyl methacrylate) microfluidic chip using phase-changing agar hydrogel as a sacrificial layer.* ELECTROPHORESIS, 2011. **32**(23): p. 3319-3323.

93. Lai, S., X. Cao, and L.J. Lee, *A Packaging Technique for Polymer Microfluidic Platforms.* Analytical Chemistry, 2004. **76**(4): p. 1175-1183.

94. Yoon, J., et al., *Poroelastic swelling kinetics of thin hydrogel layers: comparison of theory and experiment.* Soft Matter, 2010. **6**(23): p. 6004-6012.

95. Hong, W., Z. Liu, and Z. Suo, *Inhomogeneous swelling of a gel in equilibrium with a solvent*

and mechanical load. International Journal of Solids and Structures, 2009. **46**(17): p. 3282-3289.

96. Lutolf, M.P., et al., *Cell-Responsive Synthetic Hydrogels.* Advanced Materials, 2003. **15**(11): p. 888-892.

97. Zhang, H., et al., *Fabrication of Robust Hydrogel Coatings on Polydimethylsiloxane Substrates Using Micropillar Anchor Structures with Chemical Surface Modification.* ACS Applied Materials & Interfaces, 2014. **6**(12): p. 9126-9133.

98. Marcombe, R., et al., *A theory of constrained swelling of a pH-sensitive hydrogel.* Soft Matter, 2010. **6**(4): p. 784-793.

99. Hung, P.J., et al., *Continuous perfusion microfluidic cell culture array for high-throughput cell-based assays.* Biotechnology and Bioengineering, 2005. **89**(1): p. 1-8.

100. Cheng, S.-Y., et al., *A hydrogel-based microfluidic device for the studies of directed cell migration.* Lab on a Chip, 2007. **7**(6): p. 763-769.

101. Chirila, T.V., *An overview of the development of artificial corneas with porous skirts and the use of PHEMA for such an application.* Biomaterials, 2001. **22**(24): p. 3311-3317.

102. Abraham, S., et al., *Molecularly engineered p(HEMA)-based hydrogels for implant biochip biocompatibility.* Biomaterials, 2005. **26**(23): p. 4767-4778.

103. Kejlová, K., et al., *Hydrophilic polymers—biocompatibility testing in vitro.* Toxicology in Vitro, 2005. **19**(7): p. 957-962.

104. Merrett, K., et al., *Adhesion of corneal epithelial cells to cell adhesion peptide modified pHEMA surfaces.* Journal of Biomaterials Science, Polymer Edition, 2001. **12**(6): p. 647-671.

105. Guiseppi-Elie, A., C. Dong, and C.Z. Dinu, *Crosslink density of a biomimetic*

poly(HEMA)-based hydrogel influences growth and proliferation of attachment dependent RMS 13 cells. Journal of Materials Chemistry, 2012. **22**(37): p. 19529-19539.

106. Burdick, J.A. and G. Vunjak-Novakovic, *Engineered Microenvironments for Controlled Stem Cell Differentiation.* Tissue Engineering Part A, 2008. **15**(2): p. 205-219.

107. Johnson-Chavarria, E.M., et al., *Automated single cell microbioreactor for monitoring intracellular dynamics and cell growth in free solution.* Lab on a Chip, 2014. **14**(15): p. 2688-2697.

108. Cimetta, E., et al., *Micro-bioreactor arrays for controlling cellular environments: Design principles for human embryonic stem cell applications.* Methods, 2009. **47**(2): p. 81-89.

109. Lee, H.L.T., et al., *Microbioreactor arrays with integrated mixers and fluid injectors for high-throughput experimentation with pH and dissolved oxygen control.* Lab on a Chip, 2006. **6**(9): p. 1229-1235.

110. Zhao, W., et al., *A methodology to analyse and simulate mechanical characteristics of poly(2-hydroxyethyl methacrylate) hydrogel.* Polymer International, 2013. **62**(7): p. 1059-1067.

111. Tong, Z. and X. Liu, *Swelling Equilibria and Volume Phase Transition in Hydrogels with Strongly Dissociating Electrolytes.* Macromolecules, 1994. **27**(3): p. 844-848.

112. Tang, L. and N.Y. Lee, *A facile route for irreversible bonding of plastic-PDMS hybrid microdevices at room temperature.* Lab on a Chip, 2010. **10**(10): p. 1274-1280.

113. Sunkara, V., et al., *Simple room temperature bonding of thermoplastics and poly(dimethylsiloxane).* Lab on a Chip, 2011. **11**(5): p. 962-965.

114. Lee, N.Y. and B.H. Chung, *Novel Poly(dimethylsiloxane) Bonding Strategy via Room Temperature "Chemical Gluing".* Langmuir, 2009. **25**(6): p. 3861-3866.

115. Tennico, Y.H., et al., *Surface modification-assisted bonding of polymer-based microfluidic devices.* Sensors and Actuators B: Chemical, 2010. **143**(2): p. 799-804.

116. Vlachopoulou, M.E., et al., *A low temperature surface modification assisted method for bonding plastic substrates.* Journal of Micromechanics and Microengineering, 2009. **19**(1): p. 015007.

117. Setsuhara, Y., et al., *Low-damage surface modification of polymethylmethacrylate with argon–oxygen mixture plasmas driven by multiple low-inductance antenna units.* Thin Solid Films, 2010. **518**(13): p. 3561-3565.

118. Hegemann, D., H. Brunner, and C. Oehr, *Plasma treatment of polymers for surface and adhesion improvement.* Nuclear Instruments and Methods in Physics Research Section B: Beam Interactions with Materials and Atoms, 2003. **208**: p. 281-286.

119. Tsougeni, K., et al., *Plasma Nanotextured PMMA Surfaces for Protein Arrays: Increased Protein Binding and Enhanced Detection Sensitivity.* Langmuir, 2010. **26**(17): p. 13883-13891.

120. Wong, I. and C.-M. Ho, *Surface molecular property modifications for poly(dimethylsiloxane) (PDMS) based microfluidic devices.* Microfluidics and Nanofluidics, 2009. **7**(3): p. 291-306.

121. Kim, J., R. Surapaneni, and B.K. Gale, *Rapid prototyping of microfluidic systems using a PDMS/polymer tape composite.* Lab on a Chip, 2009. **9**(9): p. 1290-1293.

122. Yu, N., et al., *Correction: Benign and Malignant Renal Cells Are Differentially Inhibited during Prolonged Organ Preservation.* PLoS ONE, 2014. **9**(1): p. 10.1371/annotation/b51ed377-9d16-4082-b714-369fc36a8a22.

123. Oh, K.W., et al., *Design of pressure-driven microfluidic networks using electric circuit analogy.* Lab on a Chip, 2012. **12**(3): p. 515-545.

124. Antia, M., T. Herricks, and P.K. Rathod, *Microfluidic Modeling of Cell−Cell Interactions in Malaria Pathogenesis.* PLoS Pathog, 2007. **3**(7): p. e99.

125. Barnes, J.M., J.T. Nauseef, and M.D. Henry, *Resistance to fluid shear stress is a conserved biophysical property of malignant cells.* PLoS One, 2012. **7**(12): p. e50973.

126. Makamba, H., et al., *Surface modification of poly(dimethylsiloxane) microchannels.* ELECTROPHORESIS, 2003. **24**(21): p. 3607-3619.

14. Acknowledgement

I would like to thank my supervisor, Prof. Paolo Milani, for offering me the opportunity to work on this exciting project. I am really glad that he gave me so much space and support to develop such wonderful work.

I would like to thank my internal advisor Dr. Alessandro Podestà, for examining my research and reports on the project, and my external advisor Prof.Yosi Shacham for helpful advices on my work.

I would like to thank Dr. Tommaso Santaniello for all of the fundamental research support for me and constant help involved in all my projects, including writing.

I would like to thank Lorenzo Migliorini for the excellent work in the hydrogel actuator part.

I would like to thank Alexandra Raileanu, Riccardo Porotti, Ilaria Denti, Wondimu Gebreyes, Ana Muci, Claudio Piazzoni, Andrea Bellacicca, Gabriele Faraone, Eleonora Rossi , Claudia Cella, Margherita Tamplenizza, Chloé Minnai, Luca Giacomo Bettini, Sambat Gevorgyan and Castern Schulte for their help during the four years.

A special thank goes to the mechanical workshop in CIMaINa, that really supported me during these four years with their wonderful engineering work.